NUMERICAL MODELING OF A LIGAMENTOUS LUMBAR MOTION SEGMENT

A Dissertation
Presented to
The Academic Faculty

By

Guilhem Denozière

In Partial Fulfillment
Of the Requirements for the Degree
Master of Science in Mechanical Engineering

Georgia Institute of Technology
May 2004

NUMERICAL MODELING OF A LIGAMENTOUS LUMBAR MOTION SEGMENT

Approved by:

Dr. David N. Ku, Advisor

Dr. William C. Hutton

Dr. David L. McDowell

May 24, 2004

ACKNOWLEDGEMENT

I am most grateful for my advisor, Dr. David Ku, for his guidance and support during this study. He allowed me to manage my research with a great range of freedom, from which I earned a rich experience. I would like to express my gratitude to the other members of my committee, Dr. William Hutton and Dr. David McDowell, whom experience and advice have been most profitable to my research.

I would also like to thank the staff of the Engineering Computing Services Department for their availability and assistance with the inescapable computer-related difficulties that have arose while developing the model.

I will not forget to mention the unconditional support of the members of my family, from each side of the ocean, and I would like to express my gratitude to them with the same measure of the confidence, the force, and the love that they offered me along this year.

TABLE OF CONTENTS

LIST OF TABLES

LIST OF FIGURES

LIST OF ABBREVIATIONS

ALIF Anterior Lumbar Interbody Fusion

ALL: Anterior Longitudinal Ligament

CL: Capsular Ligament

FE Finite Element

FSU: Functional Spine Unit

IAR: Instantaneous Axis of Rotation

ISL: Inter-Spinous Ligament

IVD: Intervertebral Disc

LF: Ligamentum Flavum

PLIF Posterior Lumbar Interbody Fusion

PLL: Posterior Longitudinal Ligament

SSL: Supra-Spinous Ligament

TL: Transverse Ligament

SUMMARY

Eight out of ten people in the United States will have problems with low back pain at some point in their life. The most significant surgical treatments for low back pain can be distributed into two main groups of solutions: arthrodesis and arthroplasty. Spinal arthrodesis consists of the fusion of a degenerated functional spine unit (FSU) to alleviate pain and prevent mechanical instability. Spinal arthroplasty consists of the implantation of an artificial disc to restore the functionality of the degenerated FSU. The objective of this study is to analyze and compare the alteration of the biomechanics of the lumbar spine treated either by arthrodesis or arthroplasty.

A three-dimensional finite element model of a ligamentous lumbar motion segment, constituted of two FSUs, was built and simulated through a static analysis with the finite element software ABAQUS.

It was shown that the mobility of the segment treated by arthrodesis was reduced in all rotational degrees of freedom by an average of approximately 44%, relative to the healthy model. Conversely, the mobility of the segment treated by arthroplasty was increased in all rotational degrees of freedom by an average of approximately 52%. The FSU implanted with the artificial disc showed a high risk of instability and further degeneration. The mobility and the stresses in the healthy FSU, adjacent to the restored FSU in the segment treated by arthroplasty, were also increased.

In conclusion, the simulation of the arthroplasty model showed more risks of instability and further degeneration, on the treated level as well as on the adjacent levels, than in the arthrodesis model.

CHAPTER 1

INTRODUCTION AND BACKGROUND

1.1 Pathophysiology of the Intervertebral Disc

1.1.1 Triple Joint Complex

The intervertebral disc (IVD) is one of the most important constitutive elements of a functional spine unit (FSU). Its complex structure allows significant mobility between two adjacent vertebrae while transmitting considerable compressive loads from one vertebra to another. The IVD is consequently the focus of interest of numerous biomechanical and biochemical studies. The spine consists of three main columns which provide a triple joint interface connecting two adjacent vertebrae. This triple joint complex is made of one IVD and two articular facets. The geometric and material properties of those elements, as well as all the constitutive elements of a FSU, are extensively described in Chapter 2. Figure 1-1 illustrates the triple joint complex of a FSU.

The facet joints have an important role in the stability of the spine, in the restriction of its mobility, and in the load sharing between the anterior and posterior elements of a FSU [78], [62]. According to Sharma et al. the facets resist up to 39.7% of the load for large extensions [62] and up to 59% for large axial rotations [61]. Adams and Hutton claim that the articular facets withstand 16% of the compressive load in the erect standing posture, i.e. slightly extended [2]. Conversely, the facets' load share is not significant in flexion [61], [62] unless very large angular displacements are considered [63]. The load sharing between the IVD and the facet joints can be very important in some degrees of

freedom, and the elements of the triple joint complex may become accordingly interdependent in their pathologies [74]. For example, the reduction of the intervertebral space induced by disc excision or by the natural degeneration of the disc brings abnormal loadings on the facets, which may lead to other degenerative changes and low back pain [15]. Fujiwara et al. suggest that disc degeneration induces facet joint osteoarthritis with a delay of approximately 20 years after the onset of disc degeneration [21].

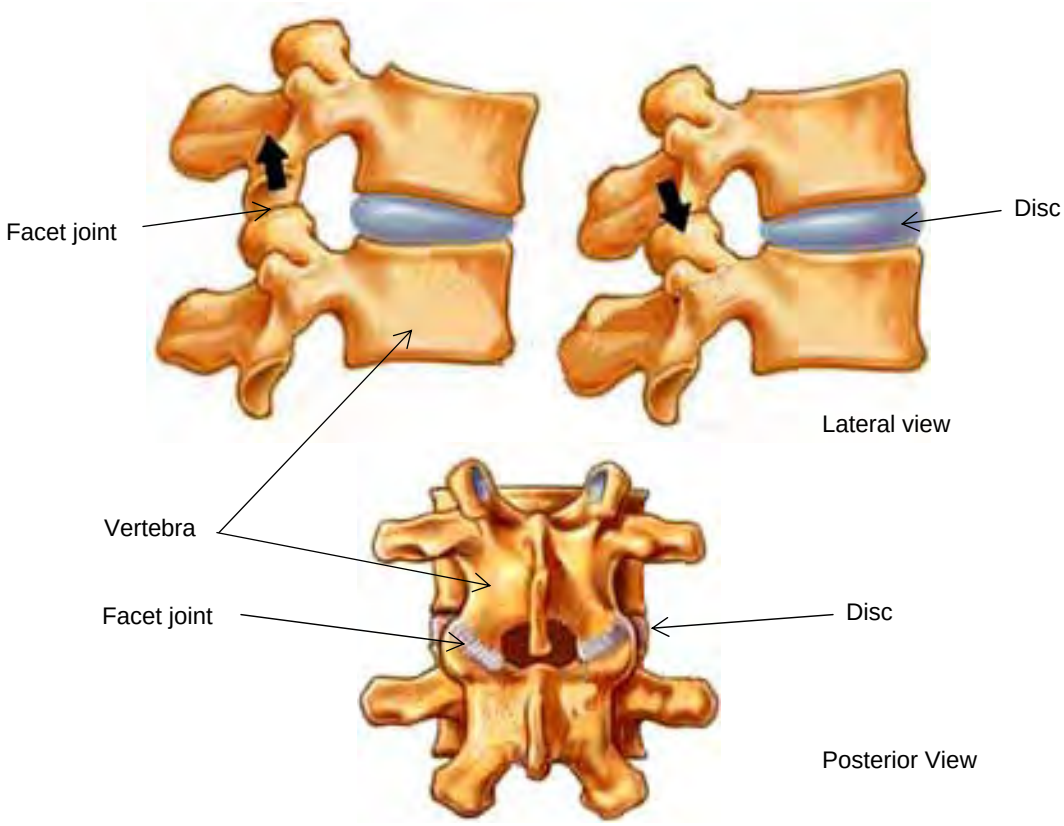

Figure 1-1: Basic constitutive elements of a functional spine unit

In conclusion, the interrelations between the disc and the facets of a FSU triple joint complex are significant and it can be assumed that any intervention on one of those elements is likely to provoke major changes in the FSU biomechanics and might contribute to further complications.

1.1.2 Low Back Pain

The mechanisms of low back pain are difficult to identify and remain for the most part unknown. On one hand, the biomechanical changes induced by numerous degenerative diseases or traumatic experiences of the lumbar spine are well known. On the other hand, the structure of the sensory innervations in the lumbar spine, which is a potential source of low back pain, is also well known. However, the paths between causes and effects relate more to expectations than to true understanding. Figure 1-2 summarizes back pain mechanisms relating abnormal biomechanics to pain. Although nothing more than a hypothesis, it illustrates how complex and numerous the mechanisms of back pain can be.

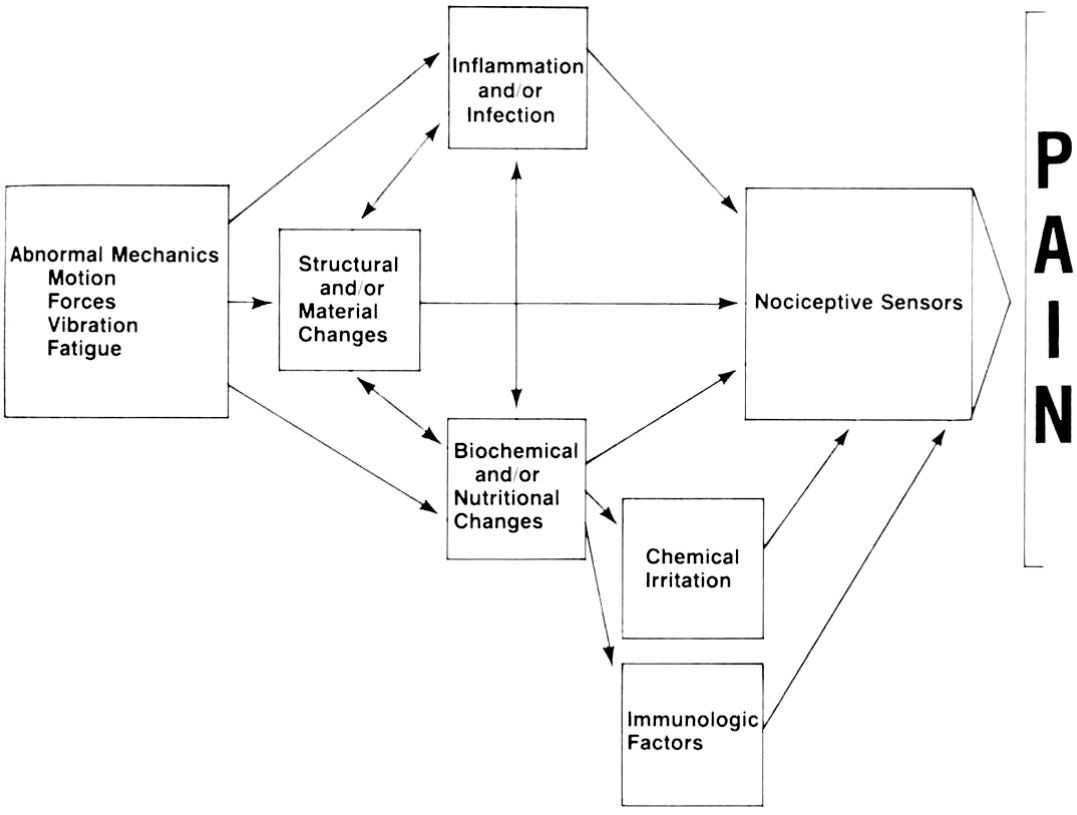

Figure 1-2: Hypothesized sequence of events linking abnormal mechanics to spine pain [76]

The sinuvertebral nerve, starting from each spinal root nerve, innervates most of the constitutive elements of a FSU [45]. Consequently, virtually any hard tissue in the lumbar spine can be a potential source of back pain. The outer layers of the annulus fibrosus [6], the cortical and cancellous bone [48], and the set of intervertebral ligaments are all innervated [76]. The only elements that cannot be a source of pain are the inner layers of the annulus fibrosus, the nucleus pulposus [6], [45], and the cartilage endplates as well as the articular cartilage of the facets [48].

In individual cases, it is difficult to clearly identify the problem and apply the right treatment for a patient's lower back pain. Moreover, it suggests that the treatments which aim to alleviate pain through a modification of the spinal structure and biomechanics, specifically surgical treatments, may be hazardous. Indeed, considering the strong interdependence of the intervertebral elements discussed in the previous section, such treatments may simply transfer the pain from one area to another.

1.1.3 Disc Degeneration

The IVD is the first component among the FSU's constitutive elements to degenerate. This process is entirely natural and starts as early as the second decade of life with biochemical alterations. The first modifications of aging are loss of water and disarrangement of the collagen organization, which induce a decrease of the disc height. Concurrently, the reduction of nutrient supply to the disc cells, due to the calcification of the cartilage endplates, results in tissue failures starting with the nucleus. The next step of the natural degeneration process occurs during the third or fourth decade of life and consists of macroscopic alterations such as fissuring of the annulus fiber layers and radial migration of the nucleus material. This is followed by a general bulging of the disc and in

certain cases of more pronounced local bulging, also known as disc herniation, illustrated in Figure 1-3 (a). Finally, the degeneration is also coupled with vascularization and innervation of the disc's inner-tissues, originally avascular and not innervated. The disc can accordingly become subject to inflammations and infections, and may develop a sensory innervation network that turns it into a significant source of pain. The intensity of the IVD degeneration depends on several other aspects such as acute traumatic events or the mechanical, nutritional, and genetic backgrounds. The model here explored biomechanical considerations but did not include the important genetic components of the disease.

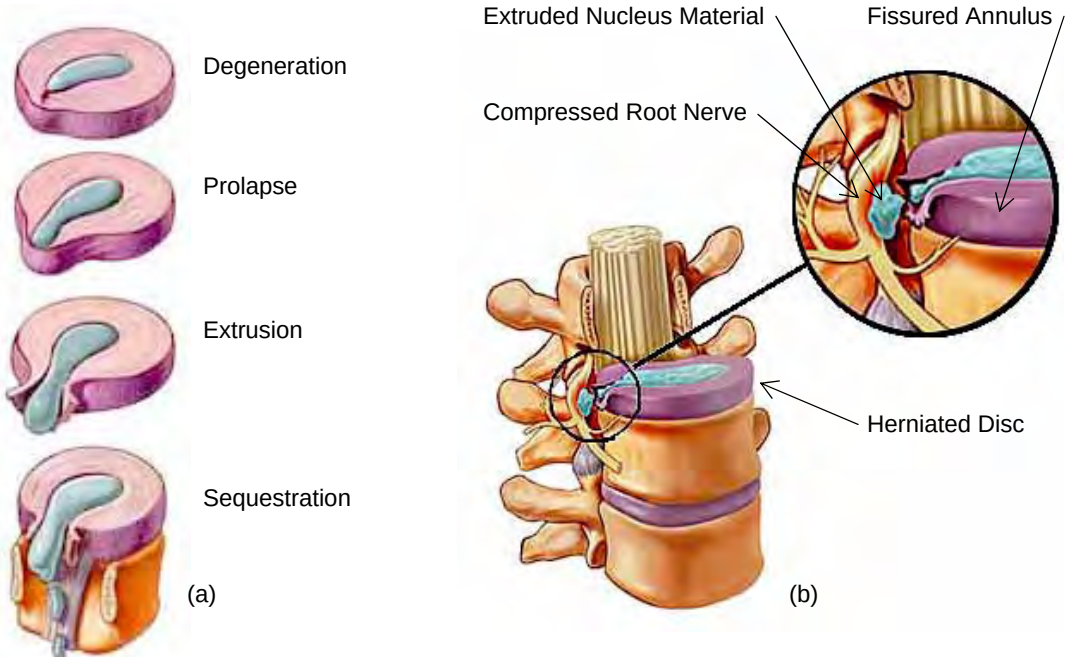

Figure 1-3: (a) Progression of disc herniation, (b) example of radiculopathy caused by disc herniation [*spineuniverse.com*]

It is important to note, however, that disc degeneration can occur without any symptomatic pain. Low back pain from IVD degeneration can be felt directly through this extra innervation of the disc itself, combined with an alteration of the spine

biomechanics. Another common source of low back pain is the sensitization of the central nervous system. Radiculopathy, often induced by mechanical events such as disc herniation (Figure 1-3 (b)), is characterized by intraneural inflammation and hypersensitivity. In a more general point of view, it can be affirmed that the biochemical and biomechanical alterations of the disc have, directly or indirectly, significant effects on lower back pain. Indeed, IVD degeneration precedes and appears to emphasize the degeneration of the various constitutive elements of a FSU. [10], [18], [45], [6], [12]

1.2 Review of Surgical Treatments for Disc Degeneration

As far as feasible, conservative treatments for disc degeneration are preferred. Such treatments include physical therapy, drugs, relaxation, braces, or even steroid injections and nerve blockage through spinal injections. The success of such treatments is mixed, however, since the first clinical symptoms usually occur when disc degeneration is already well advanced. If the conservative treatment is not successful in alleviating the clinical symptoms such as pain, sensory deficit, or motor deficit, surgical treatment should be considered. Even if surgery provides a fast relief, it remains unclear that surgical techniques such as discectomy will have a better outcome than the natural progression of the disc disease. However, it appears that outcomes are more favorable when discectomy is achieved shortly after the failure of a conservative treatment. Rothoerl et al. recommend considering surgery after two months of unsuccessful conservative treatment [60]. Baldwin recommends a period of three months [6].

Beyond the classic discectomy, which consists of the removal of the bulging disc material, various other surgical treatments for degenerative disc disease are available [11]. Less invasive, percutaneous nucleotomy and nucleoplasty respectively aim to

remove or disintegrate the excessive nucleus material that causes the disc herniation. More experimental, the intradiscal electrothermal therapy involves the pericutaneus insertion of a thermal resistance that aims to shrink the collagen fibrils of the annulus and consequently reduces the bulge of the disc [4], [75]. Alini et al. emphasize that no treatments intend to repair the degenerated disc and the authors are attempting to develop implantable engineered tissue that has similar characteristics to healthy nucleus pulposus tissue [3].

When the disc is in an advanced stage of degeneration, the removal of the excessive disc material is not sufficient and it is sometimes necessary to restore the disc height to release the compressed structures. The corresponding surgical treatments of arthrodesis and arthroplasty, described in the following section, therefore require the implantation of artificial devices.

1.2.1 Arthrodesis

Arthrodesis consists of the distraction and the surgical immobilization of a joint, here of a FSU, to alleviate pain and prevent mechanical instability. The bones subsequently grow solidly together, maintaining the interbody distraction and the stability of the joint.

Initially used for treatment of infectious conditions, deformity or trauma of the spine, and based on technical evolutions, the treatment of arthrodesis is now generally indicated for abnormal or unstable motion of a FSU, or for IVD degenerative disease. In any case, this kind of treatment is used in an attempt to control and ease acute low back pain [27].

Various techniques of spinal arthrodesis are available. Some are more adapted to specific pathologies such as spondylolisthesis, illustrated in Figure 1-4 (A).

Spondylolisthesis is a forward movement of a vertebra over the underlying vertebra, which requires an additional bearing in the sagittal direction to prevent instability (Figure 1-4 (B)). In general, arthrodesis techniques are evolving toward the improvement of the fusion rate.

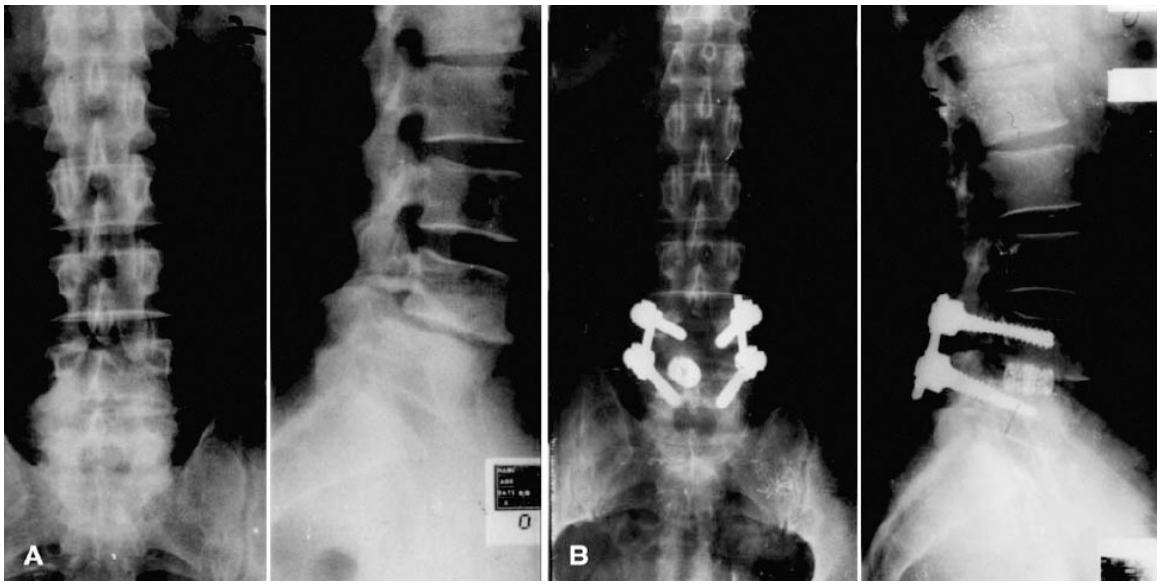

Figure 1-4: (A) 41-year-old male with symptomatic spondylolisthesis on L3-L4. (B) He was treated with posterior lumbar interbody fusion (PLIF) using one diagonal BAK cage with unilateral facetectomy and with transpedicular screw fixation [79]

The main arthrodesis techniques available are listed below [43], [50], [27], [46]:

- *Posterolateral fusion*, consists of the implantation of a bone graft in the posterolateral area of the intervertebral space with or without the use of internal fixations,
- *Pedicle/laminae screw instrumentation*, consists of the adjunction of posterior stabilization devices such as wires, hooks, or screws, that have been shown to improve the fusion rate,

- *Posterior lumbar interbody fusion* (PLIF), illustrated in Figure 1-4 (B), consists of the excision of the degenerated disc and implantation of a graft through a posterior path. It is usually associated with internal fixation and partial or total laminectomy,
- *Anterior lumbar interbody fusion* (ALIF), consists of the excision of the degenerated disc and implantation of a graft through an anterior path. It can be associated with internal an anterior fixation to improve the fusion rate,
- *Interbody fusion cage*, is used to improve the structural support of the intervertebral space in addition to the bone graft that may collapse and cause instability. It can be associated with an internal fixation to improve the fusion rate,
- *Circumferential fusion*, is characterized by the elimination of all potential sources of pain in the anterior and posterior structures, and a high stability. The procedure usually takes into account a combination of the anterior and posterior approaches.

The complete rehabilitation from the surgical operation typically takes 3 to 12 months during which the patient is required to avoid motion in order to allow bone healing [26]. The clinical outcomes can be significantly variable depending on the materials and methods used. In general, satisfactory outcomes range from 49% to 88% [19], [43], [46], [27]. According to Fritzell et al., complications increase significantly with increasing technical complexity of the surgical procedure [19].

The most common complications directly related to the treated FSU are: failure to achieve the solid bony union [44], broken screw, instrument loosening, and migration of implant [19]. Other complications are associated with changing behaviors of the levels adjacent to the treated FSU. Bastian et al. have shown that the segmental mobility of the

overlying adjacent level has been significantly increased after a double level T12-L2 posterior arthrodesis. It is also suggested that it may lead to an accelerated degeneration of the facet joints at this level and explain symptoms such as low back pain after spinal arthrodesis [9]. Penta et al. studied 52 patients ten years after an ALIF to determine the influence of spinal arthrodesis on the degeneration of the discs in the levels adjacent to the fused FSU. They reported degenerated adjacent discs in only 33% of the patients, which led to the conclusion that the procedure does not significantly increase the degeneration of adjacent discs [55]. Kumar et al. did a similar study on 83 patients who underwent lumbar arthrodesis and with a mean follow-up period of 5 years. Radiographic evidence of adjacent segment degeneration was observed in 36.1% of the patients [35]. In another study, Kumar et al. reviewed 58 patients treated for degenerative disc disease with a minimum follow-up of 30 years. Half of the patients were treated by arthrodesis and the other half by discectomy or decompression. Radiographic changes at adjacent levels occurred approximately twice as often following lumbar fusion [36].

1.2.2 Arthroplasty

The treatment of arthroplasty consists of the plastic surgery of a joint, here of a FSU, in order to alleviate pain by restoring the relevant functionalities of a degenerated IVD. Eijkelkamp et al. have identified and listed the requirements for an artificial IVD according to nine critical items: geometry, stiffness, range of motion, strength, center of rotation, fixation to the adjacent vertebra, function of the facet joints, fail-safety, and surgical procedure [17]. Additionally, other authors have raised the importance of the biocompatibility [47], [7] as well as the shock absorption properties [39], [73] of such devices.

Spinal arthroplasty is indicated for acute low back pain resultant from degenerative disc disease for which conservative treatments have failed. It has been shown that such a treatment is contraindicated for gross degeneration of the spine (such as scoliosis), secondary osteoarthritis of the facet joints, fused adjacent levels, less than 4 mm disc height remaining at the adjacent levels, and posterior segment instability (such as spondylolisthesis). More specifically, risk of subsidence makes osteoporosis a contraindication for disc replacement with metallic devices. Annulus defects may also be a contraindication for nucleus replacement as the device typically applies tension to the annulus [34], [26], [11].

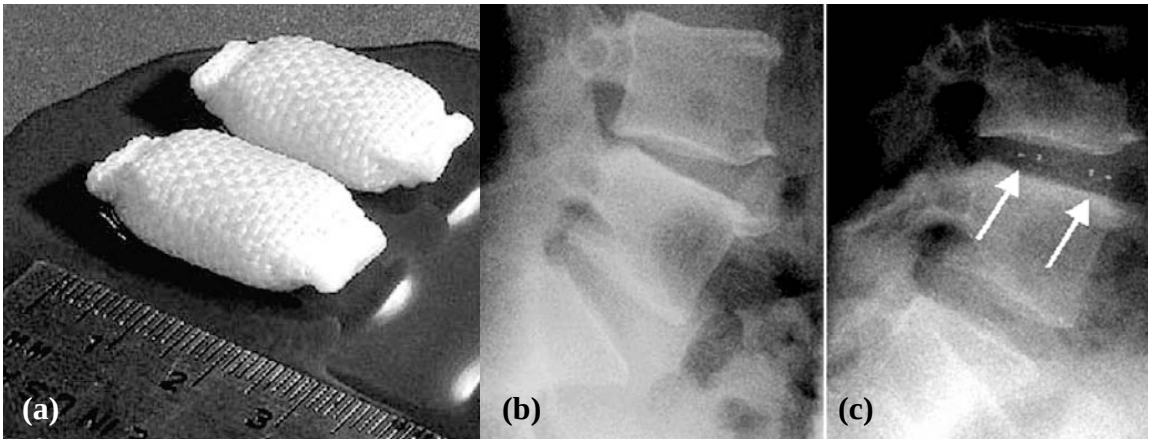

Figure 1-5: (a) Example of a nucleus prosthesis, the PDN artificial device, (b) preoperative lateral radiographic view with degenerative disc disease on L4-L5, (c) postoperative lateral radiographic view [59]

Artificial devices for spinal arthroplasty can be classified into two main groups: the nucleus prostheses for partial disc replacement, illustrated in Figure 1-5, and disc prostheses for total disc replacement. The disc prostheses can themselves be distinguished into movable devices, typically constituted of sliding solid parts, as shown

in Figure 1-6 and Figure 2-12, and flexible devices, illustrated in Figure 1-7, typically including a soft material to mimic a natural disc's behavioral characteristics [6].

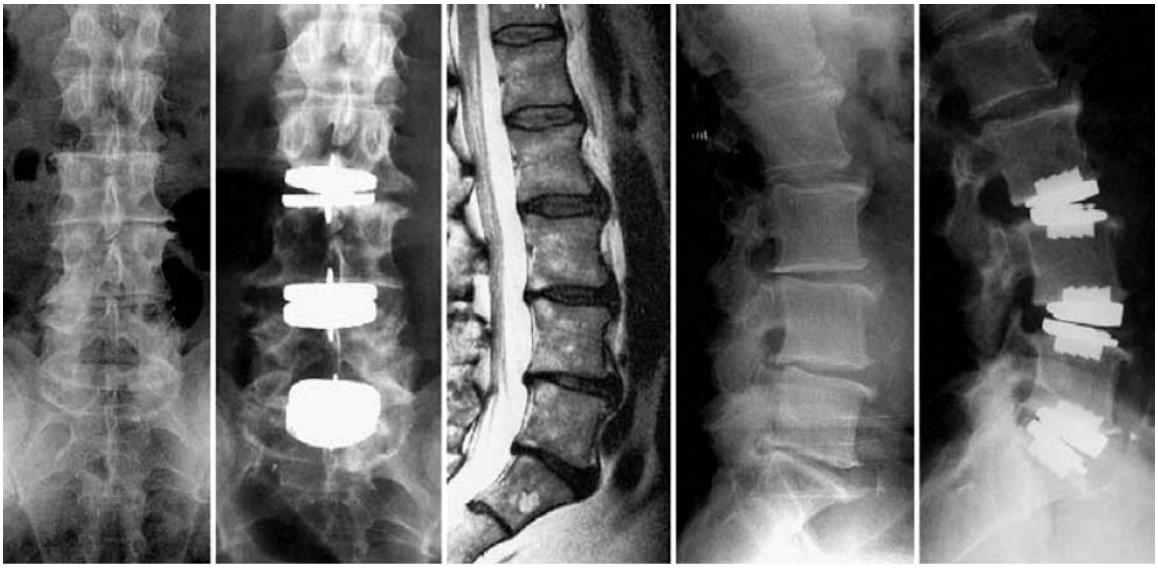

Figure 1-6: Extreme case of arthroplasty on three consecutive levels L3-S1 with the Prodisc II prosthesis, 53-year-old male with vertical segmental instabilities at L3-S1, radicular symptoms at L4, L5 and severe low back pain. He had previously undergone unsuccessful conservative treatment [11]

Szpalski et al. have extensively described the history of spinal arthroplasty, beginning in 1956 when the first intervertebral artificial device was described [71], [25]. The inventory of current clinically used intervertebral lumbar prostheses is as follow [26], [73], [71]:

- Acroflex, J&J Depuy Acromed (Raynham, MA),
- Maverick, Medtronic Safamor Danek (Minneapolis, MN),
- SB Charité, J&J Depuy Acromed, originally Link Spine Group (Hambourg, Germany),
- PDN, Raymedica (Minneapolis, MN),
- Prodisc, Synthes-Stratec, originally Spine Solutions (New York, NY).

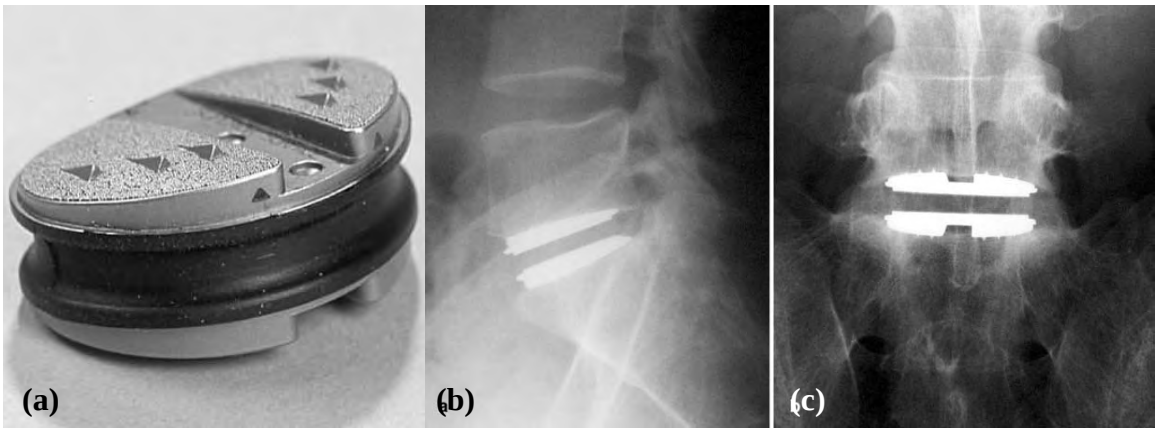

Figure 1-7: (a) Example of flexible disc prosthesis, the Acroflex artificial device, (b) postoperative lateral radiographic view with arthrodesis treatment on L4-L5, (c) postoperative anterior radiographic view [71]

The rehabilitation from arthroplasty procedures is much shorter than spinal arthrodesis and typically takes a few weeks. The patient is required to perform spinal motion exercises as soon as possible to guarantee better long term results [26].

The long term outcomes are reviewed here. The longest follow-up time period does not exceed approximately 12 years among the currently used devices. Kleuver et al. reviewed 9 studies gathered from 564 arthroplasties on 411 patients. The SB Charité was used in 8 cases and the Acroflex in 1 case. The follow-up periods range from 9 to 51 months. With the SB Charité, the ratios of good or excellent outcomes vary from 63% to 81% depending on the case, with an average of 72%. The single study involving the Acroflex shows 50% (3 out of 6 patients) of good or excellent outcomes [34]. Guyer et al. reviewed two studies with the Prodisc artificial device. In the first study, 108 patients showed 99% of good and excellent outcomes on short-term follow-up periods ranging from 3 to 24 months. In the other study, 70 patients have shown 78% of good and excellent results on long term follow-up periods ranging from 8 to 10 years [26]. Jin et al.

report 86% of satisfaction from 30 patients treated with the PDN artificial disc on a 6 month follow-up period [31].

Some devices, for which the follow-up periods are significant, allow us to understand the main complications that may be expected with spinal arthroplasty. Ooij et al. have shown that most common complications result from the degeneration of the facet joints on the same level, the degeneration of the disc and the facet joints on the adjacent levels, as well as the subsidence or migration of the artificial device [49].

1.3 Motivation of the Study

1.3.1 Biomechanical Comparison of Surgically Altered Lumbar Motion Segments

The rate of low back surgery has recently dramatically increased. As our life expectancy is continuously lengthening, problems related to the natural degeneration of the spine, specifically requiring surgical treatment, have become more common. Between 1979 and 1990, lumbar arthrodesis increased by 100%. In a more general point of view, low back surgery increased by 55% over the same period [44]. In the early nineties, the arrival of many new artificial intervertebral devices and the onset of clinical trials for some of them gave a new dynamic to spinal surgery. The growing experience base with arthrodesis and arthroplasty solutions now provides sufficient knowledge to allow engineers and surgeons to improve materials and methods in order to achieve better results. However, as described in Section 1.2, outcomes can be variable and complications diverse for both of the surgical groups of solutions. Studies on the subjects often reach the conclusion that many questions remain unanswered and that longer follow-up time periods are required for additional improvements. A more complete analysis still needs to be reached concerning the effects of the implantation of an artificial

intervertebral device, and more specifically on the alteration of spinal biomechanics resulting from such implantation. Indeed, likewise traumatic, nutritional, and genetic backgrounds, biomechanical changes can play a significant role in the intensity of the natural degeneration of the intervertebral components.

Many studies, experimental or numerical, have been made on the biomechanical characteristics of the lumbar spine. Some of these are touched on in this report. Involving a healthy or surgically altered lumbar spine, these studies help to take a step forward in the understanding of specific treatments for low back pain. Nevertheless, the literature was found to be lacking in studies offering a direct comparison of different treatments, and specifically the surgical solutions of arthrodesis and arthroplasty. It has been shown in the previous sections (1.2.1and 1.2.2) that the outcomes for these kinds of treatment are relatively similar over the available follow-up time periods. Their strengths and weaknesses compared to the behavior of the healthy lumbar spine have also been approached. Yet, there are no means of directly and quantitatively comparing the alteration of the spinal biomechanics induced by different surgical treatments.

The current study attempts to analyze and compare, through finite element (FE) methods, a ligamentous lumbar motion segment consisting of two FSUs in three different configurations. These configurations include a healthy motion segment, a motion segment in which the upper FSU has been fused, and a motion segment in which the upper intervertebral disc has been partially removed and restored by an artificial movable disc. The simulation protocol is identical for the three configurations. The model was built to be as close to actual physiological conditions as possible. However, the model cannot claim to provide absolute results for the different physical dimensions

investigated. The interest is to be able to understand and quantify, relatively to a healthy reference, the biomechanical alterations of a lumbar segment treated by arthrodesis and arthroplasty.

1.3.2 Choice of the Numerical Modeling

Finite element (FE) modeling has been commonly used in spinal biomechanics over the past 30 years. It has become an essential tool for the investigation of clinical problems. FE methods are inevitably complementary of experimental approaches. Those approaches are essential to compare the general results as well as to validate the construction of the model, specifically the geometry, the material properties, and the interactions characteristics. However, as the numerical simulations become increasingly relevant and accurate, FE models can allow significant savings on time and operating costs for clinical investigations.

A FE model consequently appears as an appropriate tool to accomplish the study. The software selected to complete the analysis is ABAQUS (ABAQUS, Inc., Pawtucket, RI). It is suitable for the current static analysis including non-linear behaviors and large displacements.

For reference, the commercially available FE software commonly used to model the lumbar spine and reported in the literature are:

- ABAQUS, ABAQUS, Inc., Pawtucket, RI [78], [14], [67], [23],
- PATRAN, PDA Engineering, Costa Mesa, CA [13], [61], [62], [37],
- I-DEAS, EDS, Maryland Heights, MO [58], [57],
- MARC, MSC Software Corporation, Palo Alto, CA [8], [70],
- ANSYS, ANSYS, Inc., Canonsburg, PA [38].

Other authors developed in-house software.

The current model was built through a review of the literature related to the FE modeling of the lumbar spine. In particular, a total of 20 studies making use of a FE analysis were selected and analyzed in order to extract the most relevant information for the construction of the model.

FE modeling provides the significant data needed to compare the biomechanical changes generated by the segment alterations. The study in particular focused on the range of rotational motions offered by the whole segments as well as by the individual FSUs in the different configurations. The stress modifications within the constitutive elements of the lower FSU's healthy disc were another center of interest. Finally, the forces relevant to the different sets of ligaments as well as to the facet joints were also investigated for the different configurations.

The model is however not limited to those particular applications. Indeed, once such a model is built, it is applicable to a broad range of additional problems.

1.4 Finite Element Modeling and Clinical Biomechanics of the Spine

Numerous FE analyses have been made on the clinical biomechanics of the lumbar spine. The published works can be distributed into four main areas. First of all, most of the studies aim at reaching a better understanding of the general clinical biomechanics of the lumbar spine. This includes healthy or injured segment behaviors as well as the mechanisms of injury. This area of study can itself be divided in two more specific groups, namely structural analyses and functional analyses. Less common in the literature but equally significant, FE studies are used for the design of artificial devices involved in treatments of the lumbar spine. Finally, another main area of study is the short and long

term understanding of the biomechanical alterations of the lumbar spine following a specific treatment. The analysis herein is among this last group.

To illustrate the finite element analysis in the clinical biomechanics of the spine, the following sections present some characteristic FE studies relevant to the four fields stated above.

1.4.1 Functional Biomechanics

The major topics in this area are the understanding and the evaluation of the role of the main constitutive elements in the lumbar spine. Those elements are the anterior column, the articular facets, the intervertebral ligaments and the spinal muscles.

In 1995, Sharma et al. evaluated the role of the ligaments, the articular facets, and the intervertebral disc in resisting the motions in a L3-L4 FSU under pure sagittal moments. The important role of the ligaments in flexion was shown as well as the complex interdependence between the load share of the facet and the spatial orientation of the FSU [62]. Three years later, the same authors demonstrated that the facet loads are very important in large extension as well as in torsion rotations and minimal in compression and flexion [61].

In 1994, Shirazi-Adl et al. explained that the load share in the facet joints was subject to increase with the loss of disc fluids, resulting from the disc degeneration [64].

Several authors have evaluated through numerical models the muscle forces in the lumbar spine [65], [13], [22].

In 1993, Goel et al. also investigated the differences provided by the model of a ligamentous L3-L4 segment with the muscles effects both considered and ignored. It was shown that the muscles provided more stability to the ligamentous model, decreased the

stresses within the anterior column and increased the load share of the articular facets [22].

Shirazi-Adl et al. have demonstrated how, in the neutral position, the activities of the lumbar muscles were dependant on the flattening of the lumbar lordosis and on the posterior pelvic tilt [65].

1.4.2 Structural Biomechanics

In this area the main concern is the understanding of the structural characteristics of the main spinal constitutive elements, namely the vertebral body and the IVD.

The load sharing between the cortical shell and the cancellous bone of a vertebral body remains controversial. In 1997, Silva et al. claim that the shell account for 10% of the vertebral strength in vivo and that the cancellous bone is the dominant structural component of the vertebral body [67].

During the same year, Smit et al. have studied the structure of the vertebral bone in the lumbar spine. They have come to the conclusion that the cancellous bone architecture and the vertical orientation of the facet joints suggest that walking may be the principal activity responsible for the architecture of the lumbar vertebral bone [70].

As proposed by Shirazi-Adl et al. in 1984, the disc is often modeled by a composite of fibers embedded into a matrix of ground substance surrounding the nucleus material [66]. Considering this type of model, Goel et al. have demonstrated in 1995 that the interlaminar shear stresses are more important in the posterolateral regions of the disc. This causes tears to occur in those regions; which reinforce statements provided by clinical studies [23].

1.4.3 Design of Artificial Devices

Publications related to the design of artificial devices for the lumbar spine are not common in the literature. Indeed, most of the devices are relatively recent and proprietary concerns restrict the disclosure of detailed information.

Langrana et al. reported in 1991 the design of an artificial lumbar IVD. A FE model was adopted in order to adapt the mechanical properties of the synthetic lumbar disc to the characteristics of a healthy disc, and thus match their behaviors [37].

Regarding the production of artificial lumbar devices, the FE method is a powerful tool used to validate and optimize a design prior to and in parallel with its experimental evaluation and clinical trial.

1.4.4 Consequences of Specific Treatments

The current study is indirectly related, through the design of the FE model, to the fields described in the three previous sections. However, it includes the most recent field in which the main concern is to predict the short and long term biomechanical alteration of the lumbar spine subjected to a specific treatment. This enables the identification of potential biomechanical side effects in order to formulate strategies to mitigate them.

In 2003, Baroud et al. investigated the potential fracture of adjacent vertebral bodies following a vertebroplasty. This treatment is used to prevent osteoporotic vertebral fractures and consists in the infiltration of bone cement in the osteoporotic cancellous bone. The study demonstrated that the treatment increases the pressure into the IVD by 19%; which results in an increase of approximately 17% of the inward bulge of the vertebral endplates directly adjacent to the treated vertebra. This increase of inward bulge was shown as a potential cause of adjacent fractures [8].

In 2003, Zander et al. assessed the influence of graded facetectomy and laminectomy on the biomechanics and stability of the lumbar spine. These treatments are used for decompression of lumbosacral spinal stenosis. The results for the muscular and ligamentous lumbar motion segment, illustrated in Figure 1-8, showed that the stability in axial rotation decreases with the extent of facetectomy. It was observed that further laminectomy has no significant additional effect. Laminectomy decreases stability in flexion and in results in increased muscle forces. With regard to load sharing, removal of bony and ligamentous posterior elements has a stronger influence on the magnitude than on the distribution of stresses and deformations in the disc. No major alterations were observed in the biomechanics of the adjacent levels [78].

In 1999, Calisse et al. estimated the spinal muscle forces in standing and flexion, both with and without an internal intervertebral fixation device. The muscle forces were varied in discrete steps for the models with and without device, until the mobility measured in an instrumented patient and a physiological mobility were reached, respectively. The results showed very little difference in the muscle forces while only a slight increase of the global dorsal muscle force in a standing position for the model with an implanted fixation device [13].

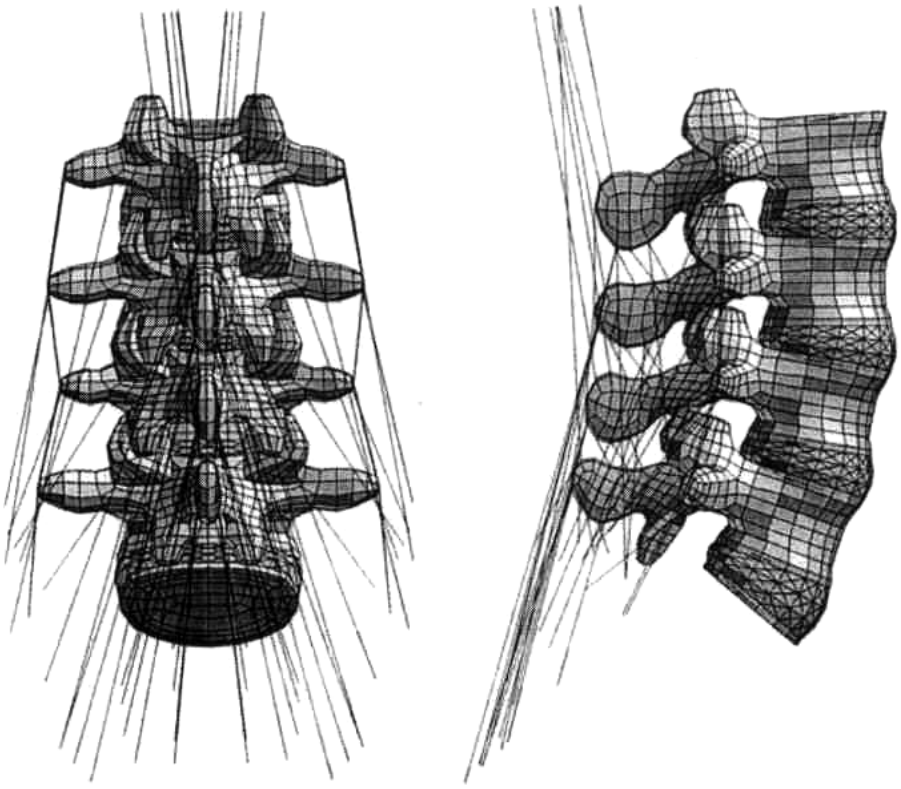

Figure 1-8: FE mesh of a ligamentous L2-S1 lumbar segment including dorsal muscle fibers, developed by Zander et al. [78]

In 2003, Polikeit et al. have studied the influence of the implantation of an intervertebral cage, or arthrodesis, in a single FSU lumbar segment. Figure 1-9 illustrates the FE model considered in their study. The results demonstrated that this type of treatment alters the load transfer which may induce bone remodeling and explain damages on the adjacent vertebral bodies. It was also demonstrated that the biomechanics of the segment and consequently the potential success of the treatment is more dependent on the density of the adjacent cancellous bone than on the material properties of the cage or the applied loads [57]. A complementary study from the same authors and using the same model has investigated the effect of the endplates properties on the stress distribution in the FSU. It was shown that harder vertebral endplates induce unusually

high peak stresses within the cancellous bone which may cause the subsidence of the prosthesis into the adjacent vertebral bodies. After inspecting different methods with and without partial removal of the endplates, it was concluded that an intervertebral cage should be designed to transfer the loads to the peripheral part of the endplates and offer more space for the bone graft [58].

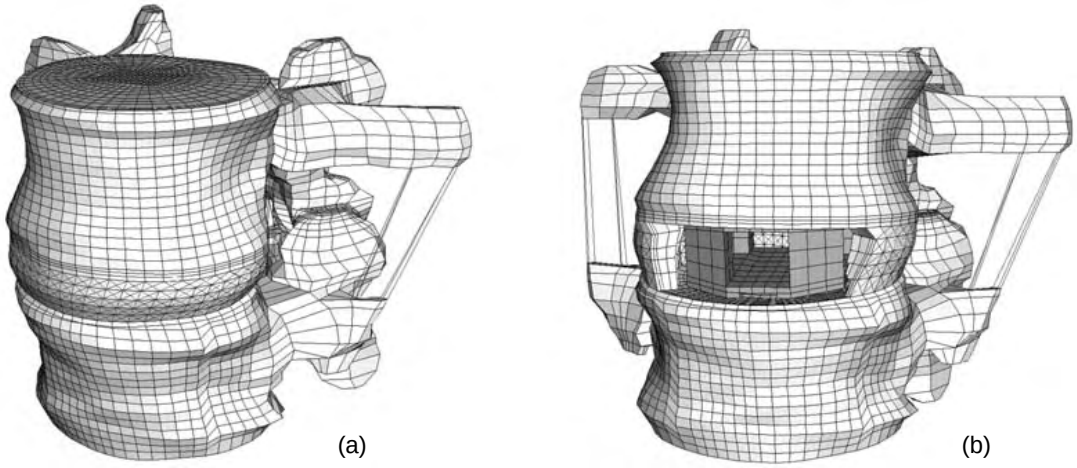

Figure 1-9: (a) FE mesh of a healthy ligamentous L2-L3 lumbar FSU, (b) FE mesh of the segment implanted with an intervertebral cage, model developed by Polikeit et al. [57]

In 2001, Dooris et al. investigated the load sharing in a lumbar FSU implanted with an artificial disc. Illustrations of the model are given in Figure 1-10. The amount of annulus removed for the anterior approach implantation and the antero-posterior position of the device were examined in axial compression, flexion and extension loading cases. It was shown that the facet loads were more sensitive to the postero-anterior position of the device than to the amount of annulus removed. The study provided as a conclusion that even if the artificial device has no rotational stiffness, the stiffness in flexion-extension

and the posterior load sharing can be modulated by the surgeon through the antero-posterior position of the artificial disc [14].

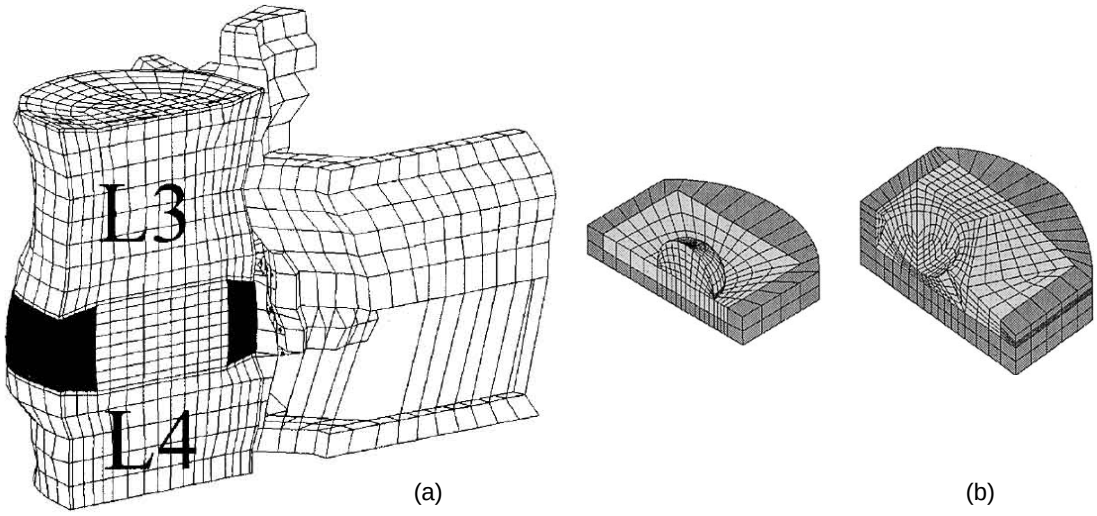

Figure 1-10: (a) FE mesh of a healthy ligamentous L3-L4 lumbar FSU, (b) FE mesh of the implanted artificial intervertebral disc, model developed by Dooris et al. [14]

CHAPTER 2

CONSTRUCTION OF THE MODEL

2.1 Component Geometries

2.1.1 Vertebra

The vertebra is the bony constitutive element of the spine. The role of a vertebra is to protect the spinal cord, to transfer loads from its upper part to its lower part while allowing a limited mobility to the spine, and to provide an anchor to the spinal muscles.

Figure 2-1 shows the main geometrical attributes of a lumbar vertebra. The vertebral body mainly conveys the axial load, whereas the articular facets limit the mobility by resisting excessive transverse and postero-anterior loads. The spinous and lateral processes interact from one level to another via sets of ligaments and muscles that operate as joint stabilizers.

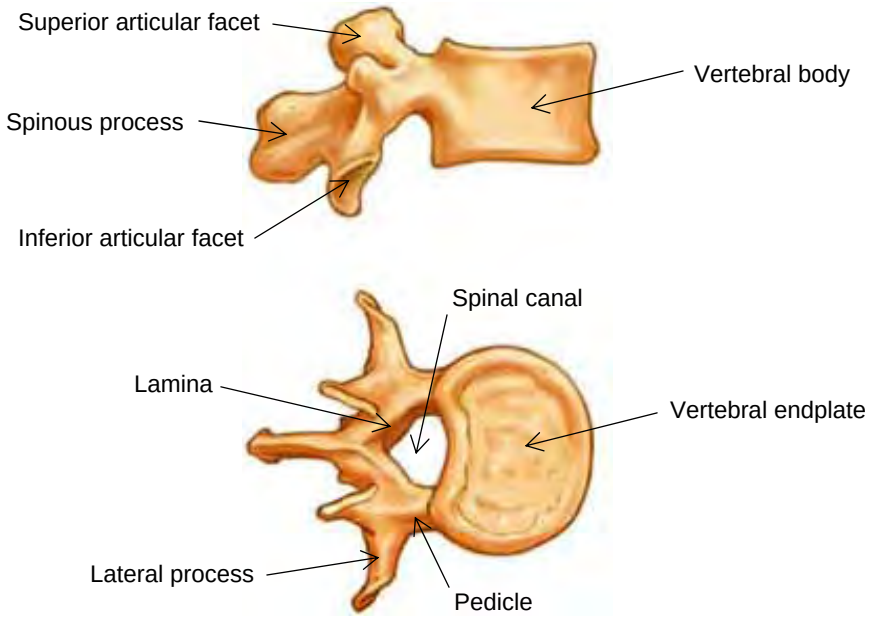

Figure 2-1: Geometry of a lumbar vertebra, (a) lateral view, (b) axial view

The following paragraphs state the features and characteristics selected through a review of the literature to model the lumbar vertebra. The chosen data generally apply to a L3 or a L4 lumbar vertebra.

The overall dimensions of the vertebral body, available in Figure 2-7, have been selected from several clinical studies as well as existing numerical models [76], [66]. For more accuracy of the stress distribution on the intervertebral disc, the model takes into account the kidney shape as well as the lateral curvature of the vertebral body. The literature is weak concerning the description of those shapes; therefore they have been extrapolated by spline curves from the available data [38]. Figure 2-2 describes the kidney shape that is typical for the vertebral body.

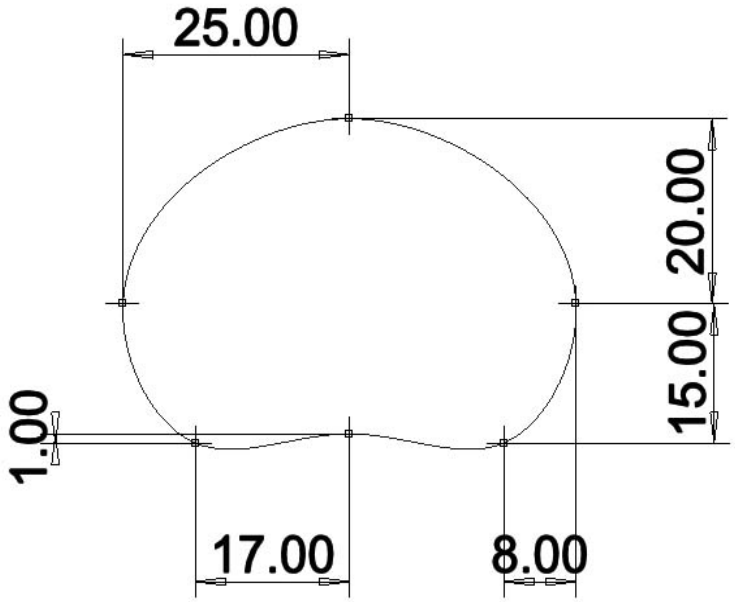

Figure 2-2: Sketch of the vertebral body kidney shape used in the model, distance in *mm*

The significance of the posterior vertebra and specifically the articular facets in the spinal biomechanics and stability has been demonstrated in several studies [78], [62], [2]. The role of the articular facets becomes even more important in the load sharing between

anterior and posterior elements of a FSU after implantation of an artificial disc [14]. As a consequence, the current study could not ignore the articular facets. The behavior of such interfaces is very complex and their accurate modeling requires special attention to the geometry, the material properties, and the contact properties [63], [64], [61]. Additionally, as the study focuses more on the relative behavior of the lumbar segment in different configurations, the articular facets will be approximated by simple planes.

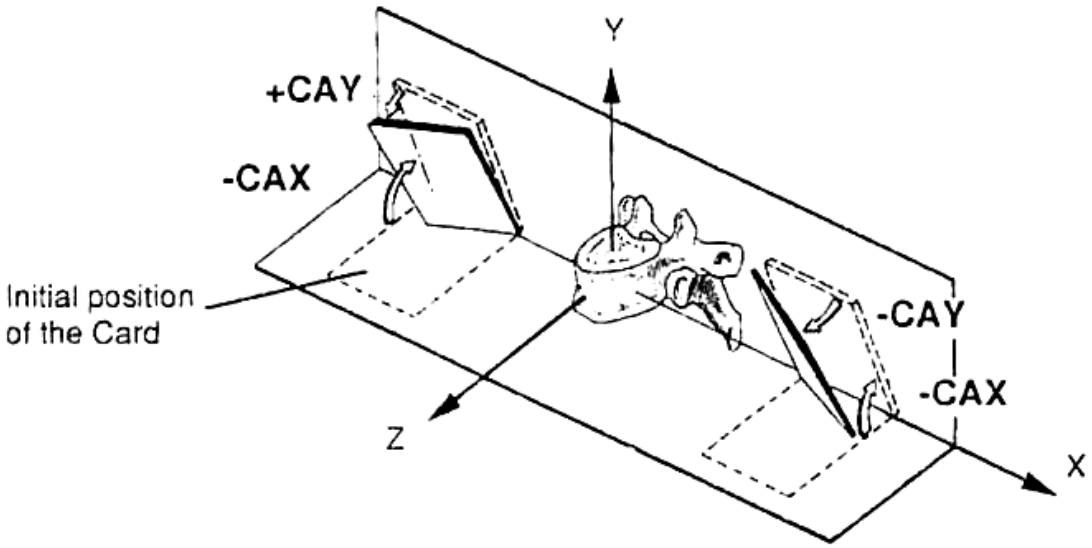

Figure 2-3: Definition of the orientation of the facet plane, initially in the transverse plane (XZ) it follows two rotations respectively around the X axis (by angle CAX°) and around the Y axis (by angle CAY°) [52]

It is also difficult to find good sets of data related to the dimensions of the posterior vertebra. The critical issues in this case are the location and the orientation of the facets as well as the length of the processes on which are attached the ligaments. The orientation and the relative positions of the facets are well described by Panjabi [52]. According to the orientation definition described in Figure 2-3, the model utilizes the following figures, relevant of a L3 lumbar vertebra: CAX=80° and CAY=±40°. The absolute position of the facets, in addition to the dimensions of the facets, the processes, the laminas and the

pedicles have been inferred from the available clinical data and some existing numerical models [76], [52], [63], [70], [23], [38]. Figure 2-4 shows the main geometrical dimensions of the posterior vertebra.

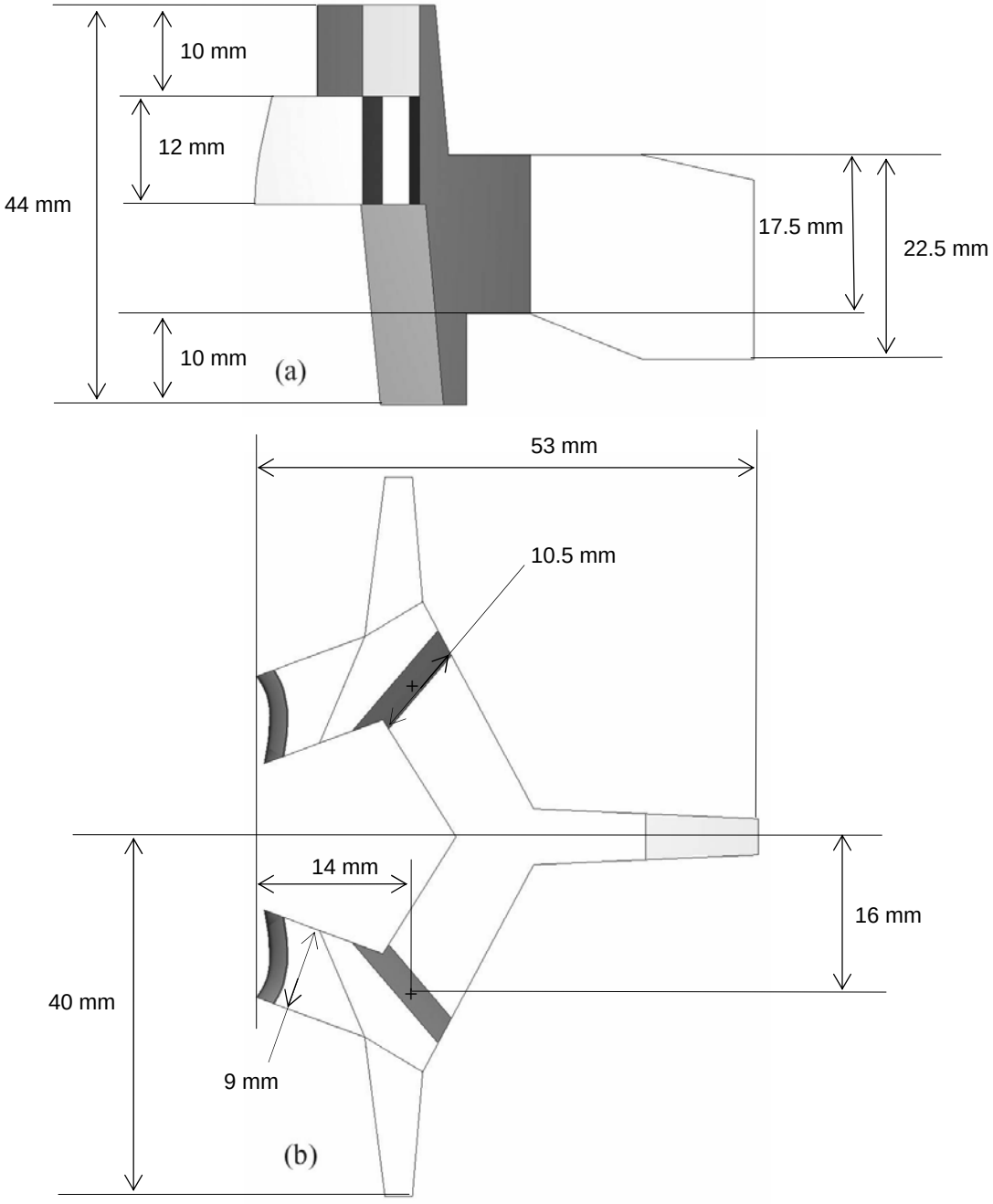

Figure 2-4: Dimensions of the modeled anterior vertebra, (a) lateral view, (b) axial view

The compressive load is the principal load transmitted through a FSU. In order to increase the accuracy of the load distribution onto the disc, the vertebral body has been modeled as two distinct parts: the cortical bone and the cancellous bone. The posterior vertebra yet remains as one homogeneous part. The cortical bone is a very dense thin layer with strong mechanical properties that surround the cancellous bone, much softer and less dense. Figure 2-5 illustrates the actual small thickness of the shell and the porous appearance of the cancellous bone. The combination of the two types of bone gives the vertebral body a very high compressive strength, yet a relative flexibility.

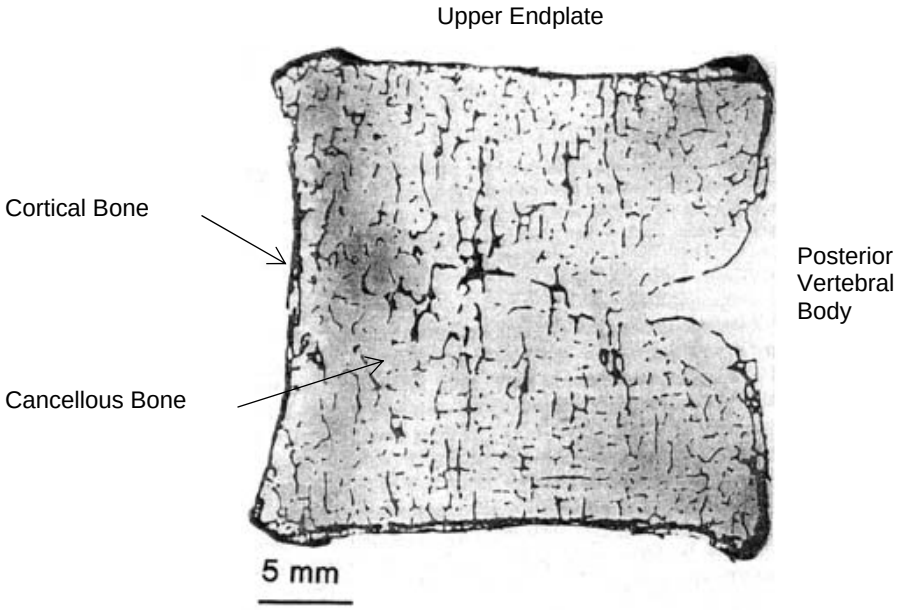

Figure 2-5: Photograph of a representative embedded section in the sagittal plane of a vertebral body, 47 year old female [68]

However, it is noted that no consensus exists concerning the load sharing between the shell and the core of the vertebral body. According to the experimental study of Rockoff et al. reported by White and Panjabi, the cortical shell contributes to 65% of the body's strength [76]. Conversely, Silva et al. support, by mean of a finite element analysis, that the share of the cortical bone is only 10% [67].

Silva et al. led another study related to thickness of the cortical shell and concluded that it has an average thickness of approximately 0.35 mm [68]. The model took into consideration this value of 0.35 mm for the thickness of the vertebral body's lateral wall.

The thickness of the vertebral endplates has been chosen as 0.5 mm. That includes the cartilage endplate which is the interface between the vertebral body and the disc. It is said to naturally calcify with age and therefore can be included with the bone [76].

Investigating the vertebral endplates, Grant et al. have shown that their mechanical properties were not homogeneous within the surface [24]. As reported in Figure 2-6, the shell is weaker above the cancellous bone, and the weakest area is located slightly on the anterior part.

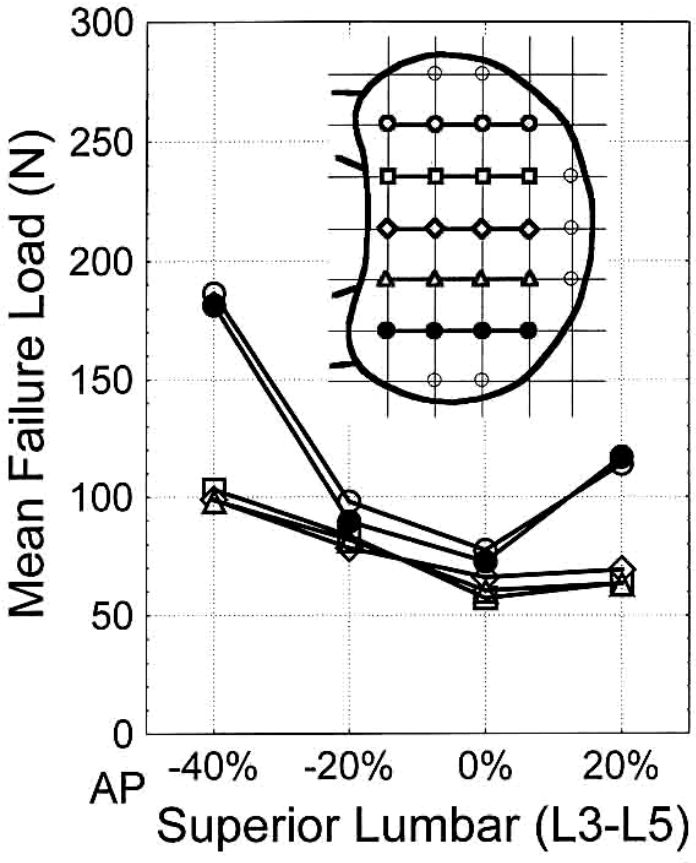

Figure 2-6: Failure loads map in the upper lumbar endplates, the lower axis shows the antero-posterior test site coordinates [24]

Nevertheless, there is no information on how the Young's modulus varies within the vertebral endplates. Studying the importance of the endplates for the implantation of intervertebral cages, Polikeit et al. propose a rough geometric distribution of the endplates' properties along with different sets of elastic modulus [58].

In the model, the endplates properties have been distributed on three discrete areas. The geometry and the Young's modulus of each area have been adapted from the results of the two previous studies. Figure 2-7 illustrates the cortical shell of the modeled vertebra.

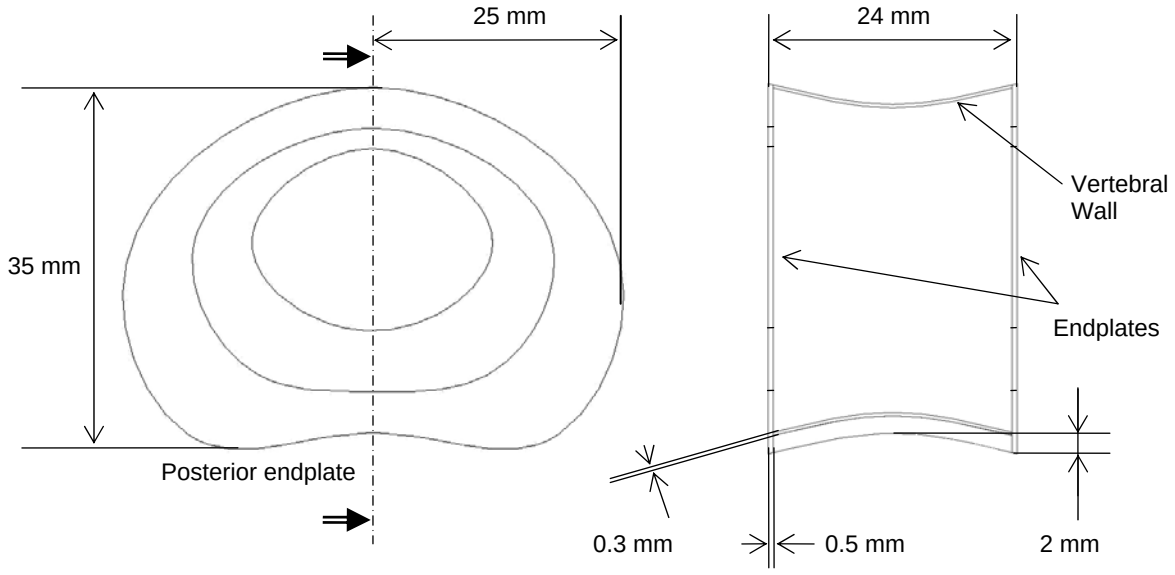

Figure 2-7: Sketch of the cortical wall and endplates of the vertebral body

It is important to note that the current model is build with a unique vertebra repeated three times on the two level lumbar motion segments. It was assumed that disregarding the slight dimension and orientation dispersions on a two level motion will not significantly affect the accuracy of the model.

Figure 2-8 shows a 3D view of the final vertebra.

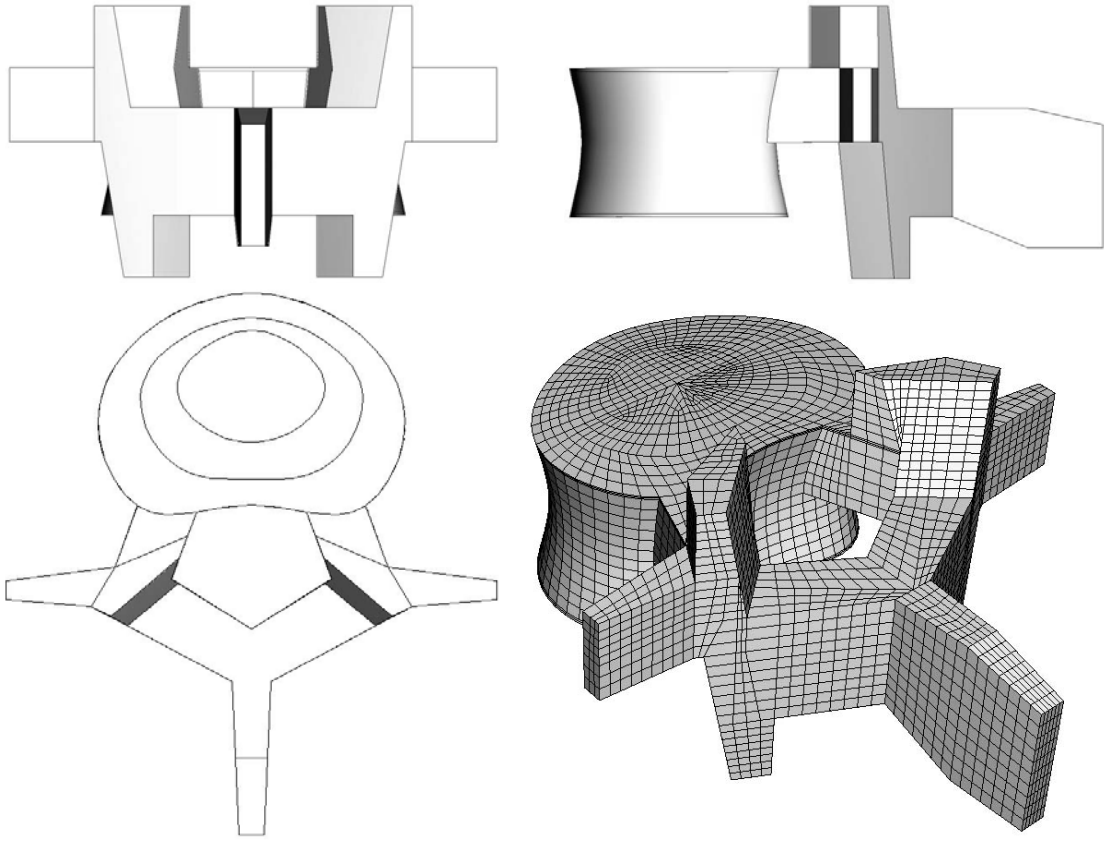

Figure 2-8: View of the modeled vertebra

2.1.2 Intervertebral Disc

The IVD is the main interface between two vertebrae. It allows a limited motion while transmitting loads from one vertebra to another. Moreover, the viscoelastic characteristics of the constitutive materials provide an IVD with shocks absorbing properties [1].

As shown on Figure 2-9, two different parts in an IVD can be distinguished: the nucleus pulposus and the annulus fibrosus.

The nucleus is originally constituted of 80% water, decreasing with age, 15% of proteoglycans, a hydrophilic and negatively charged protein, and 5% of collagen, mostly type II [30]. In the lumbar spine, the nucleus is located between the middle and the posterior third of the sagittal diameter and its volume is 30 to 50% of the total disc volume [76]. In some finite element analysis of the lumbar spine, the nucleus was chosen as 43% of the total disc volume [70], [8]; which was the value used in the current model.

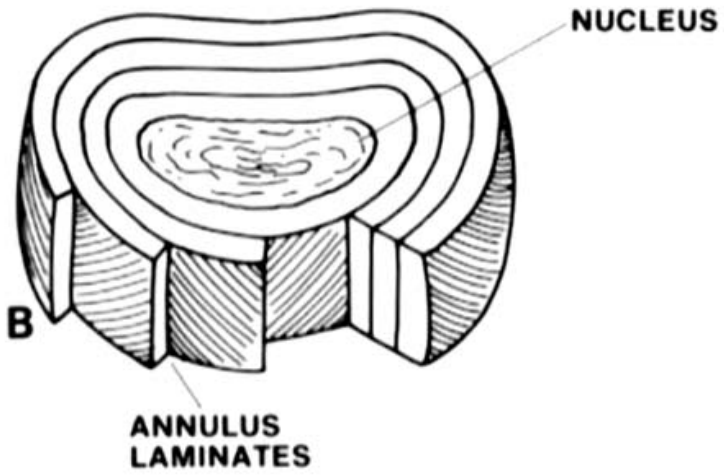

Figure 2-9: Constitution of an intervertebral disc [76]

The nucleus conforms to the kidney shape of the disc; which is assumed to be the same than the kidney shape of the vertebral body. Figure 2-10 illustrates the shape and the position of the nucleus within the disc.

The annulus is constituted of concentric layers of fibrous tissue which have an approximate thickness of 1 mm. The fibers are an aggregate of collagen fibrils type I and are alternatively oriented in regard with the transverse plane with an angle approximately equals to ±30°. The fibers are surrounded by a hydrated proteoglycan gel, or annulus ground substance [30].

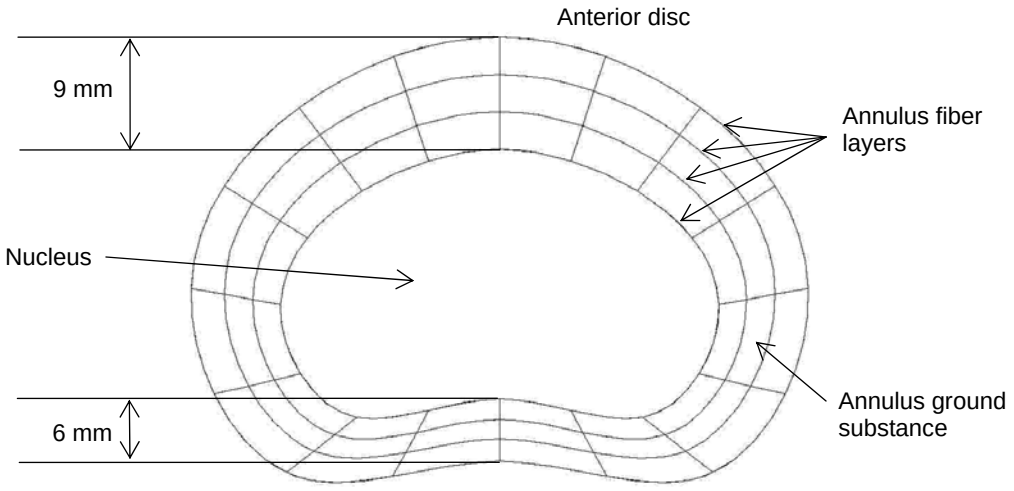

Figure 2-10: Shape and position of the nucleus within the disc, discretization of the annulus ground and fiber layers

The current model includes eight layers of fibers, represented by truss elements, with a diameter of 0.8 mm and embedded in the annulus ground substance. The fibers have a minimal inclination in regard with the transverse plane of ±15° on the two outermost layers and a maximal inclination of ±30° in the two innermost layers. The annulus fiber content can be computed and is approximately equal to 19%. This result is consistent with the value chosen by Shirazi-Adl et al. and Sharma et al. in their numerical models, which correspond to the collagen content of the annulus [62], [66]. Figure 2-11 shows a 3D view of the modeled disc.

The natural lordosis of the lumbar spine has not been considered in the model. Accordingly, the unloaded disc has a constant height that was chosen as the characteristic value of 10 mm [17], [20].

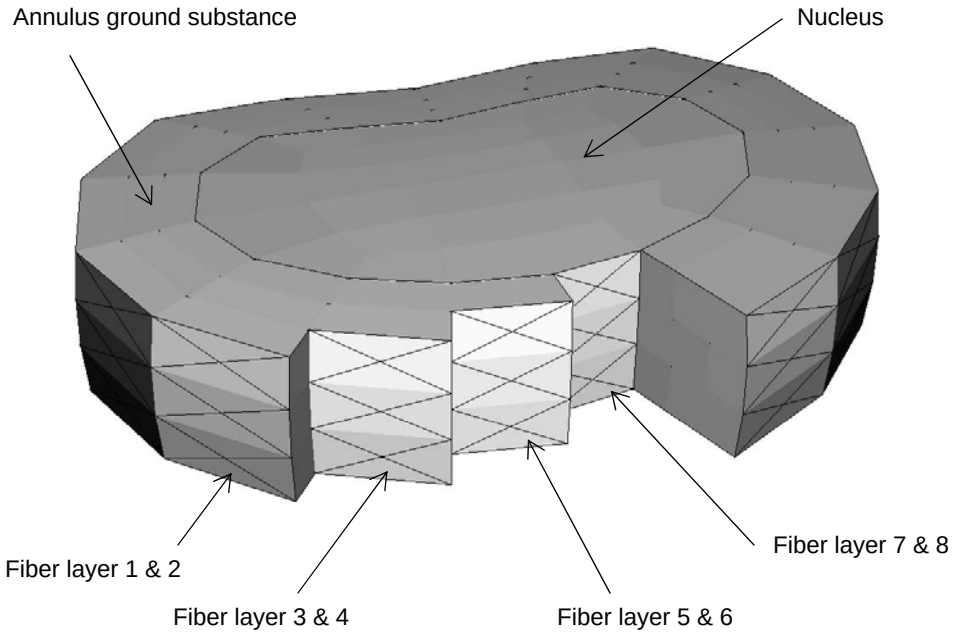

Figure 2-11: 3D view of the modeled healthy disc

2.1.3 Intervertebral Cage

As seen in Section 1.2.1, an intervertebral cage is used for the surgical treatment of arthrodesis, leading to the immobilization of a FSU. The insertion of an intervertebral cage alters the stress distribution on the adjacent vertebrae, which may lead to their remodeling and deterioration [57]. However, the current study will not take into consideration a model of an intervertebral cage that will be able to highlight these issues. The main concern, in the arthrodesis case, is the behavior of the different elements on the adjacent level and not the behavior of the structures directly in contact with the device. Therefore, only the successful ultimate condition of the treatment will be considered, i.e. where the FSU is completely immobilized. This situation is simulated by replacing the healthy disc with a homogeneous solid part that has the same dimensions than the disc along with the same mechanical properties as bone.

It has been shown that arthrodesis indeed brings slight increase of mobility on adjacent levels [9]. The current model will be able to compare this behavior with a segment treated by arthroplasty.

2.1.4 Artificial Intervertebral Disc

An artificial intervertebral disc is used for the surgical treatment of arthroplasty which aims to restore the functionality of a FSU. Among the requirements of such a device, mobility is one of the most important [17]. It is known that the translational and rotational degrees of freedom of a FSU are strongly interdependent [40]. However, the segmental rotations are dominant and are the concern of most studies. As a consequence, the artificial intervertebral discs designed for total disc replacement are often constituted of ball-in-socket joints [71]. There are for example the following recent prostheses, illustrated in Figure 2-12: the SB Charité from Link Spine Group (Hamburg, Germany), the Prodisc from Spine Solutions (New York, NY), and the Maverick from Medtronic Sofamor Danek (Minneapolis, MN).

Figure 2-12: Artificial intervertebral discs using ball-in-socket joints, respectively the SB Charité, the Prodisc and the Maverick

For the motion segment with a restored level, the model will consider a movable artificial disc similar to the Prodisc and Maverick prostheses, introduced above. The modeled device, described in Figure 2-13, consists of two homogeneous solid parts that interact with perfectly congruent spherical surfaces. The disc is accordingly restored as a simple ball-in-socket joint.

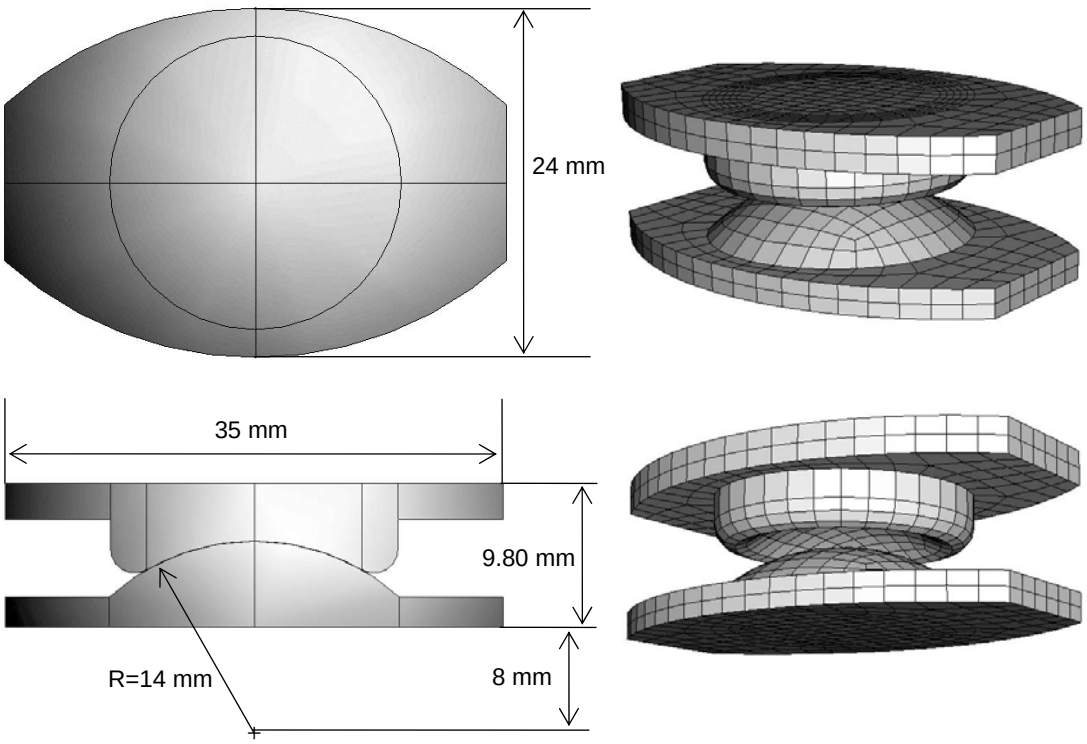

Figure 2-13: Views of the intervertebral artificial disc used in modeling

An extensive number of studies have focused on the positions of the instantaneous axis of rotations (IAR) for the different rotational motions of a FSU [76], [28]. The positions of the IARs are spread, yet, they seem to be located in the upper part of the underlying vertebra for the flexion, the extension and the lateral bending. The device utilized in the model is designed such that the center of rotation of the movable joint is

located approximately 8 mm below the upper endplate of the underlying vertebra. The radius of the spherical contact surfaces is accordingly selected equal to 14 mm. As the device aims to restore the functionality of the FSU, its thickness is chosen to be equal to the thickness of the healthy disc under compressive load in the neutral position, i.e. 9.80 mm. The maximal rotational mobility offered by the current artificial disc is ±12° with regard to the transverse plane and is not limited about the axial direction. This value of 12° corresponds approximately to the upper limit of all the rotational motions allowed by a healthy FSU [76]. The same range of rotational mobility is provided by the SB Charté, the Prodisc and the Maverick artificial prostheses. For reference, as stated in the instruction for use, the SB Charité allows a rotational motion, up to ±15.5°, with regard to the transverse plane.

2.2 Materials Properties

2.2.1 Discussion of the Material Properties of the Model Components

The material properties of each component described in Section 2.1 have been established through a review of the literature related to the numerical modeling of the lumbar spine. The most relevant data are summarized in Table 2-1.

- Cortical bone:

Most authors appear to agree on the Young's modulus of the cortical bone which is around 12,000 MPa [8], [57], [29], [56], [62], [23], [22], [38], [66].

- Cancellous bone:

Values concerning the Young's modulus of cancellous bone are slightly more variable. In the available numerical models of the lumbar spine, they range from 25 MPa [56] to 100 MPA [14], [62], [22], [38], [66], with a variety of intermediate values [8],

[32], [33]. A review of experimental studies on the compressive stiffness of vertebral cancellous bone gives results ranging from 10 to 535 MPa, with averages around 100 MPa [41]. The commonly used value of 100 MPa was used herein.

- Vertebral endplates:

Certain models regard the vertebral endplates as cortical bone, with high Young's modulus [8], [56]. Others consider homogeneous materials with reduced mechanical properties such as 500 MPa [38] or 1,000 MPa [57]. A very few models propose a distribution of the vertebral endplates' properties [58] to characterize their non-homogeneity [24]. The current model takes into account a simple geometric distribution of the vertebral endplates as shown in Figure 2-7. From the outer layer to the inner layer, the mechanical properties are respectively chosen as 12,000 MPa, 6,000 MPa and 2,000 MPa.

- Posterior bone:

Less critical than the vertebral body, which conveys most of the loads in a FSU, the posterior vertebra is modeled as a homogeneous material. As in most of the numerical models, no distinction is made between the cortical and the cancellous bone. Previous work shows a general consensus on the Young's modulus of the posterior vertebra. The values range from 1,000 MPa [38] to 3,500 MPa [8], [57], [14], [56], [62], [23], [22]. The model here considers the value of 3,000 MPa which corresponds to the stiffness of the vertebral bone seen as one homogeneous material [70].

- Annulus ground:

The literature provides a Young's modulus for the hydrated proteoglycan gel that surrounds the annulus fibers, or annulus ground, ranging from 2 MPa [38] to 8 MPa [8].

However the most commonly used value is 4.2 MPa, which has been selected for the current model [56], [70], [62], [23], [22], [66]. The Poisson ratio has the same with a value of 0.45, which suggests an almost incompressible material.

- Annulus fibers:

The annulus fibers are constituted of an aggregate of collagen fibrils. They have a non linear behavior as well as a non linear geometrical distribution within the annulus. The outer layer is subject to greater stresses and possesses accordingly a denser fibrous structure.

Some studies have chosen linear properties of the fibers, which provide an average Young's modulus of approximately 450 MPa [56], [23], [38]. Conversely, other studies have considered both non-linear characteristics. They include a continuous non-linear model specific to each fiber layer, based on the behavior of collagen fibrils. The radial non linear distribution is taken into account through different cross-sectional areas of the fibers for each layer [62], [66]. Other options have been considered, such as a bilinear model of the fibers [22]. Finally, an additional alternative takes into consideration the nonlinearities using a different linear model for each one of the fiber layers [8], [56], [70]. The current study will incorporate this last model that is simple with respect to a non-linear model, and fairly accurate with respect to a fully linear model. The mechanical properties corresponding to each fiber layer are shown in Table 2-1.

- Nucleus:

All studies agree that the nucleus is an incompressible material. However, it has been considered as a non-linear incompressible solid [8] as well as an incompressible fluid [66]. The nucleus has been modeled as a linear incompressible solid with a Young's

modulus ranging from 1 Pa [14] to 4 MPa [38] and a Poisson ratio approximately equals to 0.5. Most of the other values are in-between 0.1 MPa and 1 MPa [56], [70], [62], [23], [22]. In the current study the nucleus is modeled as an incompressible solid with a Young's modulus of 0.1 MPa.

- Intervertebral cage:

Section 2.1.3 explains how the study aims to model the ultimate condition of the fused FSU. The intervertebral space is filled with a solid prosthesis that has the same dimension as the original unloaded healthy disc. Fusion is intended to result in the bony union of the two adjacent vertebral bodies; as a consequence, the material properties of the prosthesis filling the intervertebral space are chosen to be the same as the posterior vertebra.

- Artificial disc:

The aim of this study is not to focus on the stresses within the artificial disc itself but on the adjacent elements experiencing the motion offered by the disc. Therefore the material properties of the device do not need special attention providing they are stronger than bone. The metallic parts of solid movable artificial discs usually consist of an alloy of titanium or chrome cobalt and molybdenum (CoCrMo). Those two types of material have Young's moduli approximately equal to 100 GPa and 200 GPa respectively [42]. This model will consider an artificial disc constituted of a material characterized by a 200 GPa Young's modulus.

2.2.2 Summary of the Material Properties

Table 2-1 contains the summary of the material properties for all the constitutive parts described in the Section 2.1.

Table 2-1: Material properties of the constitutive parts of the lumbar motion segment

Materials	**Young's modulus E(MPa)**	**Poisson ratio, v**	**References**
Vertebral body cortical wall	12,000	0.3	[8], [29], [56], [23], [66]
Cancellous bone	100	0.2	[14], [62], [41], [22], [38], [66]
Endplate outer layer	12,000	0.3	[58], [24]
Endplate intermediate layer	6,000	0.3	
Endplate center	2,000	0.3	
Posterior bone	3,000	0.3	[70]
Annulus ground substance	4.2	0.45	[8]
Annulus fiber layers 1&2 (outermost)	550	0.3	[8], [56], [70]
Annulus fiber layers 3&4	485	0.3	
Annulus fiber layers 5&6	420	0.3	
Annulus fiber layers 7&8 (innermost)	360	0.3	
Nucleus	0.1	0.499	[56], [70], [62], [23], [22]
Intervertebral cage	3,000	0.3	-
Artificial disc	200,000	0.3	[42]

2.3 Assembly and Interactions Properties

2.3.1 Cortical and Cancellous Bone

The complex geometry of the cancellous bone leads to difficulties in using the same type of element for the cortical and the cancellous bone when meshing the vertebra. Table 2-3 summarizes the different elements utilized. As a consequence, not all nodes at the interface of the two parts correspond, and a tie constraint has been assigned to each pair of elements within this interface. In other words, the cortical and the cancellous bone are tied together.

2.3.2 Disc Interfaces

The disc is modeled in two distinct parts. In order to bring together the nucleus and the annulus, a tie constraint is applied between the interacting surfaces.

The same tie constraint is used to connect the disc to both adjacent vertebral endplates. In physiological conditions, the interface between a disc and a vertebra is made through a cartilage endplate. This hyaline cartilage is attached to the disc by its collagen fibrils but is not connected to the bone. The disc is fixed to the vertebral body only by the outer layers of annulus fibers that are anchored into the vertebral endplate [30]. As a consequence, the tie constraint chosen to connect the disc and the vertebra indicates the ability to withstand greater shear loads than are expected in vivo. This characteristic should not induce errors in the results provided that the analyses are run with physiological loading conditions.

2.3.3 Facet Joints

The literature provides several examples of complex models dedicated to the biomechanical analysis of the articular facets in the lumbar spine. The interface is usually treated as a frictionless non-linear contact problem and modeled by gap elements [61], [64], [63]. The nonlinearities are relevant of the geometry (large displacements and non linear contact) and the materials (articular cartilage).

The current study is not focused on the mechanics of the articular facets. As explained in Section 2.1.1, their geometry is approximated by simple planes. Therefore, including contact and material properties relevant to the articular cartilage would not increase the accuracy of the model.

To save time in the computing process, a frictionless softened interface has been considered for the articular facets. This soft contact follows the exponential pressure-overclosure relationship given in the following equation and where c=0.1 mm and p_0=0.3 MPa.

$$\begin{aligned} p &= 0 && h \prec -c \\ p &= \frac{p_0}{e-1}\left[\frac{1}{c}\left(\frac{h}{c}+2\right)\exp\left(\frac{h}{c}+1\right)-\frac{1}{c}\right] && h \succ -c \end{aligned} \tag{1}$$

p, pressure
h, overclosure
c, overclosure when p=0
p_0, pressure when h=0

2.3.4 Intervertebral Cage and Artificial Disc

As with a healthy disc, the intervertebral cage and the plates of the artificial disc are tied with the vertebral bodies. If the position of the intervertebral cage is unique, the disc can be relocated as desired on the vertebral endplates.

Due to the potential for large displacements, the model chosen for the interaction between the plates of the artificial disc is similar to the model chosen for the articular facets. The contact has a friction coefficient of 0.01 and follows the exponential pressure-overclosure relationship described in Equation (1), where c=0.1 mm and p_0=0.5 MPa.

2.3.5 Intervertebral Ligaments

Ligaments exhibit a non-linear behavior which is well-known and shown in Figure 2-14.

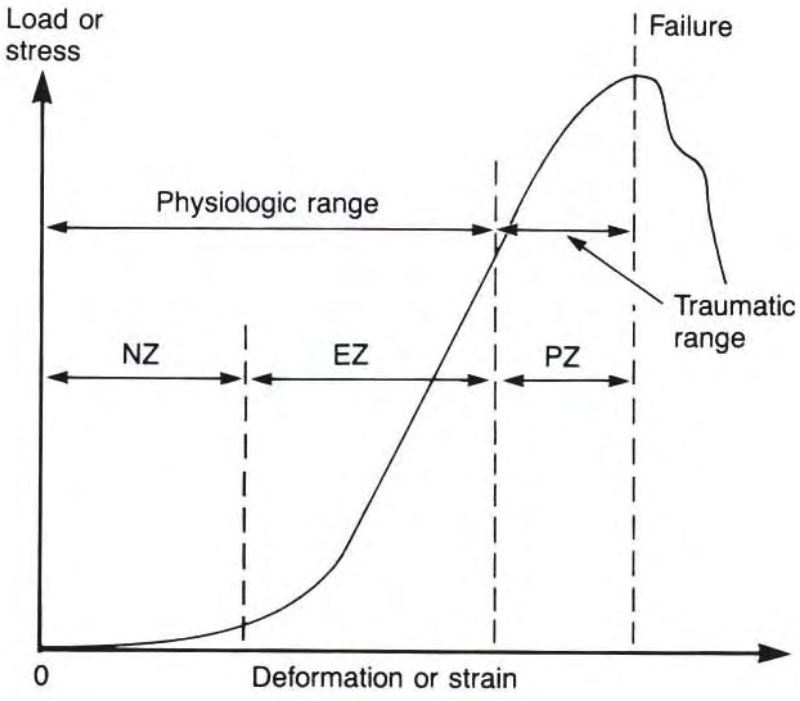

Figure 2-14: Non-linear behavior of ligaments, the curve may be divided into three main parts: the neutral zone (NZ) and the elastic zone (EZ) for the physiologic range, and the plastic zone (PZ) for the traumatic range [76]

Assuming limited physiologic range of motions, several models have considered linearly behaved ligaments [57], [38]. This approximation can however induce significant errors in the results as the radius of curvature of the stress-strain curve is the most

important within the physiologic range. As a consequence, most studies have adopted a bilinear load-deformation behavior model, each linear segment corresponding to the neutral zone (NZ) and the elastic zone (EZ) [56], [14], [70], [23], [22]. The data provided by the different experimental analyses of the spinal ligaments show significant variability resulting from the difficult experimental conditions and the diversity of the techniques [76].

Table 2-2: Summary of the ligaments' properties

Ligament		ALL	PLL	LF	TL	CL	ISL	SSL
Small strain Young's modulus (MPa)	[56] [23] [22]	7.8	10	15	10	7.5	10	8
Transition strain (%)		12	11	6.2	18	25	14	20
Large strain Young's modulus (MPa)		20	50*	19	59	33	12	15
Cross sectional area (mm^2)		63.7	20	40	1.8	30	40	30
Max. failure load (N)	[76]	510	384	340	-	284	130	200
Length (mm)		13	11	19	-	-	-	11
Length (mm)	Current study	10	10	16.5	22	4.8	13	14.25

* modified data adapted from Smit et al. [70]

The current study adopted a bilinear model based on information provided by Pitzen et al. [56] and Goel et al. [23], [22]. The spinal ligaments are not taken to be actual finite elements but have been modeled as two-node axial connectors. The data used to build the model of these connectors are summarized in Table 2-2. The large strain Young's modulus of the posterior longitudinal ligaments (PLL) has been modified from 20 MPa to

50 MPa in order to have consistent behavior relative to the behavior of the ligamentum flavum (LF) and the supra-spinous ligament [70]. The corresponding force-displacement relationship for each of the ligaments, limited by the maximal failure loads proposed by White and Panjabi [76], have been calculated from the data in Table 2-2 and the results are illustrated in Figure 2-15.

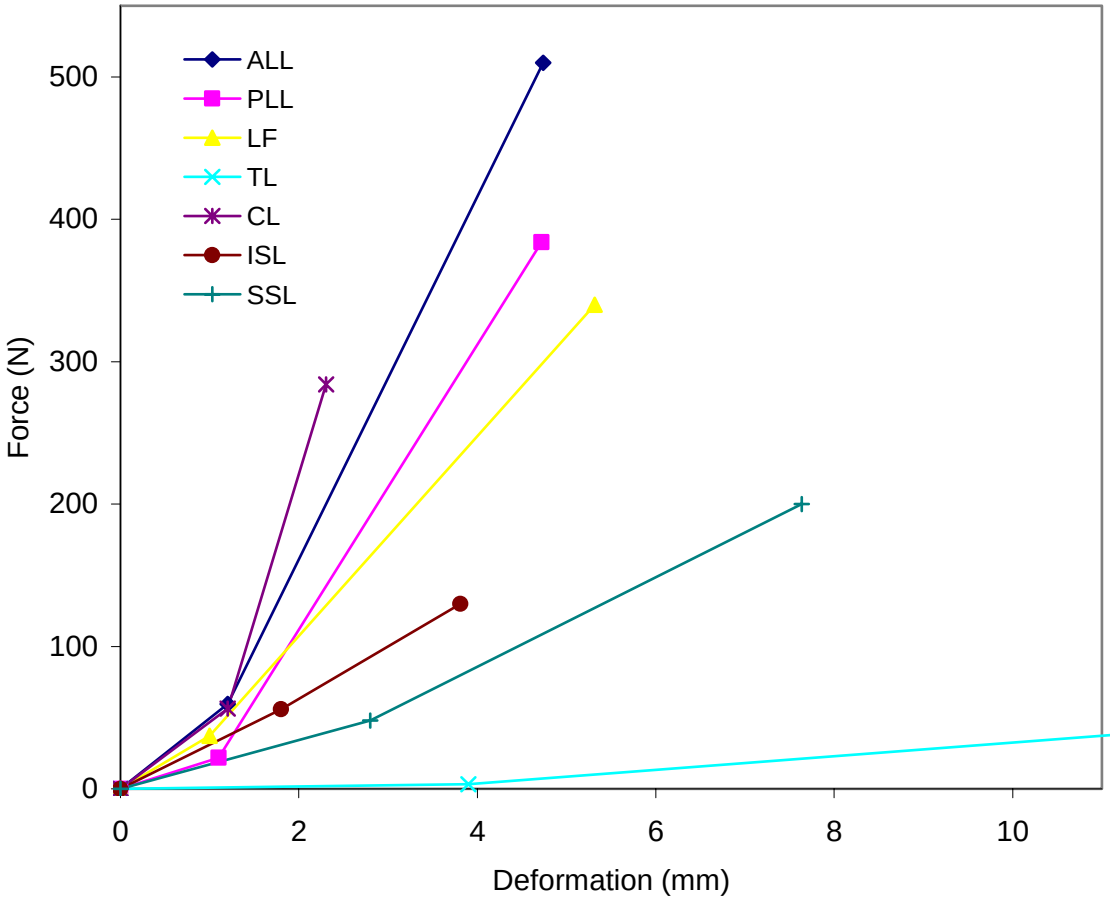

Figure 2-15: Comparison of the behavior of the spinal ligaments

It is interesting to note in Figure 2-15 that the transverse ligaments (TL) have no mechanical significance on the lumbar spine. This is due to their negligible cross-sectional area [76]. As a consequence, the literature provides very little information on the mechanical properties of this ligament and its failure load remains unknown.

Some ligaments have been divided into several individual connectors in order to model their natural distribution. The mechanical properties of the sub-elements of each ligament have been estimated and assigned accordingly. The location of the connectors is illustrated in Figure 2-16 and the number of connectors corresponding to each ligament is given in Table 2-3.

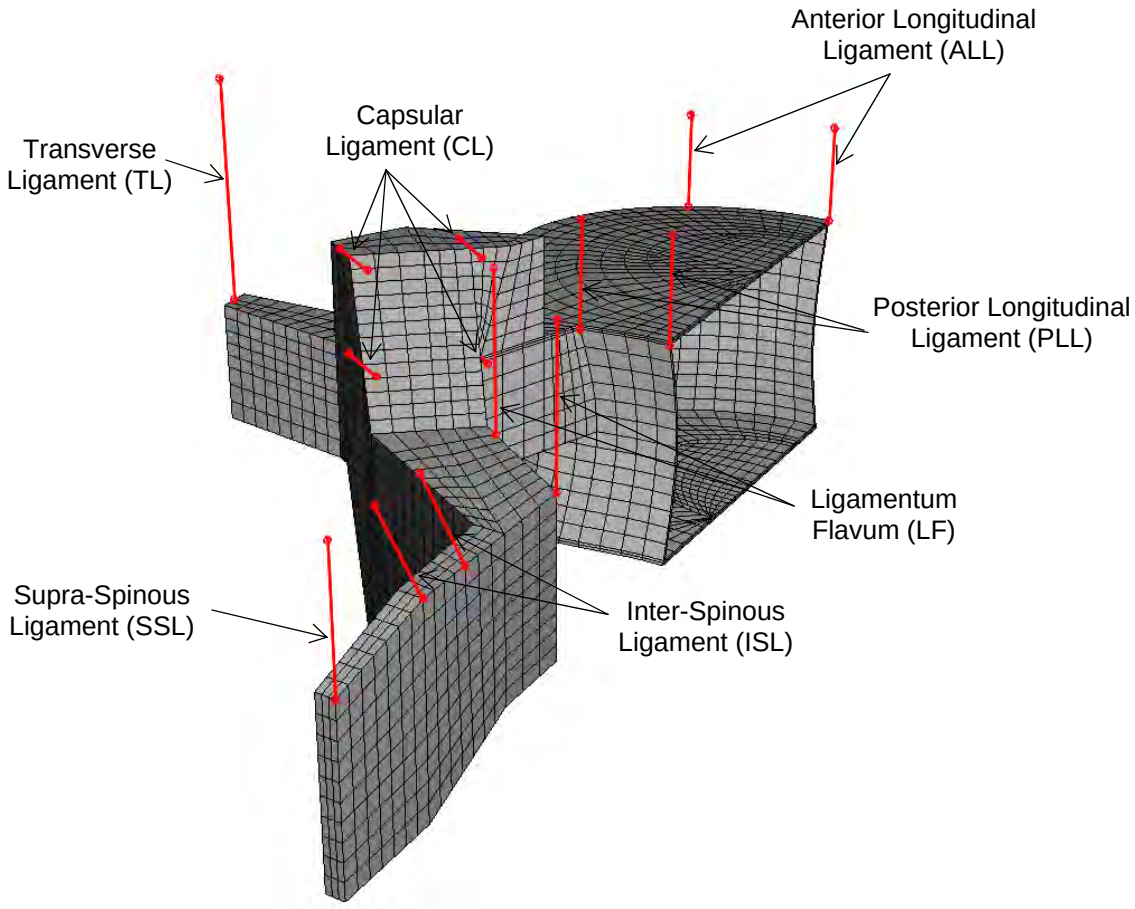

Figure 2-16: Distribution of the modeled intervertebral ligaments

2.4 Component Summary

Table 2-3 provides the characteristics and relevant information on the constitutive elements of each FSU component taken into consideration in the model.

Table 2-3: Summary of the finite element models

Parts	Element type	Number of elements	Number of nodes
Vertebra	-	28,498	15,698
Cancellous bone	C3D4, tetrahedral	20,544	-
Cortical and posterior bone	C3D8R, hexahedral	7,954	-
Annulus ground	C3D8R, hexahedral	144	256
Annulus fibers	T3D2, truss	384	256
Nucleus	C3D8R, hexahedral	96	164
Intervertebral cage	C3D8R, hexahedral	220	381
Artificial disc, upper plate	C3D8R, hexahedral	1,160	1,581
Artificial disc, lower plate	C3D8R, hexahedral	440	735
Healthy segment	-	86,669	47,923
Segment with a fused FSU	-	86,265	47,884
Segment with a movable FSU	-	87,625	49,819
ALL	Axial connector	3 / ligament	-
PLL	Axial connector	3 / ligament	-
LF	Axial connector	3 / ligament	-
TL	Axial connector	1 / ligament	-
CL	Axial connector	4 / ligament	-
ISL	Axial connector	2 / ligament	-
SSL	Axial connector	1 / ligament	-

2.5 Illustration of the Final Models

2.5.1 Healthy Lumbar Ligamentous Segment

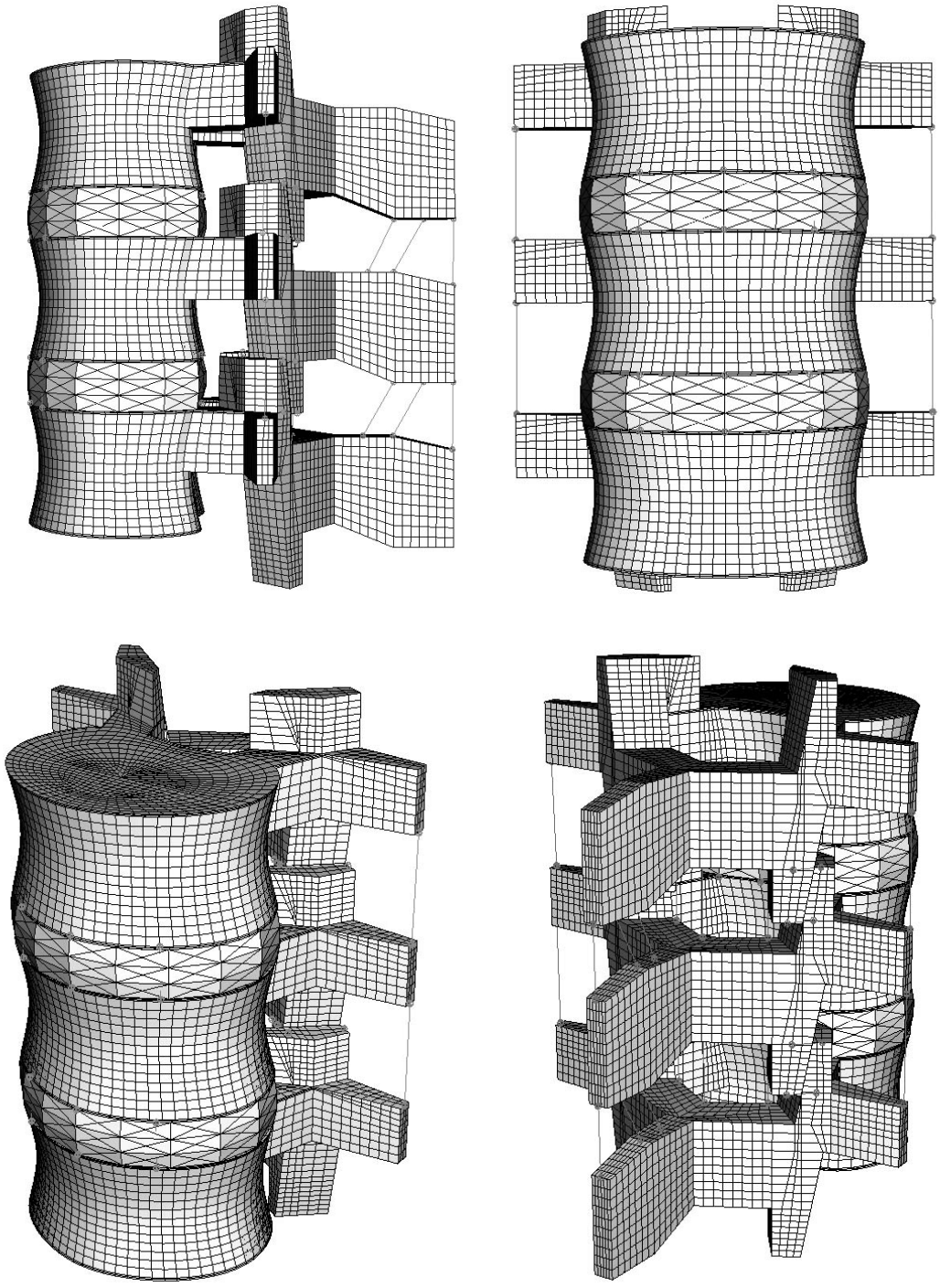

Figure 2-17: 3D views of the modeled healthy segment

2.5.2 Lumbar Ligamentous Segment with a Fused Level

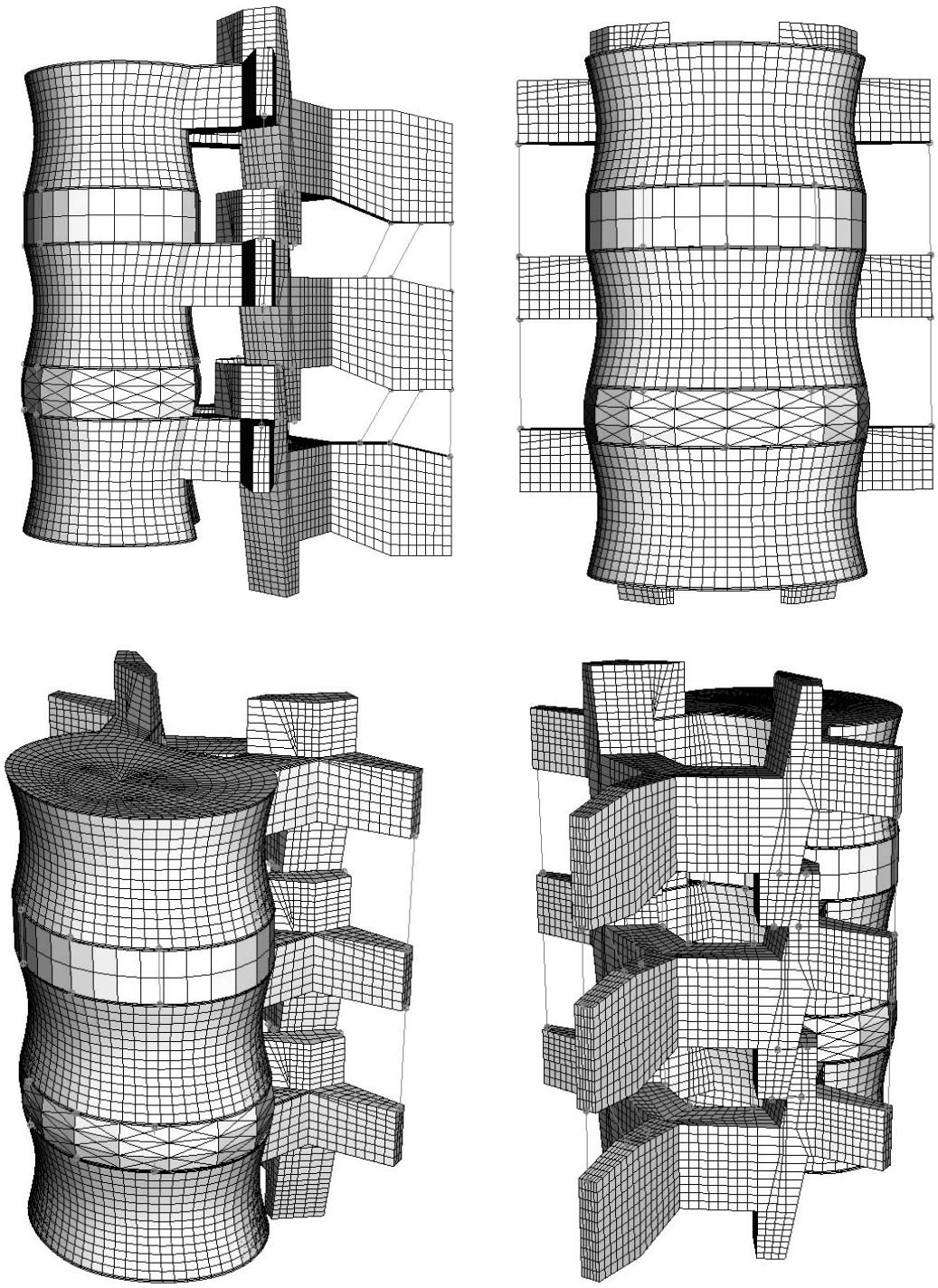

Figure 2-18: 3D views of the modeled segment including a fused FSU

2.5.3 Lumbar Ligamentous Segment with an Artificially Restored Level

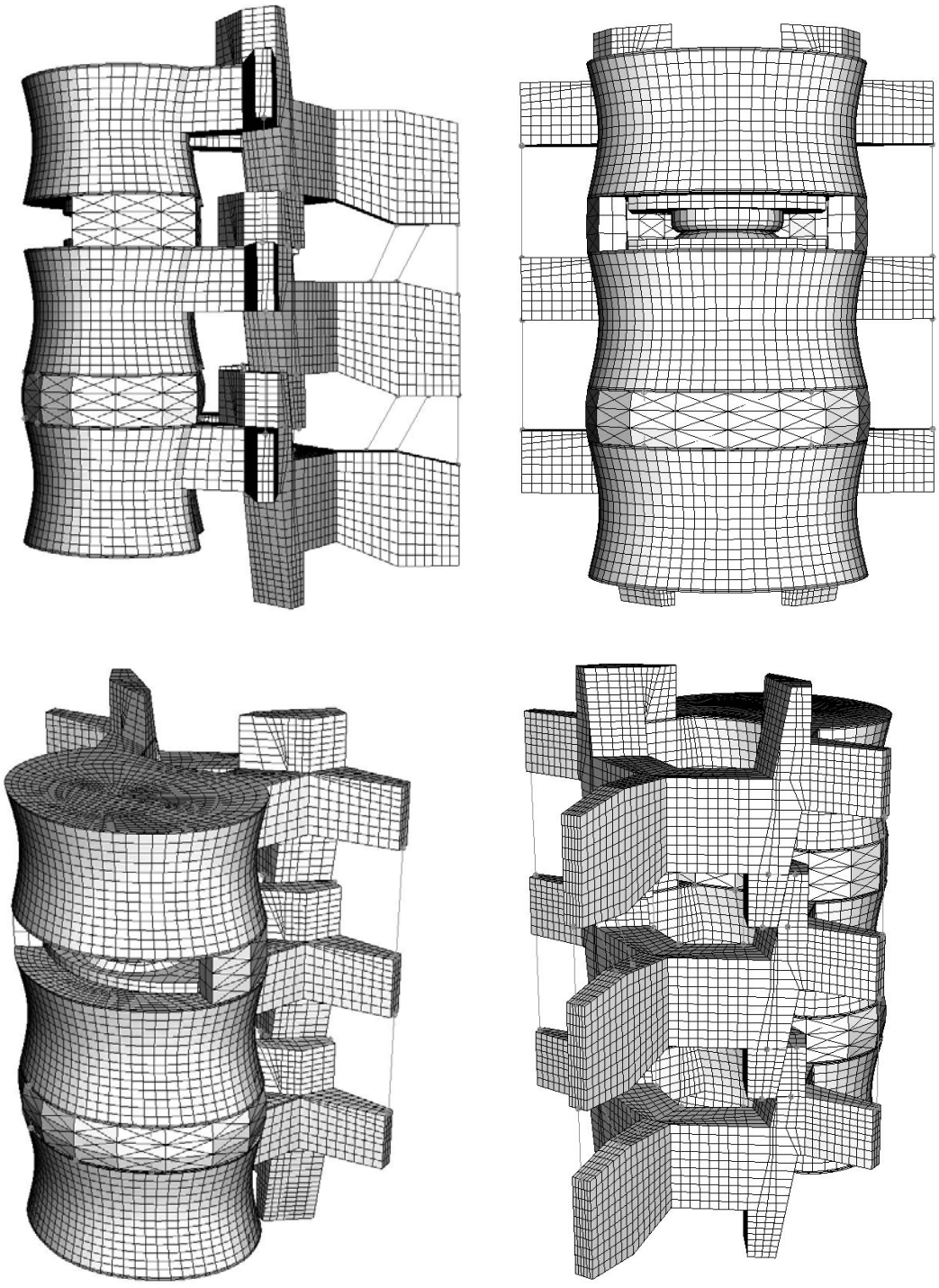

Figure 2-19: 3D views of the modeled segment including a FSU restored with an artificial movable disc

To be applicable to the post-operative conditions of an anterior approach, the anterior longitudinal ligament is not considered in the model of the artificially restored segment. Indeed, the surgeon needs to remove most of this ligament in order to be able to extract the degenerated disc and to implant the artificial device.

Moreover, the degenerated disc is usually not removed completely. It can be difficult to distinguish the boundary between the different tissues such as the annulus and the posterior longitudinal ligament. It is consequently hazardous to remove too much material. Additionally, the presence of a residual fraction of the posterior annulus can improve the stability of the movable FSU. Dooris et al. have shown through numerical models that keeping a significant amount of annulus tissue limits the undesired excess mobility in the movable FSU implanted with a ball-in-socket artificial disc [14]. In the current model, all the elements of the original disc that do not interfere with the artificial disc have been retained. The resulting residual annulus is illustrated in Figure 2-20.

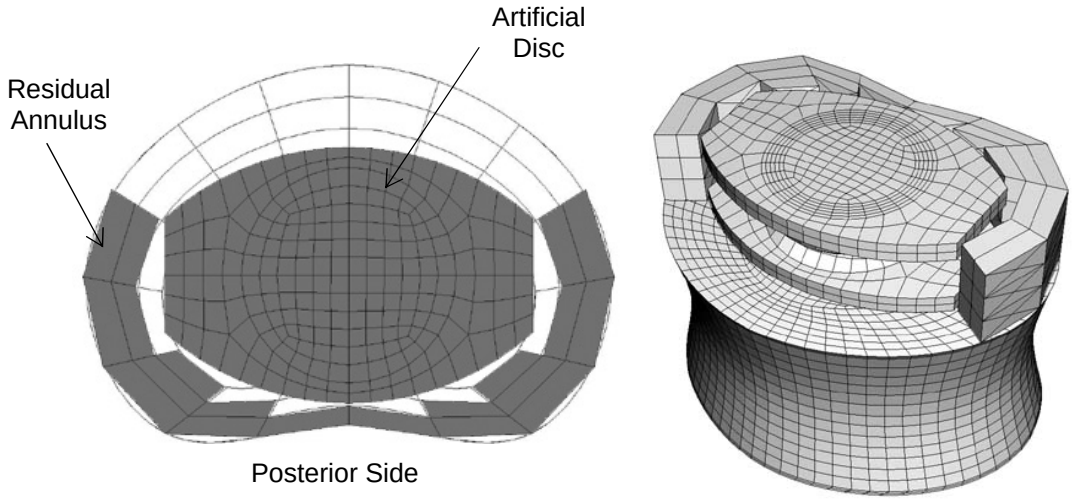

Figure 2-20: Residual annulus and location of the artificial disc

The final model considers a posterior location of the prosthesis. The influences of the antero-posterior position of the artificial disc as well as the residual annulus are discussed in Section 1.4.4. Moreover, the current study confirms that the complete removal of the annulus as well as an anterior position of the artificial disc results in an excessive instability, preventing the simulations from being run through a static analysis.

2.6 Difficulties and Limitations

The following paragraphs state the difficulties met during the construction of the models and the limitations resulting from the various choices and solutions adopted. These points stand for potential future improvements of the model.

- Spinal muscles:

The considered loading protocol described in Section 3.2.2actually results from gravity loads and forces distributed by the complex network of spinal muscles on the different parts of each vertebra. Several authors have tried to identify the role of the different muscles in the spinal biomechanics and to estimate their force in various motions [65], [13], [22]. However, as most of the forces are transmitted through the disc, applying the loads simply on the uppermost vertebral body of the analyzed segment is considered a good approximation for static analyses. The question of considering muscle forces remains for dynamic analyses as muscles play the important role of dynamic stabilizers. In the current study, muscle forces are not taken into account.

- Interaction between discs and vertebrae:

It was seen that, in vivo, the interaction between a disc and a vertebra is relatively weak above the nucleus and the inner annulus. As a consequence, the modeled tie contact

is not relevant to physiological conditions and will withstand greater shear loads prior to failure. This does not stand as a critical limiting factor for the model provided that the shear stresses at those interfaces for the surgically altered models remain realistic compared to the healthy reference.

- Mesh of the cancellous bone:

The complex geometry of the vertebral body made it difficult to partition. As a result, the vertebral body was meshed with tetrahedral elements whereas the cortical shell and the other elements were meshed with hexahedral bricks. The interface between the cortical shell and the cancellous bone is poor since the nodes between the two different kinds of element do not correspond spatially. To limit the incompatibility, the ABAQUS software automatically assigns tie constraints at the interface. Ideally, in future models, the meshing at the interface between the cortical and the cancellous bones should be redefined.

- Mesh of the disc:

The discrete modeling of the annulus, with the annulus ground and the fibers, add more complexity to reduce the size of the mesh elements. As a consequence, an element's size for the annulus and the nucleus is much larger than for an element of the vertebral endplates. This induces a poor distribution of the load transferred from discs to vertebrae and vice-versa. Stress concentrations will occur where the disc's nodes, which are less numerous, are in contact with the vertebral endplate.

Moreover, the disc is modeled by three layers of elements. This will affect the accuracy of the disc bulge calculations. Goel et al. have studied the variation of the disc

bulge with respect to the number of axial layers considered. It was shown that the choice of 8 layers seems to provide a good compromise between accuracy and computing time. A difference of approximately 15% was observed when measuring the bulge of a 2-axial-layer disc compared to the bulge of a 16-axial-layer disc under the same loading conditions [23].

- Mesh of the cortical shell:

ABAQUS sends warnings related to the disproportion of the mesh elements of the cortical shell. Indeed, most of the elements are much thinner relative to length and width. This is due to the very small thickness of the shell. It would require many more nodes to have proportional elements and the system will require much more computing time. As the cortical shell is much stiffer than the other elements, its deformation is limited and the element disproportion does not represent a threat to the accuracy of the results.

- Interaction between ligaments and vertebrae:

The ligaments are modeled by simple axial connectors. At most one ligament is modeled by three connectors and each connector is attached as its extremities to one node. The tensile force of each ligament is thus transmitted to very few nodes. Therefore, the stress concentrations generated at the ligament's connection areas are not representative of true physiological conditions and can be extremely important. The forces provided by the ligaments are pertinent. Their allocation could be reviewed to provide more accurate stress distributions within the vertebrae.

- Bulging and ligaments:

One of the roles of the ligaments, specifically the ALL and the PLL, is to limit the disc bulge. The swelling of the disc tends to extend the ligaments which consequently provide more resistance. However, the ligaments, modeled by axial connectors, are not actual elements and accordingly are not deformable in any other fashion than axially. In the current model, the disc bulge does not influence the extension of the ALL and PLL, and conversely, the force on those ligaments does not influence the disc bulge. This suggests that the calculated protuberance of the disc might be over-estimated and that the force in the ALL and PLL might be under-estimated.

- Pressure in the disc:

The high water content of a healthy IVD provides a hydrostatic pressure which distributes the compressive stress within the disc [18]. However, the current model considers a disc that has been modeled by two different sections, the annulus fibrosis and the nucleus pulposus. Those two sections have significantly different mechanical properties. As a consequence, calculations show a compressive stress much higher in the annulus. This behavior does not represent physiological conditions. The compressive stress will not even be always homogenous within the annulus or the nucleus as they are modeled by deformable solids. A better, although more complex, model of the disc could be achieved through a poroelastic solid which would take into consideration fluid flow and hydrostatic pressure.

CHAPTER 3

SIMULATION PROTOCOL

3.1 Biomechanics of a Lumbar Motion Segment

3.1.1 Motions

The motion of a vertebra relative to the underlying vertebra in a FSU is highly complex. It consists of a combination of displacements with six degrees of freedom. However, the three rotational motions are recognized to be dominant and are described, according to the coordinate system illustrated in Figure 3-1, as follow:

- Flexion, positive rotation around the lateral axis (x),
- Extension, negative rotation around lateral axis (x),
- Lateral bending, rotations around the sagittal axis (z),
- Axial rotation, rotations around the vertical axis (y).

Numerous authors have studied the range of motion of the rotational degrees of freedom. The results converge and show a variability of the range of motions within each portion of the lumbar spine. Representative data reviewed by Dvorak et al. [16], Eijkelkamp et al. [17], and White and Panjabi [76] are shown in Table 3-1.

More specific studies have been made to understand coupling patterns between the different degrees of freedom. It has been shown that the lateral bending and the axial rotation are strongly interdependent [76]. Furthermore, the flexion/extension and the lateral bending are tied to the translational motions in the sagittal direction and the lateral direction, respectively [20], [16]. This latest observation can also be interpreted through the displacement along a certain path of the instantaneous axes of rotation [28]. The data

collected by Dvorak et al. concerning the translational displacement in the sagittal and lateral directions are summarized in Table 3-2 [16].

Table 3-1: Review of average range of motion of the rotational degrees of freedom for lumbar FSU

Motion	Author	L1-L2	L2-L3	L3-L4	L4-L5	L5-S1
Flexion (°)	Pearcy, 84	8	10	12	13	9
Extension (°)	Pearcy, 84	5	3	1	2	5
Flexion + Extension (°)	Yamamoto, 89	10.7	10.8	11.2	14.5	17.8
	Hayes, 89	7	9	10	13	14
	Dvorak, 91	11.9	14.5	15.3	18.2	17.0
Lateral Bending, one side (°)	Pearcy, 84	5.5	5.5	5	2.5	1
	Yamamoto, 89	4.9	7.0	5.7	5.7	5.5
	Dvorak, 91	5.2	6.2	6.2	4.8	2.6
Axial Rotation, one side (°)	Pearcy, 84	1	1	1.5	1.5	0.5
	Yamamoto, 89	2.1	2.6	2.6	2.2	1.3

Table 3-2: Average values of translational displacements in lumbar FSUs from 41 healthy adults aged from 22 to 50 years-old. The value measured is the displacement of a point located on the edge of the lower endplate of the overlying vertebra in a specific direction, relative to the underlying vertebra [16]

Motion	L1-L2	L2-L3	L3-L4	L4-L5	L5-S1
Total translation in the sagittal direction (*z*) induced by flexion + extension (mm)	2.6	3.0	3.1	2.6	0.9
Total translation in the lateral direction (*x*) induced by lateral bending in both directions (mm)	2.0	1.4	1.4	0.8	1.2

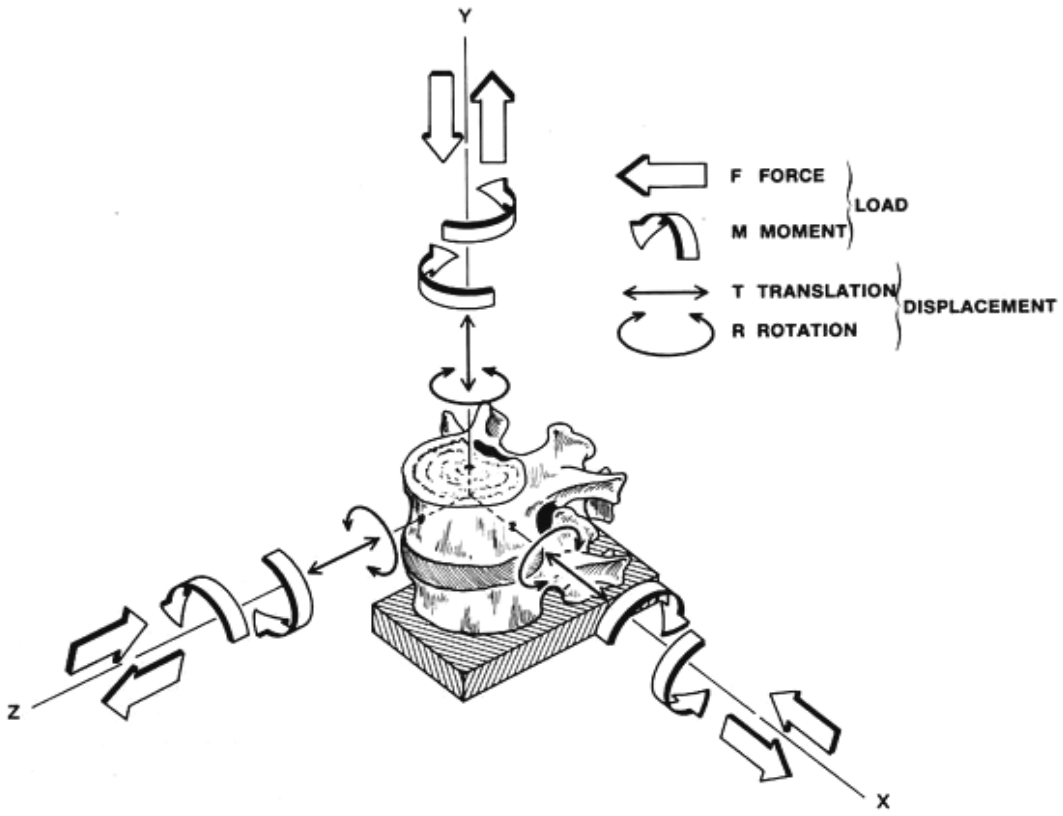

Figure 3-1: 3D coordinate system used to describe the complex biomechanics of a FSU; *x*, lateral direction; *y*, vertical direction; *z*, sagittal direction; *xy*, frontal plane; *yz*, sagittal plane; *zx*, transverse plane [76]

3.1.2 Loads

As shown in Figure 3-1, while a lumbar FSU provides six degree of freedom from one vertebra to another, it is also able to withstand axial and rotational loads in all directions. Yet, the principal load transmitted by a FSU is the axial compressive load conveyed by the intervertebral disc along the vertical axis and is the main concern in spinal biomechanics. Wilke et al. have shown, through in vivo measurements in a healthy L4-L5 FSU, that intradiscal pressures range from 0.1 MPa in the prone position, up to 2.3 MPa when lifting 20 kg bent over with a round back [77]. Using the geometry of the current model, an estimation of the actual load can be calculated. Indeed, assuming a

homogeneous pressure on the surface of the disc (S=1440 mm²), one can estimate the compressive load in a lumbar FSU to range from 144 N in the prone position up to 3,312 N when lifting 20 kg bent over with a round back. A pressure of 0.5 MPa in the standing position would be equivalent to 720 N of compressive load. The load capacity as well as the height of an IVD is said to decrease with time [18]. Consequently, a compressive load of 3,312 N can be well beyond failure load, especially for degenerated discs. Figure 3-2 gives an idea of the intradiscal pressure in the common postures and activities.

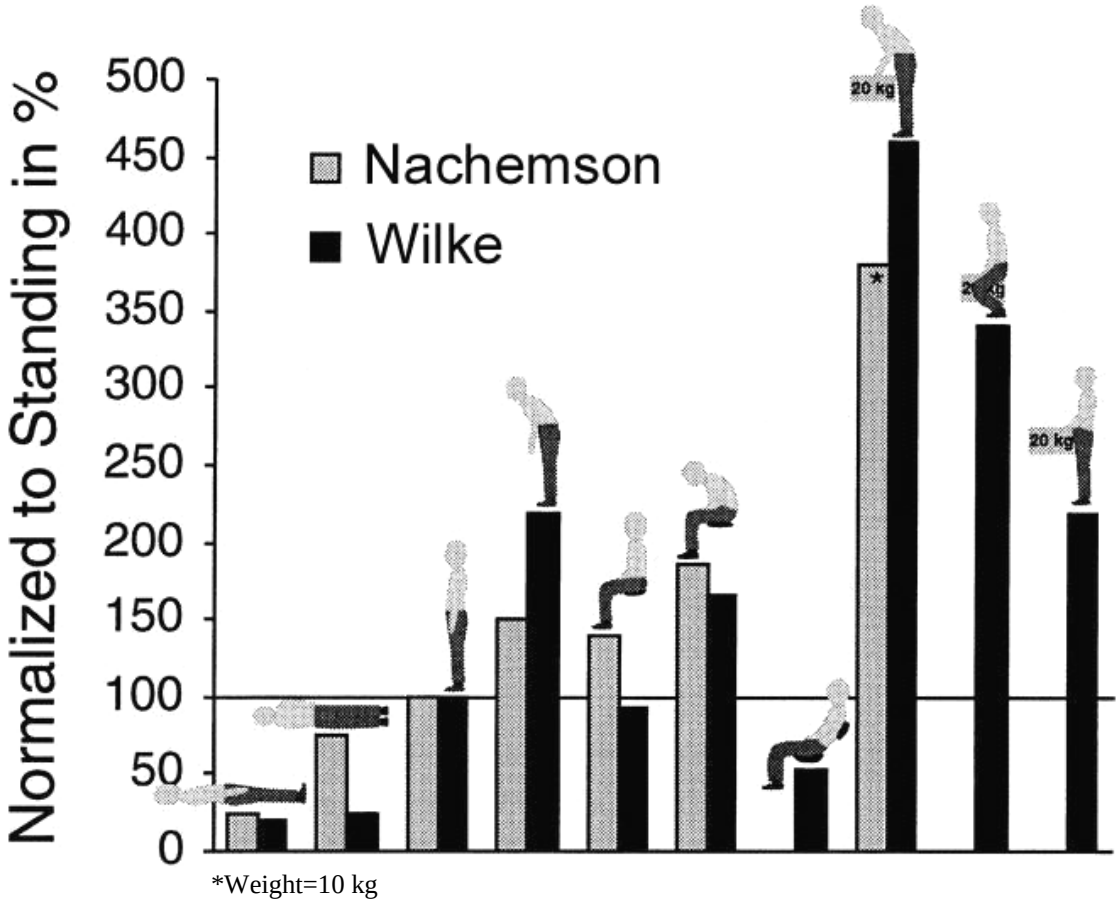

Figure 3-2: Intradiscal pressure in vivo in common postures and activities. Normalized to standing (0.5 MPa, equivalent to 720 N with respect to the current model). Comparison between the data of Nachemson (1960) and Wilke (1999) both for 70 kg healthy individuals [77]

Other factors can play a significant role in the load sharing in a FSU. Namely, the facet joints sustain a large amount of load in the postero-anterior direction for sagittal translation, as well as for lateral translation. The facets also have an important function in the limitation of the axial rotation. They are, however, not involved greatly in the compressive load. It has been noted that the facet joints participate in about 16% of the compressive load in the erect standing posture, and that this ratio tends to increase with respect to the amount of extension [2].

White and Panjabi propose a simple linear representation of the behavior of a lumbar FSU, summarized in Table 3-3 and Table 3-4 [76]. These data provide a relatively good understanding of the FSU behavioral differences in each direction.

Table 3-3: Average translational stiffness coefficients of a representative lumbar FSU [76]

Force	Tension (+Fy)	Compression (-Fy)	Ant. Shear (+Fz)	Post. Shear (-Fz)	Lat. Shear (Fx)
Stiffness (N/mm)	770	2000	121	170	145

Table 3-4: Average rotational stiffness coefficients of a representative lumbar FSU [76]

Moment	Flexion (+Mx)	Extension (-Mx)	Lateral Bending (Mz)	Axial Rotation (My)
Stiffness (N-m/°)	0.74	0.48	0.57	0.20

Moreover, this simple model allows an approximate estimation of the shear loads induced by rotational motions in the sagittal and lateral directions. For example, the maximal translational displacement in the postero-anterior sagittal direction is at most

about 4 mm [20], [16]. Considering the corresponding stiffness of 121 N/mm in that direction, it can be concluded that the shear load does not exceed 484 N in this direction. Patwardhan et al. have shown that a “follower load” (i.e. a load whose path approximates the tangent to the curve of the spine) considerably increases the compressive load capacity of the lumbar spine [54]. This characteristic explains why the compressive load greatly raises in a FSU when shear loads occur. Indeed, in physiological conditions, the compressive load in a FSU modulates in order to keep as much of the resultant load as tangent to the curve of the spine as feasible. In particular, this also explains why lifting a load bent over with a round back, which induces large shear loads, dramatically increases the compressive load and should be avoided to maintain spine integrity.

3.2 Boundary Conditions and Applied Loading

3.2.1 Boundary Conditions

The boundary conditions are applied to the underlying endplate of the lowermost vertebral body. The translational degrees of freedom of the nodes on the outer surface of the endplate have been immobilized.

This type of boundary condition applied to the lowermost vertebra is commonly used in numerical analysis as well as in experimental studies. However, it should be addressed whether boundary conditions should be applied to the whole vertebra or to the vertebral body only. The case where boundary conditions are applied to the whole vertebra is appropriate if the lowermost vertebra is S1, which is much more massive and less deformable than the other vertebrae. If the boundary conditions are not applied to the whole vertebra, the analysis cannot take into account the deformation of the posterior vertebra relative to the vertebral body. In the current model, the posterior part of the

lowermost vertebra is not constrained. This implies that the interaction with the underlying posterior vertebra, through the facets, muscles and ligaments are not taken into account. It may result in an extra stress on the lowermost vertebra by the overlying elements. The situation is similar with the uppermost vertebra, for which the model provides quite poor boundary conditions. Nevertheless, it does not limit the model as the current study aims to compare relatively the behavior of the three different motion segments modeled and does not claim to provide absolute results concerning stresses and displacements.

3.2.2 Loading Protocol

The loads have been chosen to be the controlled parameters of the study. The same set of loads is applied to each of the three numerical models and the induced motions and stresses in the relevant constitutive elements are compared and analyzed.

Loads are applied on the upper endplate of the uppermost vertebra. As explained in the previous section, the interactions with the upper part of the posterior vertebra, through the facets and the processes, are not taken into consideration. But, in a similar fashion, that does not affect the model as the study is interested principally in the relative behaviors of the three models. Moreover, it has been shown that the compressive load is the most important in the spine biomechanics and that it is mainly transmitted through the vertebral endplates and the intervertebral disc. As a consequence, the loads applied on the uppermost endplate in the model are only compressive loads. Initially, a permanent pressure, equivalent to the intradiscal pressure in neutral position, is assigned to the surface of the endplate. Vertical volumic loads distributed appropriately are then applied in order to generate the different rotational motions. It is important to note that, as the

motions occur, the vertical loads produce a combination of compressive and shear loads, as in natural behavior.

The magnitudes of the loads applied to generate each rotational motion have been established through iterative tests applied to the healthy model, as well as the data provided in Section 3.1.1, concerning the range of motions, and in Section 3.1.2, concerning the loads involved in a lumbar FSU. As a result, the loads applied to the models are relevant of physiological conditions. The loading protocol used in the simulation of the models is summarized in Table 3-5 through Table 3-8.

3.2.3 Simulation Protocol Summary

Each rotational degree of freedom described in Section 3.1.1, i.e. flexion, extension, lateral bending and axial rotation, is independently simulated on the three modeled segments under loading conditions appropriate to the upper limit of physiological conditions. The magnitudes and the location of the loads, applied to simulate each rotational motion, are tabulated below.

Appendix A shows the structure of the section of the ABAQUS input files that includes the simulation protocol and also summarizes the material properties, the interactions properties, the boundary conditions, and the interactions. The code proposed is taken from the input run to simulate the healthy model in all rotational degrees of freedom.

Table 3-5: Summary of the simulation protocol, magnitude and location of the loads applied to generate flexion

	Pre-compression pressure	**Additional volumic force in the vertical direction**	**Total load**
Magnitude	0.5 MPa	7.7 N/mm^3	-
Location	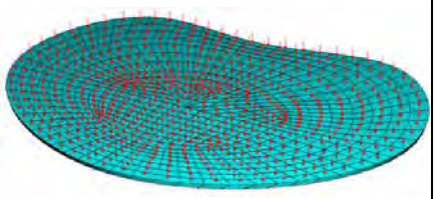 Total endplate surface S=1440 mm^2	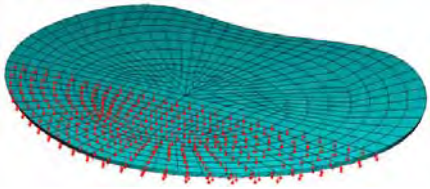 Anterior endplate volume V=260 mm^3	-
Equivalent load (N)	720	2,000	2,720

Table 3-6: Summary of the simulation protocol, magnitude and location of the loads applied to generate extension

	Pre-compression pressure	**Additional volumic force in the vertical direction**	**Total load**
Magnitude	0.5 MPa	2.2 N/mm^3	-
Location	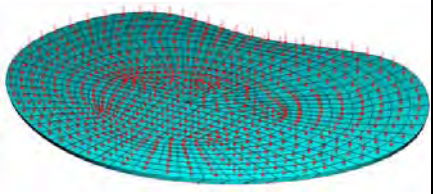 Total endplate surface S=1440 mm^2	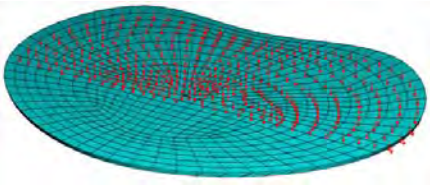 Posterior endplate volume V=460 mm^3	-
Equivalent load (N)	720	1,000	1,720

Table 3-7: Summary of the simulation protocol, magnitude and location of the loads applied to generate lateral bending

	Pre-compression pressure	**Additional volumic force in the vertical direction**	**Total load**
Magnitude	0.5 MPa	3.6 N/mm^3	-
Location	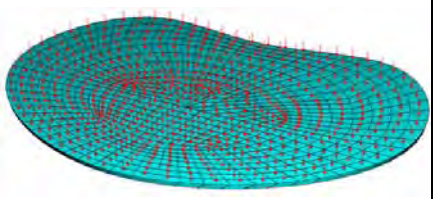 Total endplate surface S=1440 mm^2	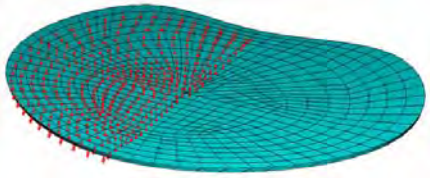 Lateral endplate volume V=360 mm^3	-
Equivalent load (N)	720	1,300	2,020

Table 3-8: Summary of the simulation protocol, magnitude and location of the loads applied to generate axial rotation

	Pre-compression pressure	**Additional nodal force in the sagittal direction**
Magnitude	0.5 MPa	50 N per node
Location	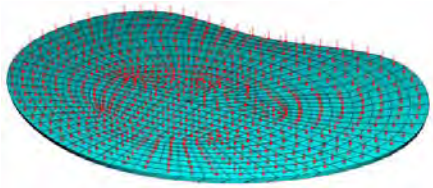 Total endplate surface S=1440 mm^2	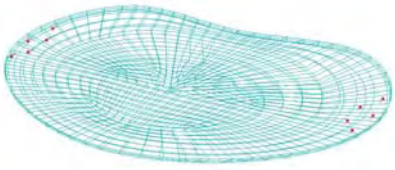 5 nodes on each side with opposite loading direction
Equivalent load	720 N	11.45 N-m

CHAPTER 4

MODEL VALIDATION

In order to validate the global consistency of the models developed in the course of this study, characteristic results from the model of the healthy spine (the "healthy model") was compared to clinical data. The comparisons, discussed in the following sections, demonstrate that the model provides a relatively good match to the physiological behavior of a lumbar motion segment. Some limitations of the model have been noted and analyzed. Specifically, the negative initial strain of the ligaments under pre-compression slightly reduces their ability to resist the intervertebral motions. Isolated peak stresses are seen in the different components due to some of the geometrical modeling approximations. Bulging of the intervertebral disc is slightly increased for the rotational motions due to the simpler nature of the mesh in the disc and the absence of interaction between the ALL, the PLL, and the annulus. However, these restrictions do not limit the model for overall comparisons of the behavior of the surgically altered motion segments to the healthy model.

4.1 Range of Motions

A common way to compare the behavior of a FE model with the natural behavior of the lumbar spine is to evaluate and compare the mean stiffness of the segment for the different degrees of freedom. The mean stiffness of a lumbar FSU in all the translational and rotational degrees of freedom was reported in Table 3-3 and Table 3-4. This information provides a relatively good understanding of the behavioral differences of a FSU in the different directions. However, this is not truly representative of a lumbar FSU.

This type of model does not take into consideration the nonlinearities of the segment. It is consequently difficult to compare results to different studies by other authors as they are variable with respect to the selected loading conditions.

Accordingly, it was chosen to evaluate the mobility of the FSUs rather than their stiffness. Knowing that the loading protocol, described in Section 3.2.3, has been established to be representative of the upper limit of admissible physiological loads, the induced ranges of motion should be representative of maximum physiological ranges of motions. The average rotational motions of a FSU, resulting from the simulation of the healthy model, are reported in Table 4-1.

According to the experimental data collected and reported in Table 3-1, the ranges of motion in Table 4-1 are appropriate for actual physiological conditions. It was stated previously that the vertebra used in the model was built from information typically related to L3 and L4 vertebrae. As a consequence, it is possible to evaluate with more accuracy the result of the simulation with experimental results. Figure 4-1 compares different experimental assessments of the rotational mobility of a L3-L4 lumbar motion segment with the results of the current study. Note that on Figure 4-1, the rotational displacements in flexion and extension have been added up (12.7°) in order to be compared to the available clinical data, usually presented in this fashion.

It is readily seen that the model yields excellent physiological ranges of rotational motions in view of the considered simulation protocol.

Table 4-1: Average maximal rotational displacements calculated in the FSUs of the healthy model; expressed in the physiological coordinate system described in Figure 3-1

	Flexion	Extension	Lateral Bending one side	Axial Rotation one side
Rotational Motion (deg.)	8.4	4.3	5.9	1.5

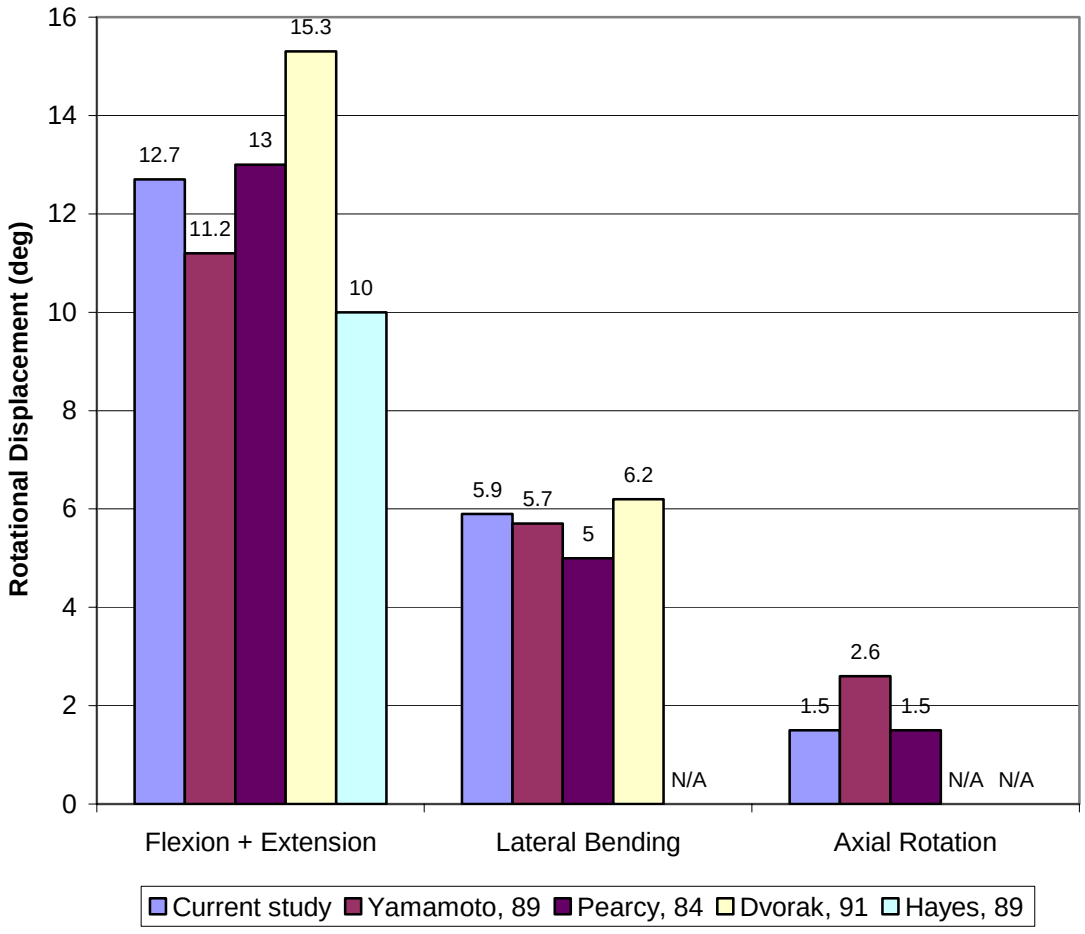

Figure 4-1: Rotational motion of a lumbar FSU, comparison of the results calculated in the healthy model with experimental data pertaining to a L3-L4 FSU; results for lateral bending and axial rotations consider only motions on one side

4.2 Coupling of the Motions in a FSU

A significant characteristic of the functional biomechanics of the spine is the coupling of the different intervertebral motions. Specifically, in the lumbar spine, it is well known that the rotations in the sagittal plane (flexion and extension) and the rotation in the frontal plane (lateral bending) are associated with the vertical translation and with, respectively, the sagittal translation and the lateral translation. Moreover, it is understood that the generation of an axial rotation induces rotational motion in the sagittal and in the frontal planes. Likewise, lateral bending is coupled with rotations in the transverse plane (axial rotation) and in the sagittal plane. However, sagittal rotations are not coupled with any other rotational displacement.

Coupled motions were evaluated while simulating the healthy-spine FE model. The different displacement components, related to each simulated rotational motion, are summarized in Table 4-2.

For both FSUs of the healthy segment, the displacements in the six degrees of freedom were computed according to the following equations, which refer to the parameters and the coordinate system described in Figure 4-2. The coordinate system (x,y,z) is attached to the lower endplate of the underlying vertebra. It is oriented according to the physiological directions illustrated in Figure 3-1.

Method of calculation of the intervertebral displacement in the six degrees of freedom, the used parameters are referring to Figure 4-2:

$$R_x = \tan^{-1}\left(\frac{y_D - y_C}{z_C - z_D}\right)$$

$$U_x = \overrightarrow{V_L F}.\vec{x} \qquad \textit{for left leteral bending}$$

$$U_x = \overrightarrow{V_R E}.\vec{x} \qquad \textit{for right leteral bending}$$

$$R_y = \tan^{-1}\left(\frac{z_H - z_G}{x_G - x_H}\right)$$

$$U_y = \frac{\left(\overrightarrow{V_E A} + \overrightarrow{V_F B}\right).\vec{y}}{2} - L_0$$

where L_0 is the disc height in neutral position

$$R_z = \tan^{-1}\left(\frac{y_G - y_H}{x_G - x_H}\right)$$

$$U_z = \overrightarrow{V_F B}.\vec{z} \qquad \textit{for flexion}$$

$$U_z = \overrightarrow{V_E A}.\vec{z} \qquad \textit{for extension}$$

Table 4-2: Average coupling motion components observed in the FSUs of the healthy model, expressed in the coordinate system described in Figure 4-2

Simulated Motion	Rx (deg.)	Ry (deg.)	Rz (deg.)	Ux (mm)	Uy (mm)	Uz (mm)
Flexion	+8.4	0.0	0.0	0.0	-2.3	+1.1
Extension	-4.3	0.0	0.0	0.0	-0.9	-0.7
Lateral Bending	-0.2	-0.6	+5.9	-0.7	-1.1	+0.2
Axial Rotation	+0.4	+1.5	-0.2	+0.2	0.0	-0.1

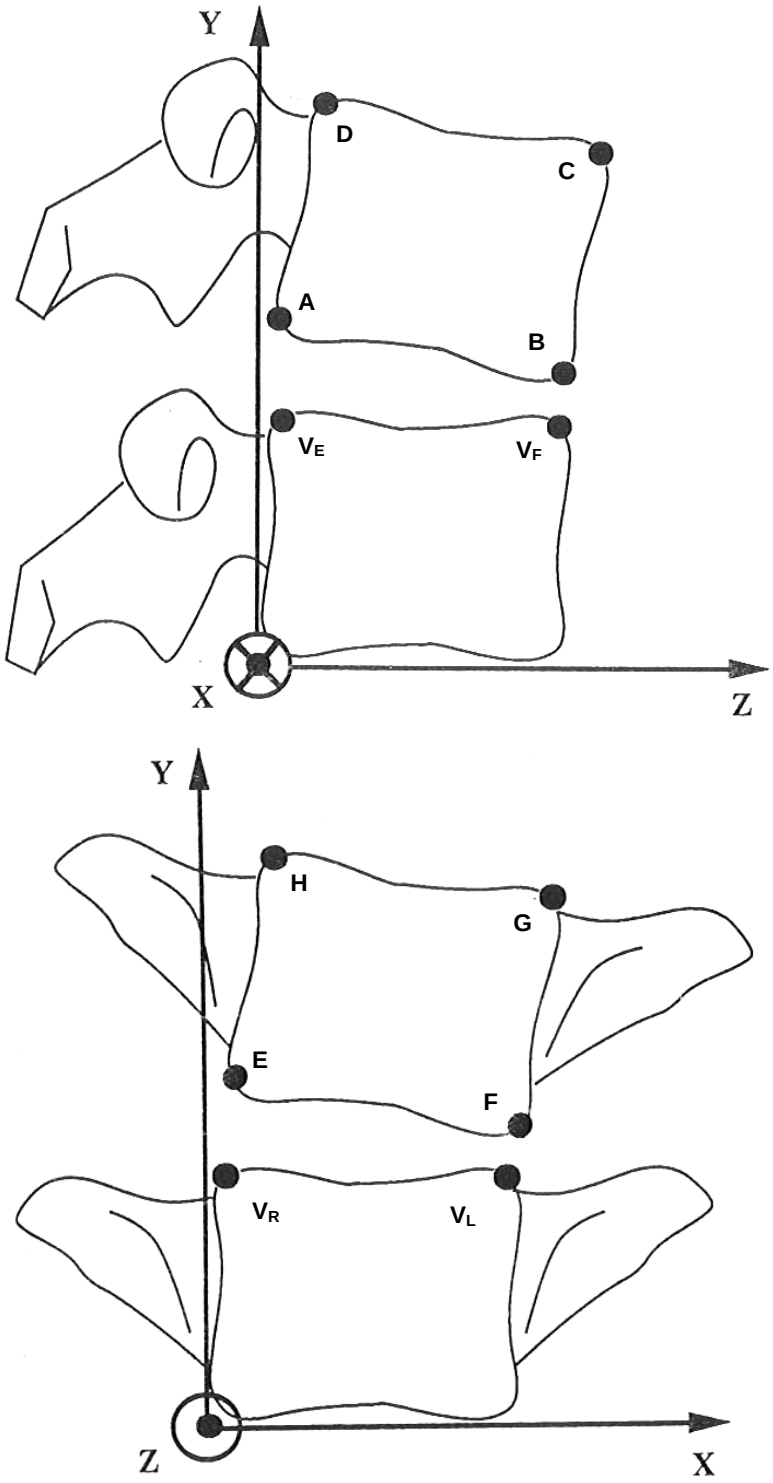

Figure 4-2: Illustration of the parameters utilized to compute the displacements of a FSU in the six degrees of freedom; (*x*,*y*,*z*): *x*, lateral direction; *y*, vertical direction; *z*, sagittal direction; *xy*, frontal plane; *yz*, sagittal plane; *zx*, transverse plane

The couplings observed while simulating the healthy model confirm the significant interrelation between the rotational motions and the translational displacements, in particular for flexion, extension, and lateral bending.

The total translational displacement in the sagittal direction for flexion and extension, $Uz = 1.8\ mm$, is less than the displacement, $Uz = 3.1\ mm$, reported by Dvorak et al.; cf. Table 3-2. This significant difference can be accounted for by two main factors. First, as observable in Figure 4-1, the reported range of motion for flexion and extension, $Rx = 15.3°$, is larger than the 12.7° measured in the current study. As a result, the translational displacement in the sagittal direction would also be larger. The second factor comes from the slightly different methods used to measure the displacement. According to Figure 4-2, Dvorak et al. report the total displacement of point *A* in the sagittal direction (*z*), for flexion and extension. The current study uses the displacement, in the same direction, of point *A* for extension, and of point *B* for flexion; which, according to the position of the instantaneous axis of rotation, can result in significant discrepancies.

The displacement in the lateral direction, $Ux = 0.7\ mm$, induced by lateral bending on one side, is consistent with the 1.4 *mm* reported by Dvorak et al. for lateral bending on both sides.

Coupling of the three rotational motions were observed when simulating lateral bending and axial rotation on the healthy model. Those data are difficult to compare with experimental values as the interrelations between the different motions are highly dependent on the spinal level considered, the loading conditions, and on the initial orientation of the lumbar segment. Figure 4-3 compares the calculated coupled motions

while simulating lateral bending and axial rotation with the results of a study on cadaveric whole lumbar spines reported by Panjabi et al. [53].

The 10 N-m considered in this experimental study for the simulation of the axial rotation is similar to the 11.45 N-m proposed in the loading protocol to generate the same motion in the model. Referring to Figure 4-3 (A), the calculated results (1.5° of axial rotation, 0.4° of flexion, and -0.2° of lateral bending) are in-between the coupling measured by Panjabi et al. for the L3-L4 and L4-L5 levels. In view of the modeled vertebra, which pertains to the L3 and/or L4 levels, this result is encouraging regarding the global model validity.

However, the measured coupling related to the simulation of lateral bending (5.9° of lateral bending, 0.2° of extension, and -0.6° of axial rotation) appears dissimilar with respect to the experimental data, see Figure 4-3 (B). The interrelation of the rotational motions is much more pronounced as reported by Panjabi et al. than it is currently observed, where coupled motions are reversed and almost absent. In this case, the divergence can mainly be attributed to differences in the loading conditions. The model simulates the lateral bending with a laterally shifted compressive load, whereas the cadaveric lumbar spines where tested with a torque of 10 N-m in the sagittal direction.

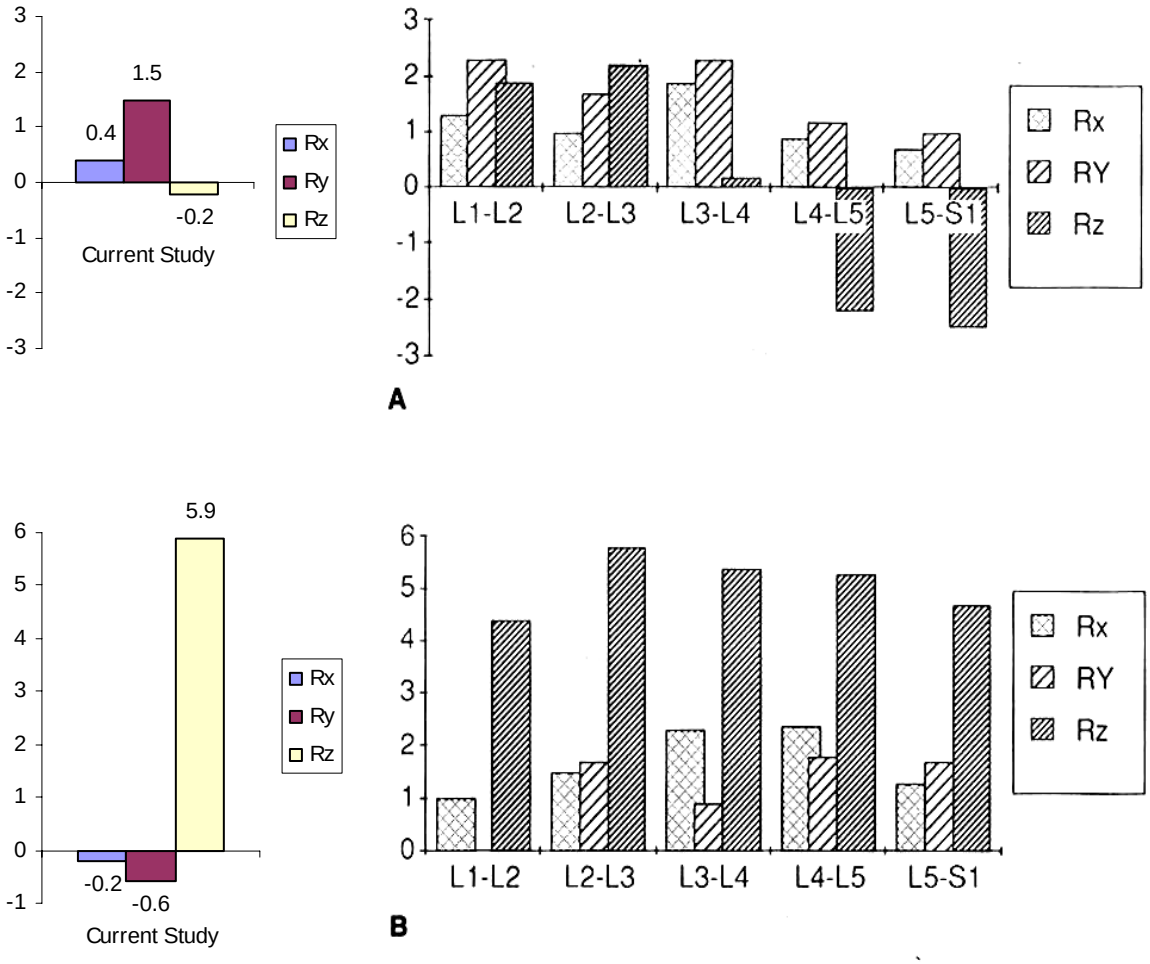

Figure 4-3: Coupling of intervertebral rotational motions in the lumbar spine. Experimental measurements (on the right) result from the investigation of fresh cadaveric whole lumbar spine specimens [76] data from [53]. (A) Simulation of left axial rotation due to axial torque: My=+11.45 N-m in the current study, My=+10 N-m in the experimental study. (B) Simulation of right lateral bending. Note that lateral bending should not be compared directly due to significant differences in the loading conditions (see text)

4.3 Strain in the Ligaments

In order to validate the segmental behavior of the healthy model, the ligaments' activities were analyzed. The relevant, most reliable data available in the literature are related to the strains of the ligaments. The model was compared with the average physiological strains in the lumbar spinal ligaments, with respect to the rotational motions, as measured by Panjabi et al. (Figure 4-4). To facilitate the comparison, Figure 4-5 follows the structure of Figure 4-4 and illustrates the average strains observed in the intervertebral axial connectors of the healthy model, with respect to the rotational motions.

The first obvious difference between the two figures is the absence of values, in the numerical analysis, of the majority of the ligaments for which the strain is below approximately 15% as reported by Panjabi et al.. This is due to the calibration of the connectors, in which strains and force are set equal to zero in unloaded conditions. As a result, the compression preload, typical of the segment neutral position, shifts the mechanical characteristics of the connectors, which then have neutral configurations than slightly mismatch the segment neutral position.

Connectors such as the SSL, the ISL, the LF, the PLL, and the ALL, are compressed approximately one millimeter after the compression preload and lose some of their resistance capacity. Adding to this inaccuracy of calibration the lack of reactivity of the ALL and the PLL to the bulge of the annulus (stated in Section 2.6), those connectors lose all their functionality in the healthy model.

The strains in the left and right capsular ligaments (CLl & CLr) are reversed on the two figures. This reveals that the axial rotation is generated in opposite directions in

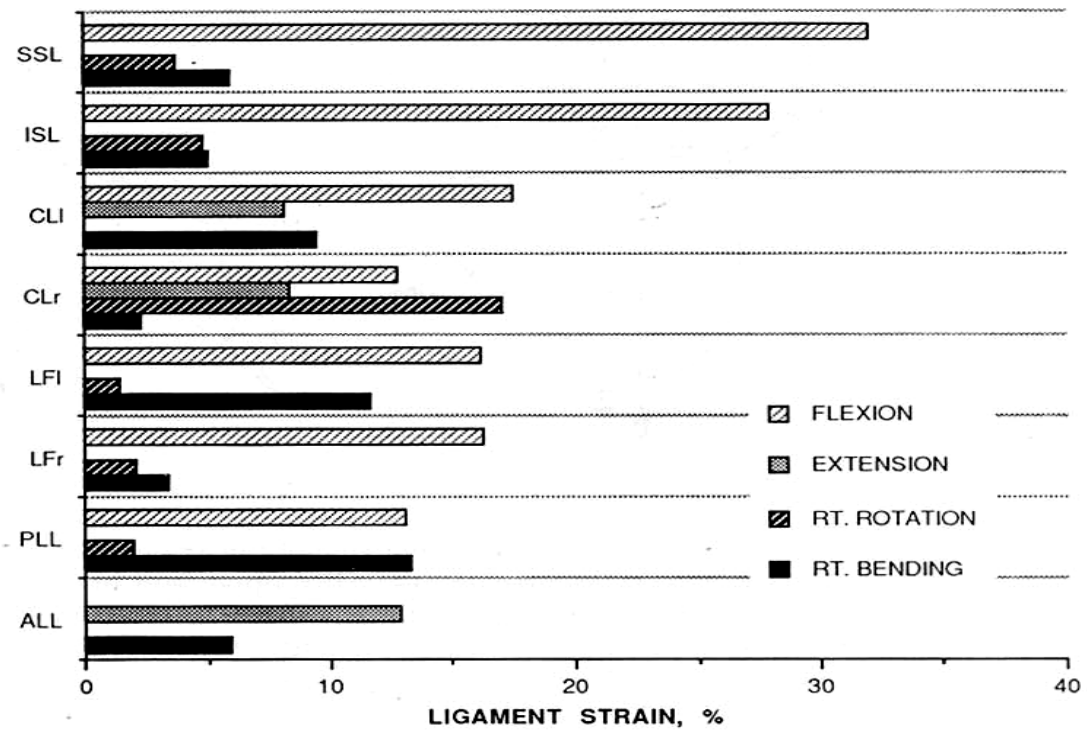

Figure 4-4: Physiological strains in lumbar spinal ligaments function of the intervertebral rotational motions, [76] data from [51]

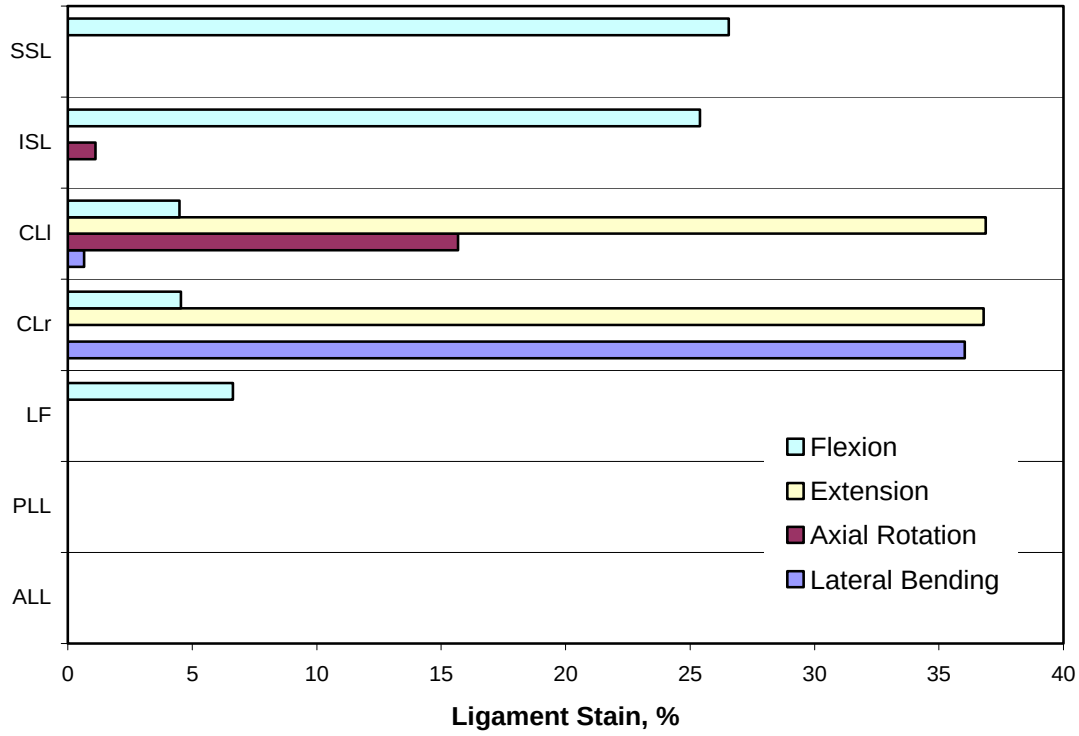

Figure 4-5: Strains in the intervertebral axial connectors for the healthy model function of the rotational motions

both studies. The CL connectors are constrained in tension toward the underlying vertebra when pre-loaded. Consequently, their strain is increased in extension and lateral bending, whereas it is decreased in flexion. The difference between the experimental and the numerical analysis is more significant relative to the CLs than to the other ligaments. This would be explained by the original length of the modeled CLs, smaller than actual CLs, which make them subject to greater strain for identical displacements. For the axial rotation, the CLs seem to have a comparable behavior in the study of Panjabi and in the present FE analysis, as shown on Figure 4-4 and Figure 4-5.

The initial-condition inaccuracy concerning the ligaments might slightly affect the results of the analysis. However, the comparison between the three modeled segments will remain consistent as they all utilize the same initial conditions. Apart from this issue, no aberrations were observed in the behavior of the intervertebral connectors of the healthy model.

4.4 Force in the Ligaments

According to the characteristics of the intervertebral axial connectors and to their strains, reported in Section 4.3, one can compute the maximum force provided by each set of connectors in the healthy model while simulating the different rotational motions. Figure 4-6 compares those results with the failure loads of the lumbar intervertebral ligaments gathered in Table 2-2. None of the ligament forces exceed the failure load in the healthy model. Moreover, the calculated values may be overestimated since the shifted initial conditions of the ligaments (discussed in Section 4.3) prevent the ALL and the PLL, which can provide significant resistance, from contributing to the static equilibrium of the FSUs. The significant difference between the calculated force and the

failure load of the ligaments shows that the intervertebral connectors of the healthy model are disposed to experience greater loads.

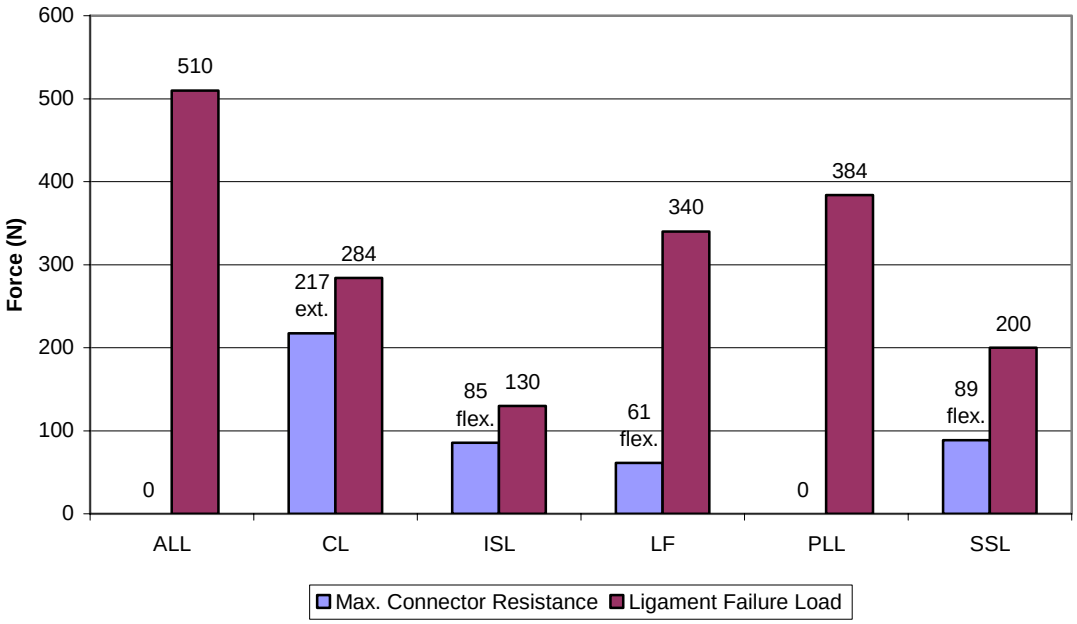

Figure 4-6: Comparison between the maximum force provided by each set of connectors in the healthy model, while simulated in the different rotational motions, and the failure load of the intervertebral ligaments reported in Table 2-2

4.5 Maximum Von Mises Stresses

To ensure the structural coherence of the model, the maximal Von Mises stress in each component of the model were examined and compared to the approximate failure stress of the related material. Table 4-3 reports the yield and/or ultimate stress of the cortical bone, the cancellous bone, and the annulus fibers. The maximum Von Mises stresses calculated while simulating the healthy model are listed in Table 4-4.

Some limitations of the model described in Section 2.6, specifically related to the meshing of the disc, are confirmed by the occurrence of spurious high peak stresses in the

Table 4-3: Yield stress of the main components of the lumbar segment models

Component	Yield or Ultimate Stress (MPa), average ± SD [range]	Source
Cortical Bone	Compressive strength of human femoral cortical bone: **[167-215]**	[5]
Cancellous Bone	Yield stress of human femoral cancellous bone in compression: **8.2 ± 2.6** Compressive strength of L4 & L5 vertebral cancellous bone: **14 [0.69-72.75]**	[29] From [72]
Annulus Fibers	Tensile strength of anterior outer fibers: **10.3 ± 8.4** Correlation between the tensile modulus (E) and the failure stress (σ_f)given by the linear regression equation: $E = 11.8 \times \sigma_f + 5.7$	[69]

Table 4-4: Maximum Von Mises stresses, and corresponding location and conditions, in the main components of the healthy model while simulating the different rotational motions. The maximum stresses observed are usually not typical of physiological conditions and are caused by modeling defects

Component	Calculated Max. Stress (MPa)	Relevant Max. Stress (MPa)
Cortical Bone	**175** Coincidence of a node from the anterior annulus and a node from the adjacent endplate – lowermost vertebra – flexion	< **90** Anterior wall of the vertebral body – lowermost vertebra – flexion
Cancellous Bone	**38** Coincidence of a node from the anterior annulus and a node from the adjacent endplate – lowermost vertebra – flexion	< **3.5** lowermost vertebra – flexion
Posterior Vertebra	**70** Connection nodes with the SSLs – intermediate vertebra – flexion	< **35** Sharp angle between the posterior wall of the vertebral body and the lower part of the pedicles – lowermost vertebra – flexion
Annulus Fibers	**49** Outer vertically intermediate layer of the annulus fibers, on the lateral side of the annulus – lower disc – lateral bending	< **25** Outer and vertically intermediate layer of the annulus fibers, on the antero-lateral portions of the annulus – lower disc – flexion

bony components and in the annulus fibers. The regions where these unrelated peak stresses are taking place can be located and their origin can be identified without difficulty. It is consequently possible to evaluate and locate the pertinent peak stresses in the component of the model, as reported in Table 4-4.

An inaccuracy of 94% was observed for the maximum Von Mises stress in the cortical bone due to the unexpected coincidence of two nodes from the upper endplate of the lowermost vertebra and the lower disc's annulus. Ignoring this defect, the maximum Von Mises stress in the cortical bone of the healthy model reaches at most approximately 90 MPa on the anterior wall of the lowermost vertebral body in flexion. This result, away from the edge, shows that the cortical bone presents no risks of failure.

The high unrelated peak stress occurring in the cortical bone is transmitted for the same reasons to the cancellous bone. A discrepancy of 986% was calculated between the maximum stresses with and without the consideration of the modeling defect in the cancellous bone. The maximum relevant Von Mises stress in the cancellous bone of the lowermost vertebra was evaluated to 3.5 MPa, which is far below the average strength of the material.

The peak stresses in the anterior vertebrae expose other expected limitations of the model. The nodal connection of the intervertebral ligaments generates high peak stresses that are not reflective of physiological conditions. These peak stresses are maximized by the interaction between the lower SSL and the intermediate anterior vertebra in flexion. Another limitation relates to the geometry of the vertebrae. A peak occurs at the interface between the pedicles and the vertebral body of the lowermost vertebra. This is due to the sharp angle between the surfaces in contact, which are in reality curved to moderate the

stress distribution. These peak stresses in the anterior vertebra remain, however, less than the material strength.

High stresses are observed in very few localized truss elements, which model the annulus fibers of the intervertebral discs. These elements are located on the outermost radial layer of the intermediate vertical level of the disc. The simple geometric modeling of the discs confers to these specific elements greater strains than in physiological conditions. This is confirmed by the significant bulge observed in the lower disc of the healthy model, reported in Section 4.7. The discrepancy in the maximum Von Mises stress of the annulus fibers, resulting from the geometric modeling, is estimated to be approximately 96%. Accordingly, the relevant maximum Von Mises stress in the annulus fibers, calculated during the simulation of the healthy model, is approximately 25 MPa on the anterior outer annulus. This value exceeds the tensile strength of the anterior outer fibers of the annulus, equal to 10.3 ± 8.4 MPa, experimentally established by Skaggs et al. [69]. However, the authors have also observed a strong correlation between the tensile modulus and the failure stress of the fibers, for which they have determined a linear regression equation: $E = 11.8 \times \sigma_f + 5.7$ (Table 4-3). With a tensile modulus of 550 MPa (Table 2-1), the tensile strength of the modeled outer layer of fibers would be approximately 46 MPa. In conclusion, the fibers' tensile moduli used in the model are greater than the value measured by Skaggs et al. (ranging from 60 MPa to 140 MPa). However, according to this correlation between the tensile modulus and the failure stress, the calculated relevant maximum Von Mises stress in the annulus fibers (~25 MPa) is significantly less than their hypothesized strength (46 MPa).

4.6 Force and Pressure on the Articular Facets

To illustrate the contribution of the facets in the segment stability, the magnitude of the force transmitted through the facet joints of the healthy model have been calculated for the different rotational degrees of freedom (Table 4-5). The forces conveyed by a joint range from 0 to 161 N. It clearly appears that the load is not transmitted in the same fashion through the different FSUs of the considered multilevel segment. In particular, the loads on the facets are significant for the upper FSU in flexion whereas they are practically nonexistent on the facets of the lower FSU. The loading and boundary conditions are responsible for this disparity as they are only applied on the vertebral endplates and do not take into consideration the facet joints. This limitation was expected and has been described in Section 3.2.1.

Adams and Hutton have shown through experimentations on cadaveric lumbar FSUs, tested in flexion and extension (from -4° to +4°) under physiological conditions, that the facets' load share was significant in extension and close to zero in flexion [2]. Extrapolating this statement to larger motions in flexion, and in view of the results reported in Table 4-5, the forces in the facets of the lower FSU of the healthy model would be more typical of physiological conditions than in the upper FSU.

Table 4-5: Magnitude of the force (N) transmitted through the facet joints of the healthy model for the different rotational motions

Facet	Flexion	Extension	Lateral Bending	Axial Rotation
Superior Left	115	54	16	0
Superior Right	116	54	161	109
Inferior Left	1	79	24	0
Inferior Right	1	79	140	114

To understand the involvement of a facet joint, it is more accurate to investigate the pressure at the interface than the force transmitted through the joint. Indeed, the contact area changes with the orientation of the FSU as well as with the applied loads. With respect to the magnitude of the force transmitted through the facet joints and to the contact area calculated while simulating the healthy model, the equivalent average compressive pressure on the facets have been estimated and are reported in Table 4-6. The pressures appear to be more uniform than the loads and remain in general below 1 MPa. More significant pressures, between 2.2 and 2.6 MPa, occur on the upper facets in severe flexion and on the upper and lower right facets in lateral bending. These values remain under the characteristic ultimate strength of cartilage, approximately equal to 3 MPa [5]. However, these values being averages, more significant peak stresses might occur at the joint interface. These results are difficult to interpret as the ultimate strength of articular cartilage is different for each type of joint. Further investigations are required to evaluate the ultimate strength of the cartilage from the articular facets.

Table 4-6: Equivalent average compressive pressure (MPa) on the elements of the facet joints of the healthy model for the different rotational motions; bolded figures are exceeding 2 MPa

Facet	Flexion	Extension	Lateral Bending	Axial Rotation
Superior Left	**2.2**	1.0	0.5	0.0
Superior Right	**2.2**	1.0	**2.6**	1.0
Inferior Left	0.1	0.9	0.7	0.0
Inferior Right	0.1	1.0	**2.3**	1.0

Alternatively, Dunlop et al. have investigated, using pressure recording paper, the peak pressure in the facet joints of lumbar FSUs tested in flexion and extension under physiological loading conditions. The averages of the reported measured peak pressures (Table 4-7) are significantly larger than the calculated average pressures.

Table 4-7: Average peak pressure (MPa) from 12 pairs of lumbar facet joints, measured with pressure-recording paper in different configuration of rotation in the sagittal plane, simulated by 1000 N in compressive load and 200 N to 400 N in shear load [15]

Facet	Flexion 4°	Neutral Position	Extension 4°	Extension 6°
Left	4.2	4.9	5.8	6.1
Right	3.2	4.2	5.9	6.1

In view of the geometric, material, and interaction approximations considered in the model (described in Sections 2.1.1, 2.2.1, and 2.3.3) the results obtained from the facet joints of the healthy model are reasonable.

4.7 Bulge of the Lower Disc

The radial bulge of the lower disc was investigated in the healthy model. The bulge was calculated at three characteristic locations of the disc, as shown on Figure 4-7, when simulated in axial pre-compression, flexion, extension, and right lateral bending. The results are reported in Table 4-8 and illustrated in Figure 4-8.

The experimental data available on lumbar disc bulge are typically generated from axial compressive forces. As a result, only the bulge resulting from pre-compression of the segment can properly be compared to clinical data.

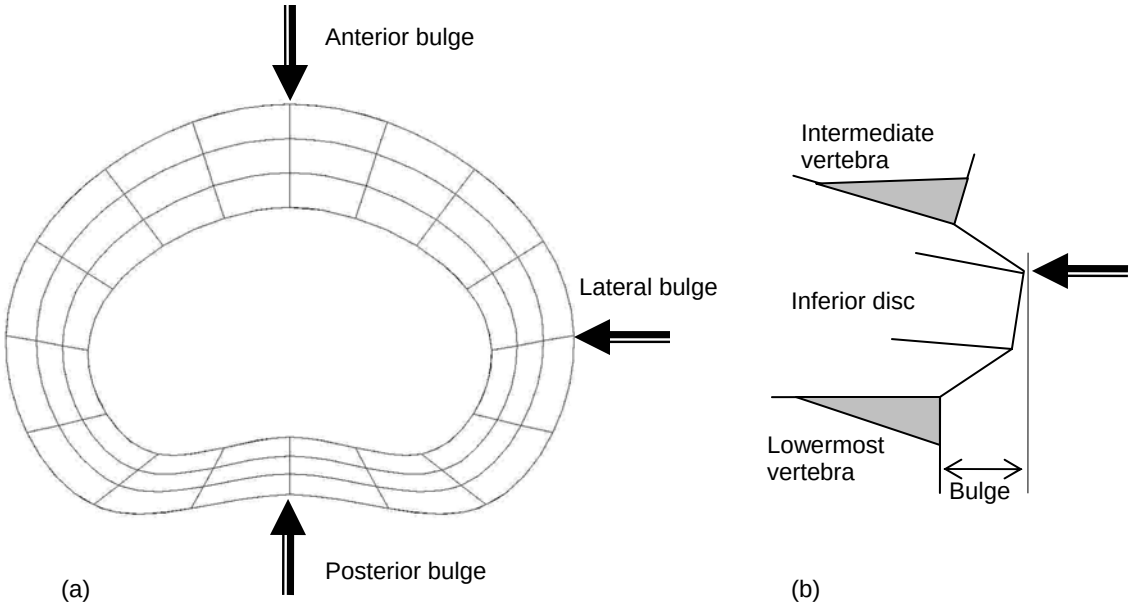

Figure 4-7: Location (a) and method (b) for the calculation of disc bulge

Shirazi-Adl et al. reviewed several studies related to the experimental measurement of disc bulge under axial compression [66]. For a compression of 720 N, as applied on the modeled segment for pre-compression, a bulge ranging from 0.4 to 1 mm is commonly reported. These figures match with the bulge calculated in the present model, which range from 0.4 mm for the lateral bulge to 0.7 mm for the posterior bulge under the same loading conditions (Table 4-8).

The same review shows a maximum reported bulge of approximately 2.5 mm under 2,500 N of compression. If we compare this result with the calculated bulge of the disc in flexion, for which the equivalent compressive load is 2,720 N, it appears that the model overestimates the bulge. Indeed, an anterior bulge of 3.9 mm and a posterior bulge of 2.5 mm were indicated by the model. This significant difference was expected, as described in Section 2.6, and can be accounted for by the simple geometric model of the

disc, with only three vertical layers of elements, as well as the absence of interaction between the disc and the ligaments, specifically the ALL and the PLL.

It is interesting to note in Figure 4-8 that the geometry of the annulus confers a bulge greater in a particular region of the posterior annulus (foraminal zone). This is particularly visible in extension and in lateral bending. According to clinical and analytical studies, annular tiers are more likely to occur in this area [23], gratifyingly consistent with the model.

Table 4-8: Lower disc bulge in the healthy model for different degrees of freedom, bold figures are exceeding 2 mm

Motion simulated	Anterior Bulge (mm)	Posterior Bulge (mm)	Right Lateral Bulge (mm)
Pre-compression	0.5	0.7	0.4
Flexion	**3.9**	**2.5**	1.7
Extension	0.4	1.8	1.1
Right Lateral Bending	1.3	1.9	**2.6**

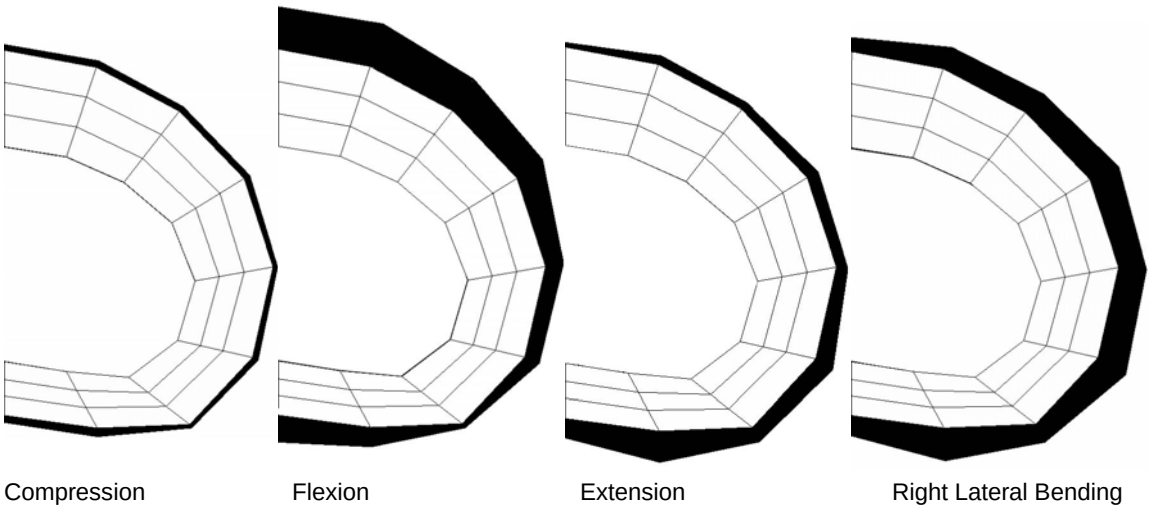

Figure 4-8: Illustration of the lower disc bulge from the healthy model for different degrees of freedom

CHAPTER 5

RESULTS

After presenting the results obtained through the simulation of the FE models, this chapter offers a discussion on the major outcomes of the study.

5.1 Results

The primary objective of this study is the comparison of the behavior of the surgically altered models relative to the behavior of the healthy model. Accordingly, the results of the fused and artificially restored models, referred to as ‘fused’ and ‘mobile’, respectively, are presented normalized to the results of the healthy model. The pertinence of the healthy model was investigated in Chapter 4 through the assessments of the FE analysis, which were compared with experimental data from the literature. The comparative results of the healthy and the surgically altered segments are presented in the following sections.

5.1.1 Mobility of Whole Segments and Individual FSUs

As intuitively expected, the mobility of the fused segment is significantly reduced by an average of 44% in the different rotational degrees of freedom (Figure 5-1). In contrast, the mobility of the mobile segment is excessive and shows an average increase of 52% in the different rotational degrees of freedom. The difference of mobility of the surgically altered segments, relative to the healthy segment, predominantly occurs in the upper FSU, where the prostheses are implanted (Figure 5-2). Fusion induces little change in the mobility of the lower healthy FSU (Figure 5-3). A maximum increase of 11% in flexion,

and a maximum decrease of 7% in extension are found. Arthroplasty, however, transfers a significant amount of its augmented mobility to the lower healthy FSU. Indeed, the mobility in the lower FSU is increased by 42% in extension and 32% in lateral bending (Figure 5-3), with an average of 25% in the different rotational degrees of freedom.

The variation of translational displacements in the lower healthy FSUs behave in the same fashion as the variation of the rotational displacements (Figure 5-4). The translational displacements remain similar in the fused and the healthy models. An average decrease of 7% is observed in the fused model for the sagittal translation in flexion and extension, and an increase of 2% is observed for the lateral translation in lateral bending. In the mobile model, however, a large average increase of 35% is found for the sagittal and lateral translation in flexion/extension and lateral bending, respectively.

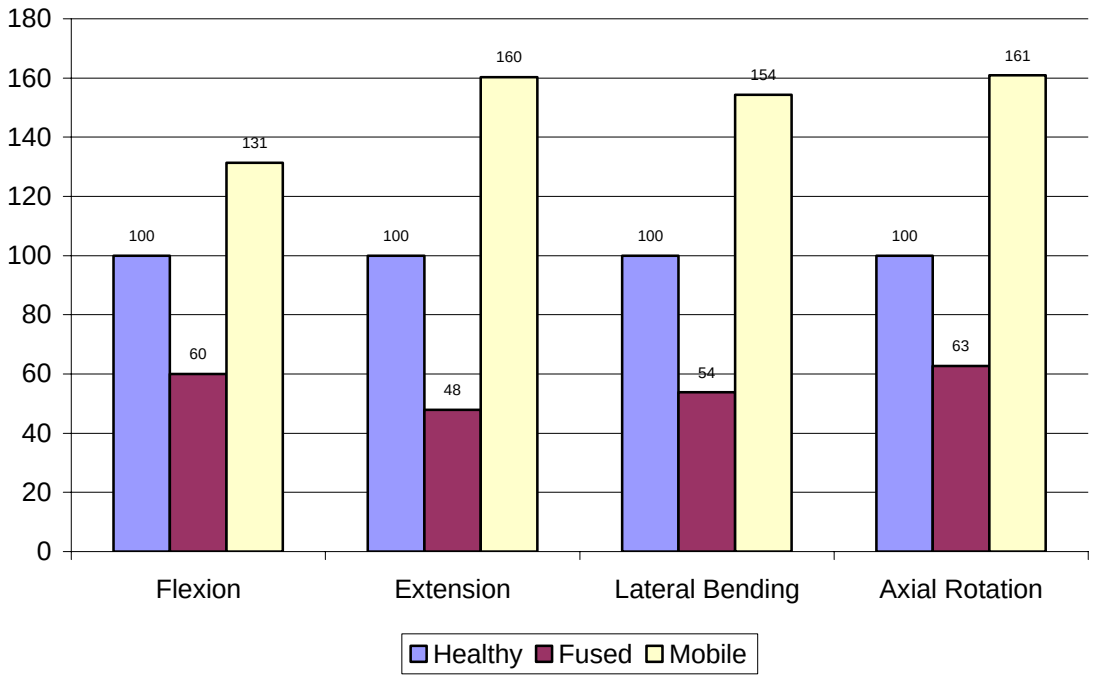

Figure 5-1: Comparison of mobility in the three modeled segments for the different rotational degrees of freedom; normalized to the results of the healthy model

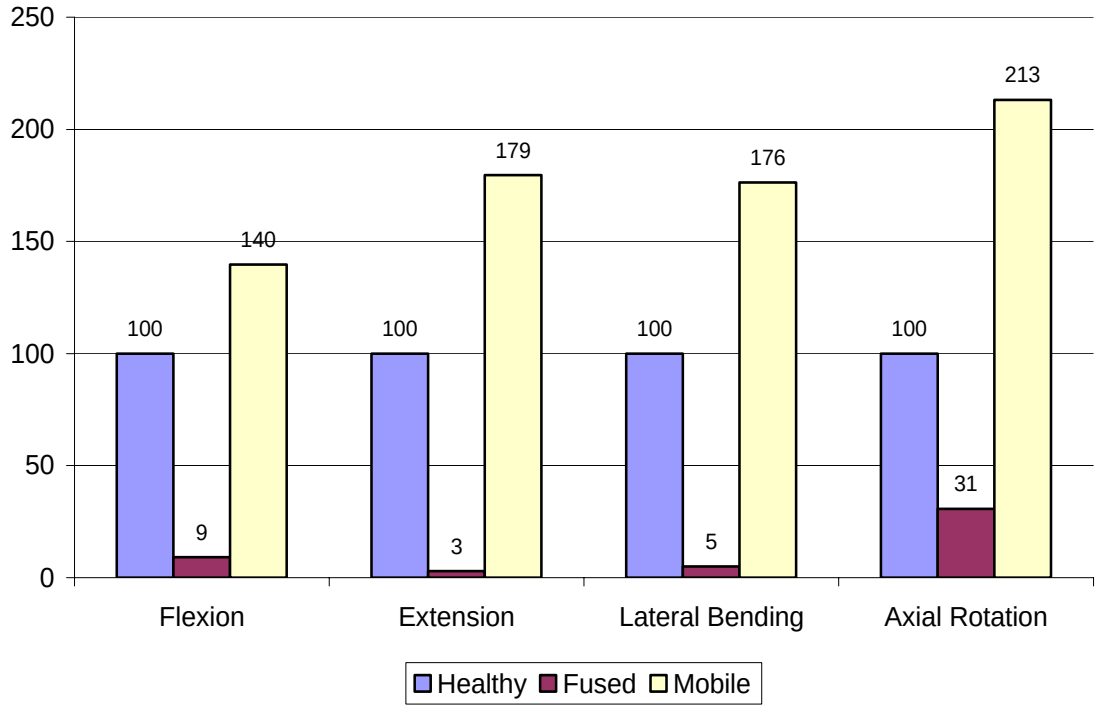

Figure 5-2: Comparison of mobility of the upper FSU in the three modeled segments for the different rotational degrees of freedom; normalized to the results of the healthy model

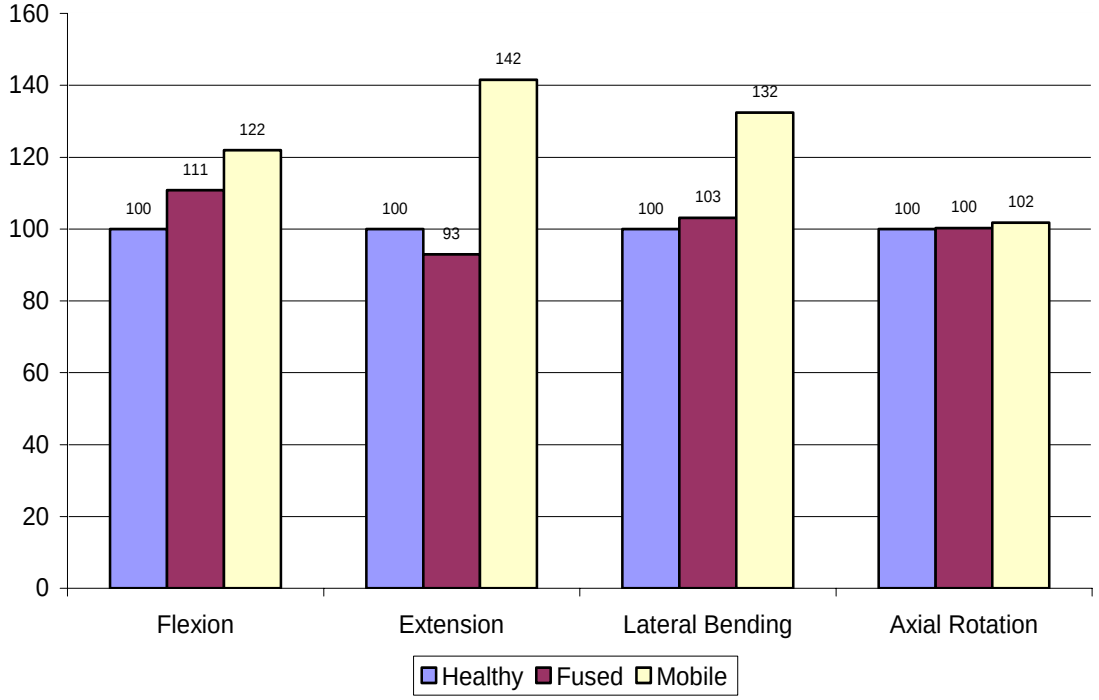

Figure 5-3: Comparison of mobility of the lower FSU in the three modeled segments for the different rotational degrees of freedom; normalized to the results of the healthy model

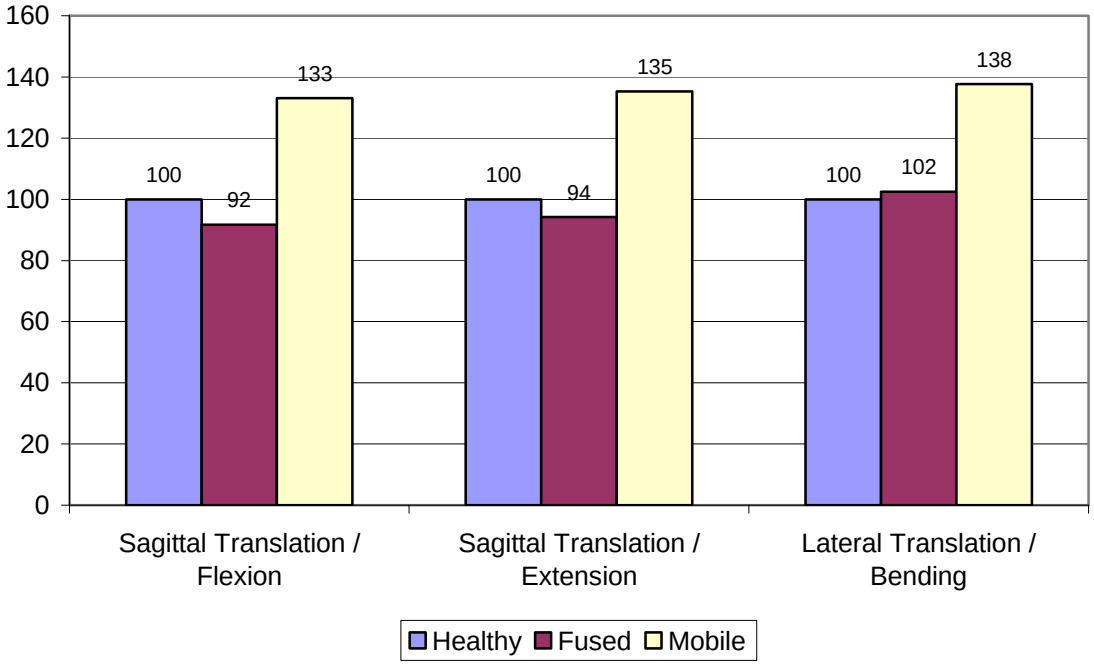

Figure 5-4: Comparison of main translational displacements of the lower FSU in the three modeled segments for the main rotational degrees of freedom; normalized to the results of the healthy model

To illustrate the comparison of the mobility of the surgically altered models to the mobility of the healthy model, graphic representations are proposed from Figure 5-5 to Figure 5-7.

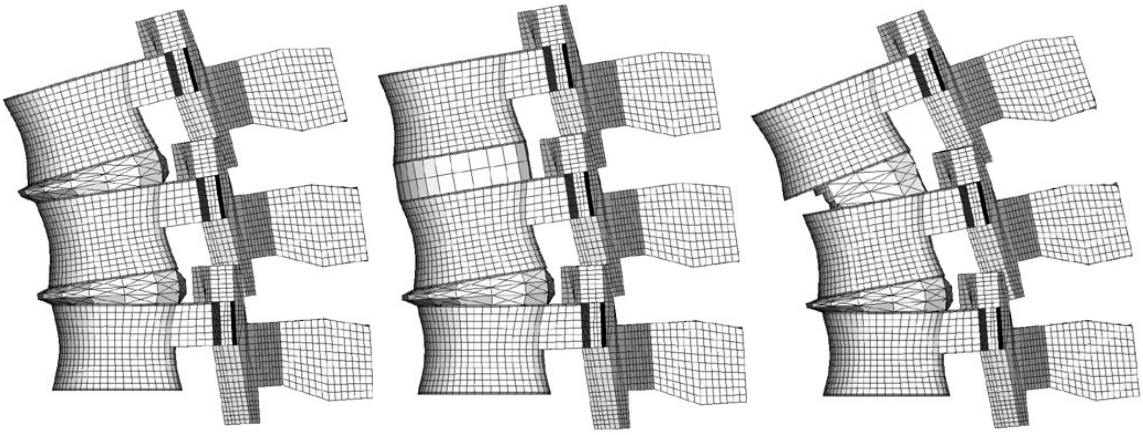

Figure 5-5: Illustration of flexion in the healthy, fused, and mobile models, respectively; the ligaments are not represented

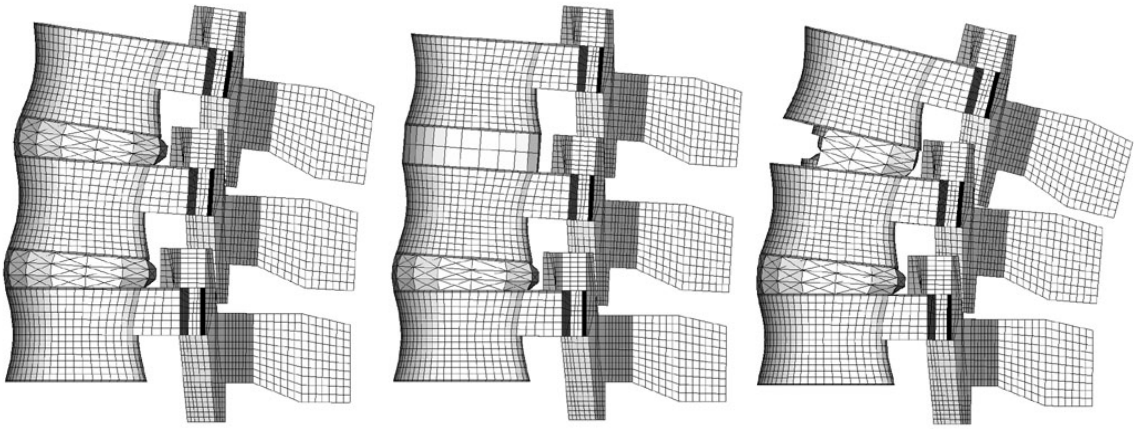

Figure 5-6: Illustration of extension in the healthy, fused, and mobile models, respectively; the ligaments are not represented

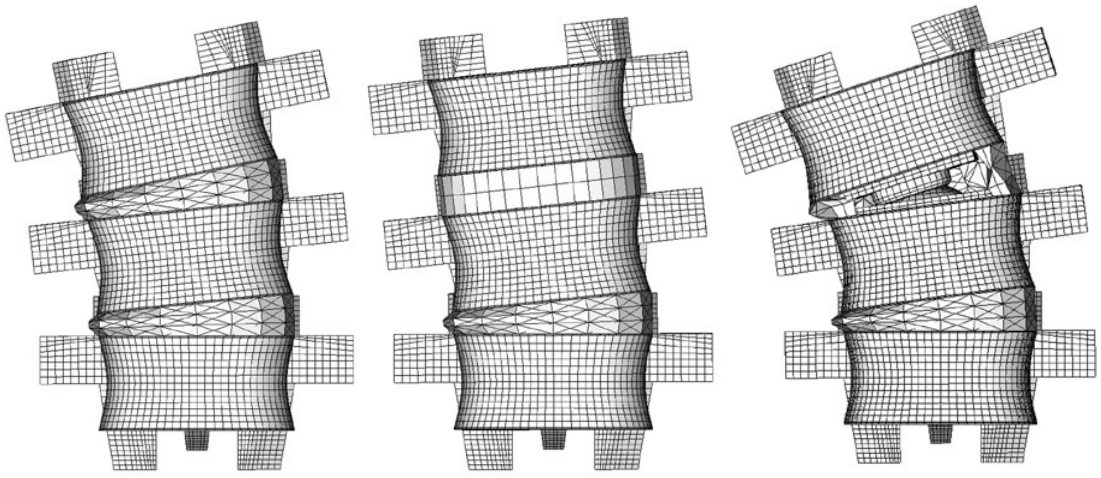

Figure 5-7: Illustration of lateral bending in the healthy, fused, and mobile models, respectively; the ligaments are not represented

5.1.2 Force in the Ligaments

The activity of the ALL and the PLL cannot be compared in the different configurations as their load is found to be zero for all the motions of the healthy model due to the calibration issue for the ligaments discussed in Section 4.3. The only significant force provided by these ligaments is 83 N in the upper PLL for the mobile model in flexion. The role of the TL is known to be negligible in the biomechanics of the lumbar spine and will not be analyzed in this section. The force provided by each ligament in the different configurations and different motions is provided in Table B-7.

The force generated in the intervertebral ligaments is generally decreased for the fused model in the different degrees of freedom. The only exception is a 28% increase in the force provided by the lower LF in flexion. In contrast, due to the important augmentation of mobility in the mobile model, the force generated in the intervertebral ligaments for this configuration is considerably amplified. Four ligaments experience a force that exceeds their expected failure load reported in Table 2-2. These ligaments are the lower right CL in right lateral bending (maximum force of 292 N, expected failure at 384 N), the left and right upper CLs in extension (maximum force of 503 N each), and the upper ISL in flexion (maximum force of 145 N, expected failure at 130 N). The rupture or avulsion of a ligament upon reaching its failure load was not taken into consideration in the model. As a consequence, other components of the mobile segment might be subject to failure after the loss of the force provided by the affected ligaments.

The role of the SSLs is major in flexion. The induced force in these ligaments is largely increased in the mobile model, by a maximum of 120% for the upper SSL in flexion, in which the force reaches 195 N (Figure 5-8). In the same conditions, the force

in the SSL of the lower FSU also increases considerably, by 64%, and attains 113 N (Figure 5-9). The reported increase in the force on the SSLs for the mobile model in axial rotation appears also very large on a relative scale but is actually not significant. This contrasts sharply with the negligible forces on the SSLs in the healthy model in axial rotation (<1.43 N).

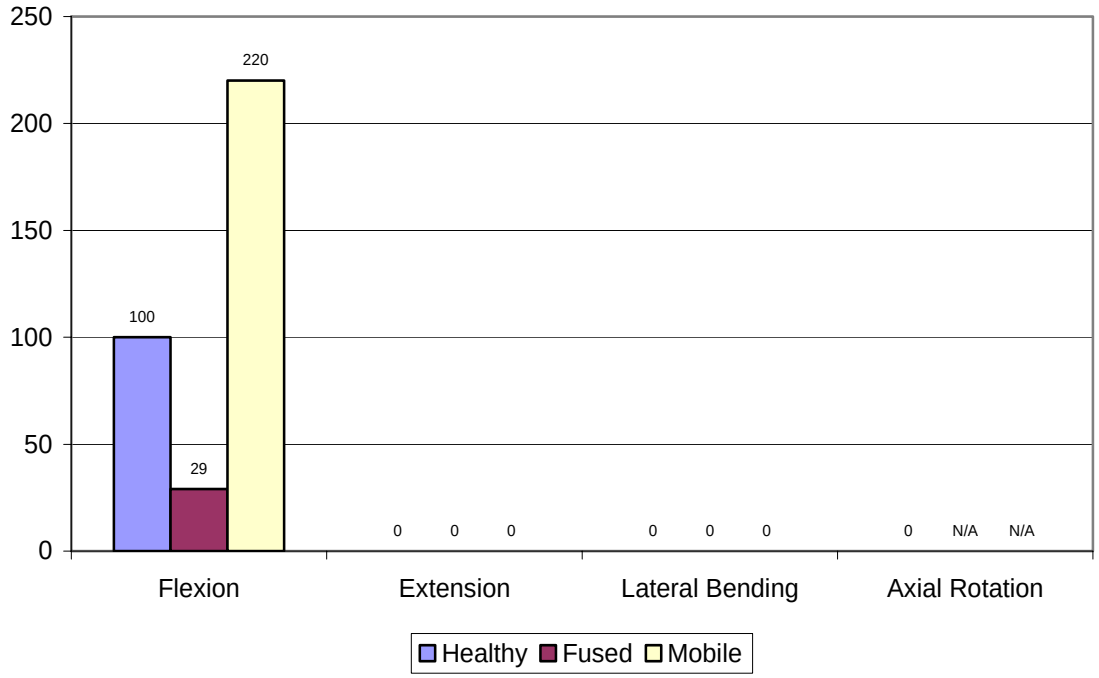

Figure 5-8: Comparison of the force in the upper SSL in the three modeled segments for the different rotational degrees of freedom; normalized to the results of the healthy model

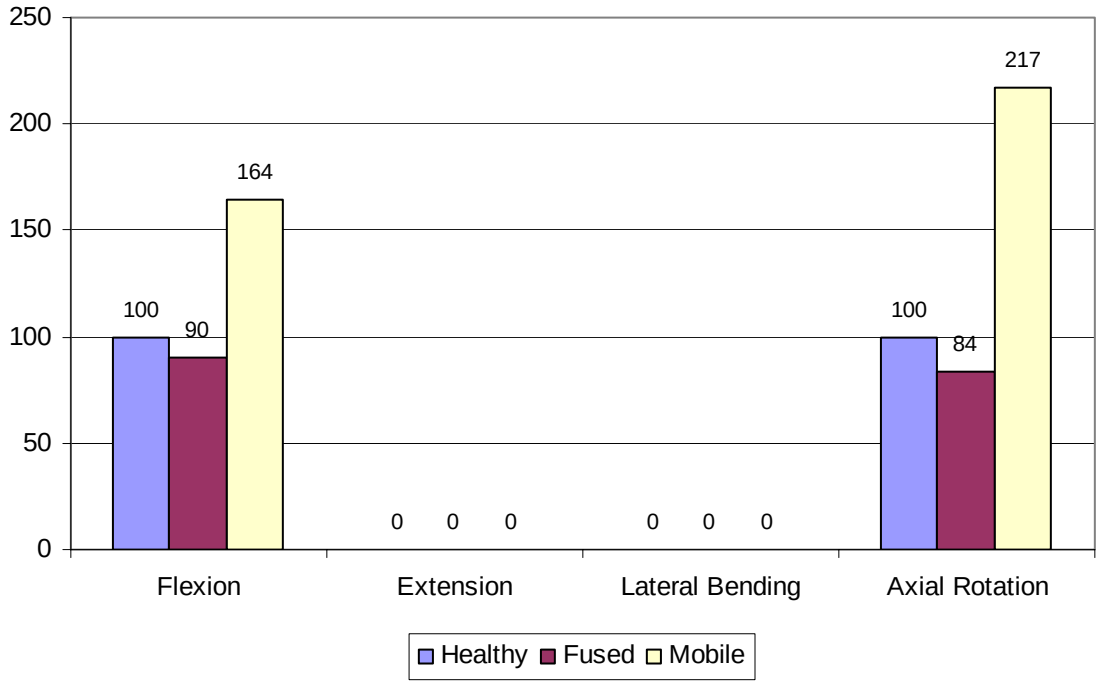

Figure 5-9: Comparison of the force in the lower SSL in the three modeled segments for the different rotational degrees of freedom; normalized to the results of the healthy model

In the same manner, the difference of force found for the ISLs between the healthy and the mobile models is large, on a relative scale, for axial rotation (Figure 5-10 and Figure 5-11) but is not relevant to large loads as they remain below 18.32 N. The significant result for the ISLs is the increase of 70% in the force on the upper ISL of the mobile model in flexion, for which the force, of 145 N, exceeds the expected failure load of 130 N.

The role of the CLs is considerable in the mobile model than in the healthy model (Figure 5-12 to Figure 5-15). Below 13 N for the healthy model in flexion, the force on the CLs shows an increase of up to 1,429% in the upper FSU of the mobile model (Figure 5-12 & Figure 5-13), although, the force in the CLs does not exceed 140 N. The increase in the force of the CLs has more repercussions in extension. The force on the lower CLs in the mobile model in extension is increased by approximately 94% and the loads reach 252 N (Figure 5-14 & Figure 5-15). The force on the upper CLs is even greater, the loads reaching 503 N, an increase of 132%, and exceeding the failure load of a CL (Figure 5-12 & Figure 5-13). The right capsular ligaments are also significantly involved in right lateral bending. In the mobile model, an increase of 63% in the force on the lower right CL leads to a force of 293 N, which exceeds the failure load of the ligament (Figure 5-15).

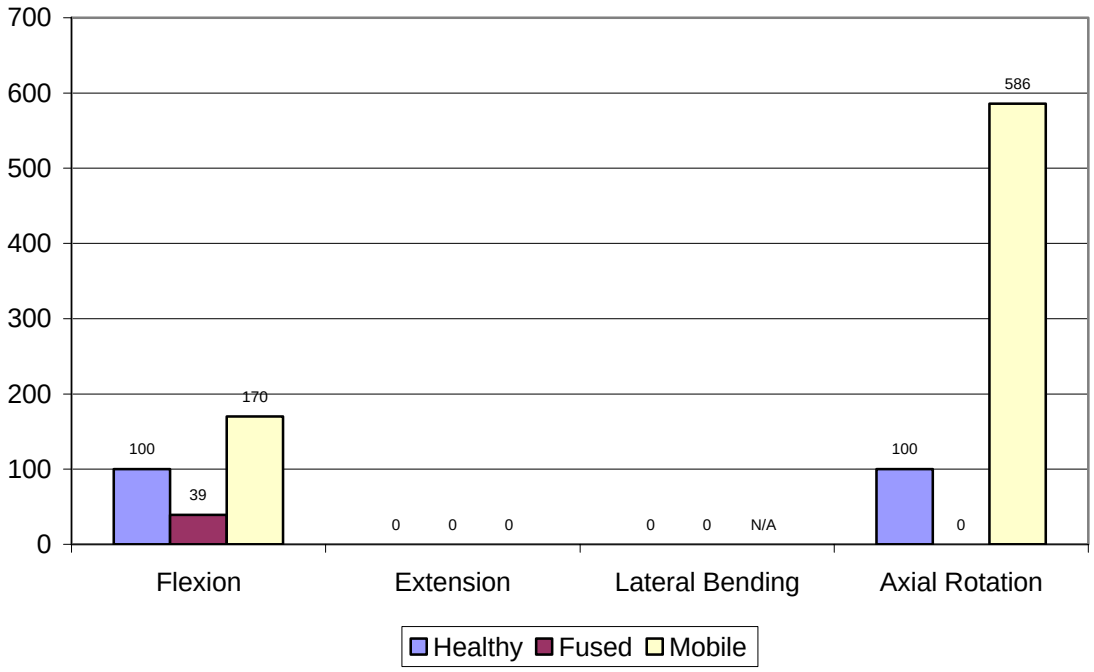

Figure 5-10: Comparison of the force in the upper ISL in the three modeled segments for the different rotational degrees of freedom; normalized to the results of the healthy model

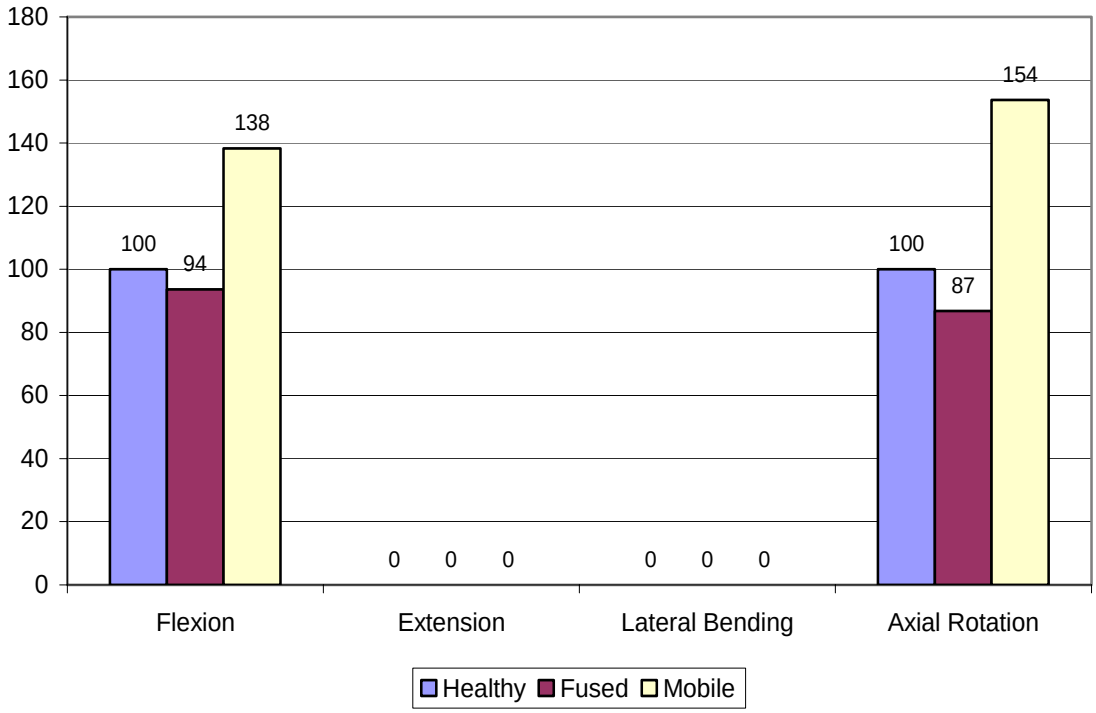

Figure 5-11: Comparison of the force in the lower ISL in the three modeled segments for the different rotational degrees of freedom; normalized to the results of the healthy model

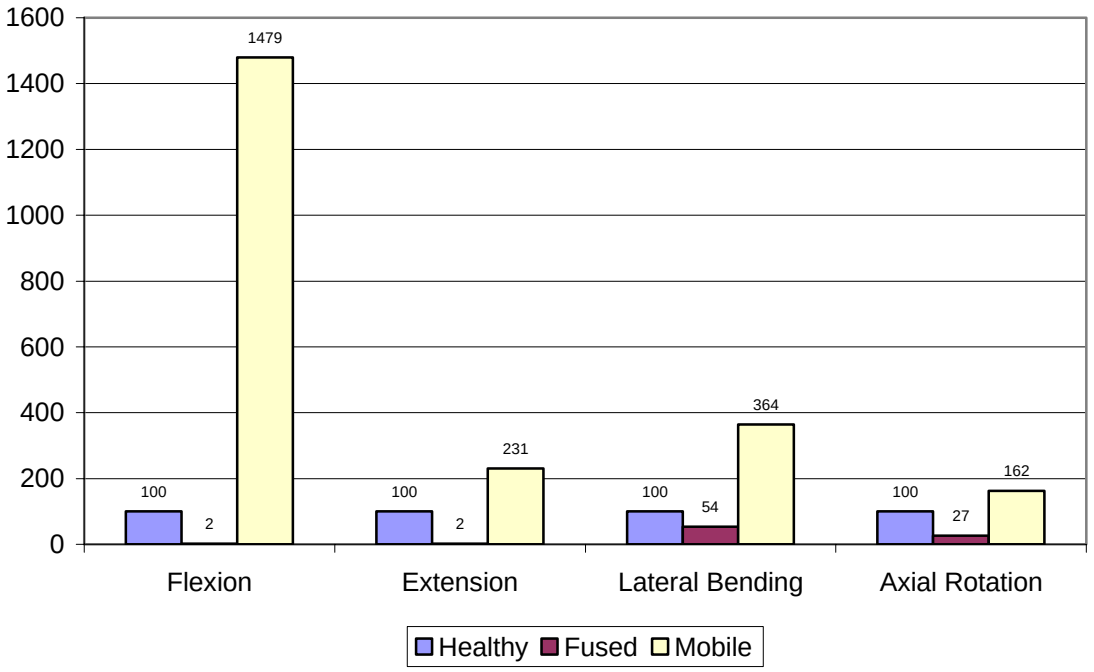

Figure 5-12: Comparison of the force in the upper left CL in the three modeled segments for the different rotational degrees of freedom; normalized to the results of the healthy model

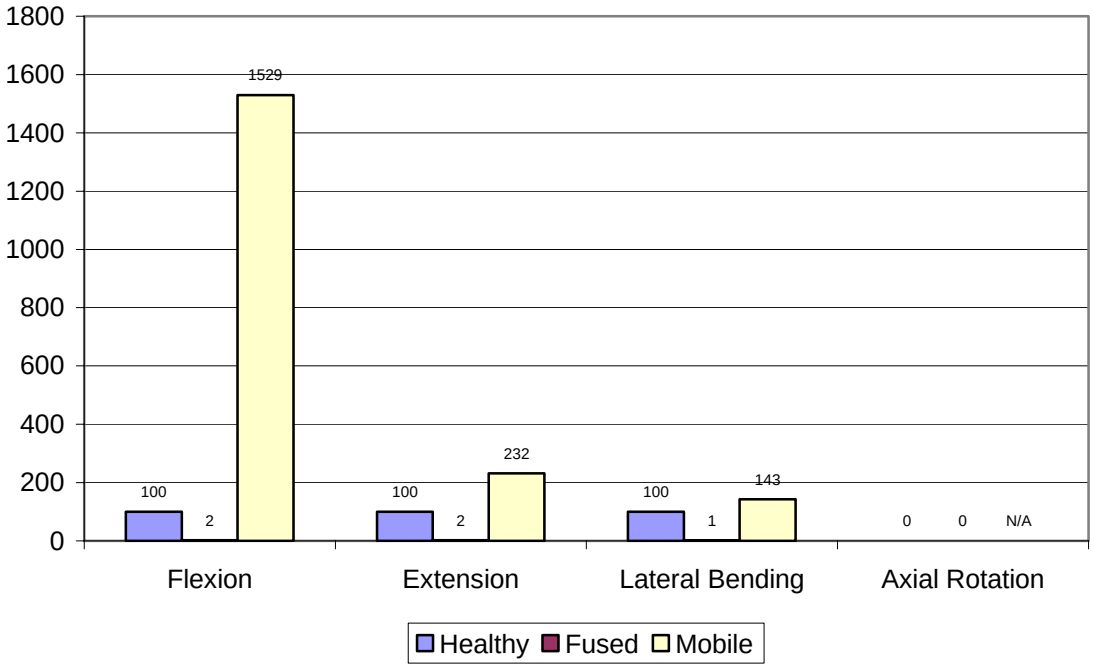

Figure 5-13: Comparison of the force in the upper right CL in the three modeled segments for the different rotational degrees of freedom; normalized to the results of the healthy model

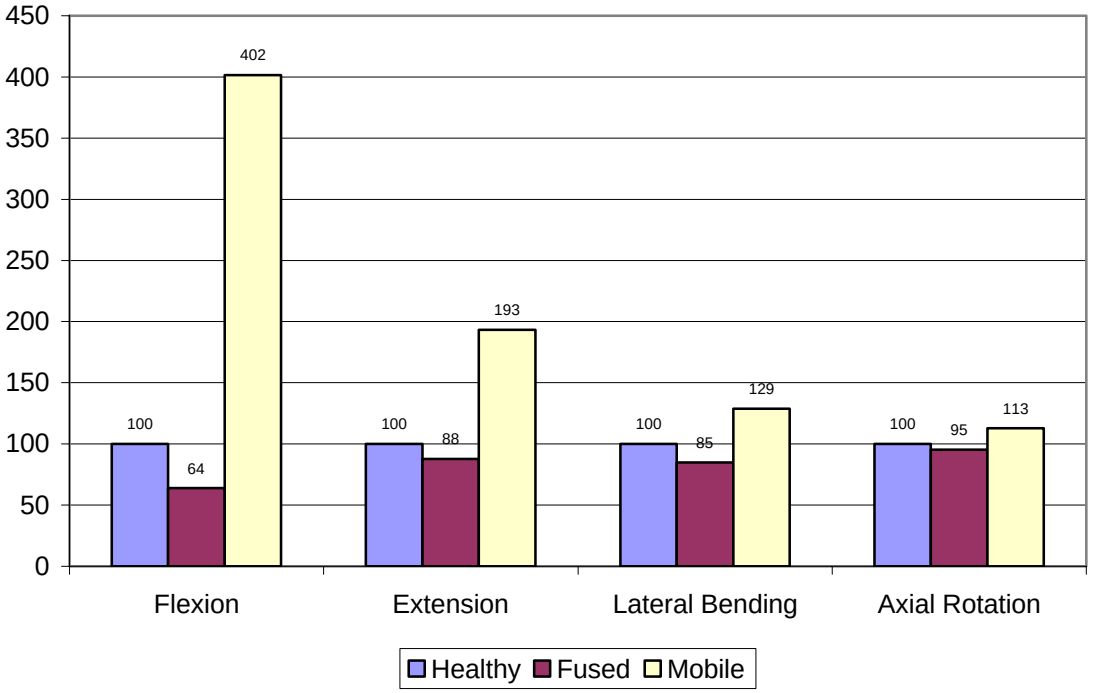

Figure 5-14: Comparison of the force in the lower left CL in the three modeled segments for the different rotational degrees of freedom; normalized to the results of the healthy model

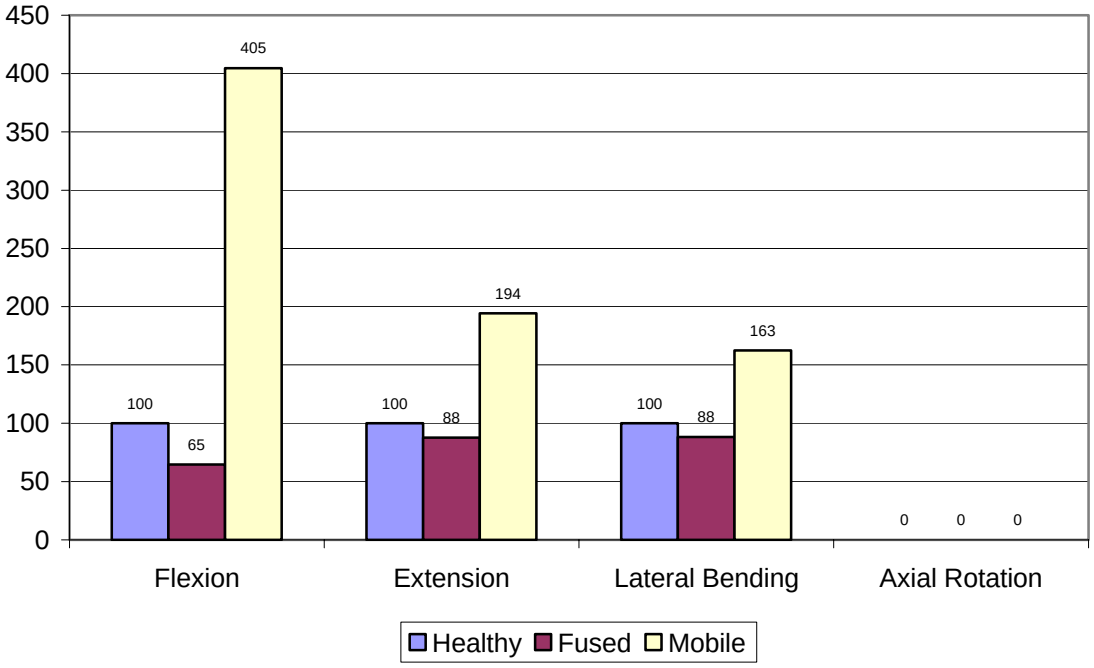

Figure 5-15: Comparison of the force in the lower right CL in the three modeled segments for the different rotational degrees of freedom; normalized to the results of the healthy model

In conclusion, four ligaments from the mobile model, illustrated in Figure 5-17, showed risks of potential failure (upper ISL in flexion, upper left and right CL in extension, and lower right CL in right lateral bending). The calculated forces in those ligaments are compared in Figure 5-16, normalized to their expected failure load. For the upper ISL in flexion and the lower right CL in lateral bending, the calculated force only exceeds the failure load by 12% and 3%, respectively. This underlines the risks of failure but does not stand as a critical result. The upper CLs, however, showed a calculated load that exceeds the expected failure load by 77%. This observation reveals a high probability of rupture of the upper CLs from the mobile model in extension.

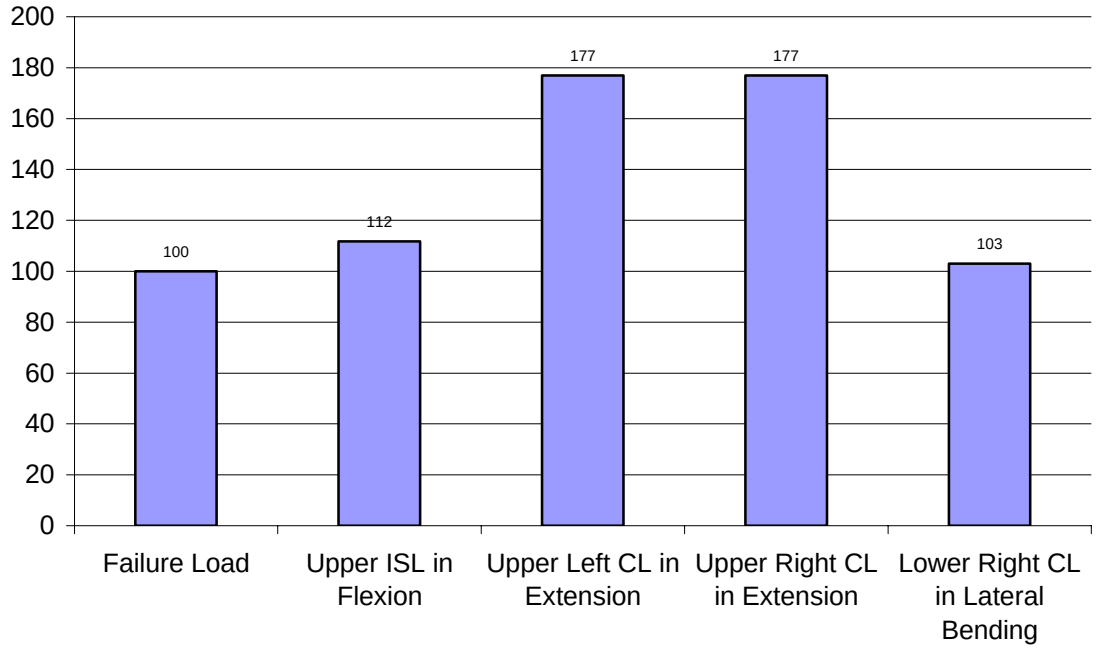

Figure 5-16: Comparison of the calculated maximum forces on the ligaments of the mobile model which force exceeds the failure load, data normalized to the ligaments' failure loads

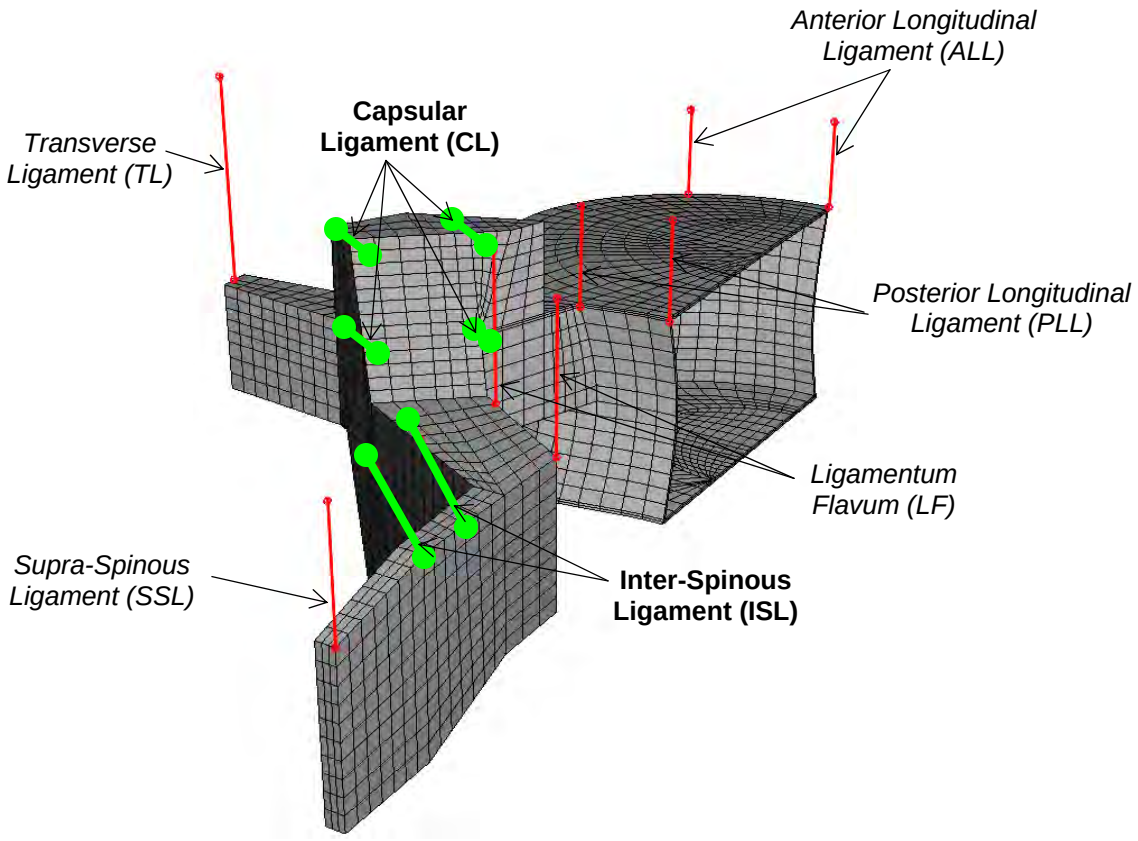

Figure 5-17: Illustration of the ligaments (in green) which calculated force exceeds the expected failure load in the mobile model (upper ISL in flexion, upper left and right CL in extension, and lower right CL in right lateral bending)

5.1.3Force and Pressure on the Articular Facets

The data concerning the force and the equivalent average compressive pressure in each facet joints of the three models are summarized in Table B-8. The forces transmitted through the facet joints remain consistent for the lower FSU of the fused model (Figure 5-22 & Figure 5-24) and do not exceed 145 N on the lower right facet joint in right lateral bending. A large relative difference (~4,500%) between the forces transmitted through the lower facet joints in the healthy and fused models is only caused

by an increase of 40 N in the fused configuration, which appears large compared to the small relative load in the healthy configuration. In the mobile model, the differences are much more significant in an absolute sense. Large increases of load were shown in the facets of the upper FSU in flexion and lateral bending (Figure 5-18 & Figure 5-20). In particular, the load in the upper facets reaches 365 N in the mobile model in flexion, compared to 115 N in the healthy model. The articular facets of the upper FSU do not do not contact and lose their functionality in the mobile model in extension and the load transmitted becomes zero.

It is more relevant to investigate the response of the facets through the pressure involved in the joints instead of the load transmitted. Indeed, the equivalent average pressure in a joint does not vary proportionally to the related load as the contact area also changes with respect to orientation of the FSU. The increase of pressure in the joints is usually smaller than the load for both fused and mobile models (see Figure 5-18 to Figure 5-25). The only exception is on the lower facets of the mobile model in extension, for which the load increases by 27%, and the related average pressure increases by approximately 155%, reaching about 2.5 MPa (Figure 5-22 to Figure 5-25). In comparison to the healthy model, the upper FSU of the mobile model shows significant increases of pressure in the upper facets. The pressure attains 5.5 MPa in both upper facets in flexion and 3.3 MPa in the upper right facet in right lateral bending (Figure 5-19, Figure 5-21, Table B-8). These values exceed the characteristic ultimate failure stress of 3 MPa for the articular cartilage [5].

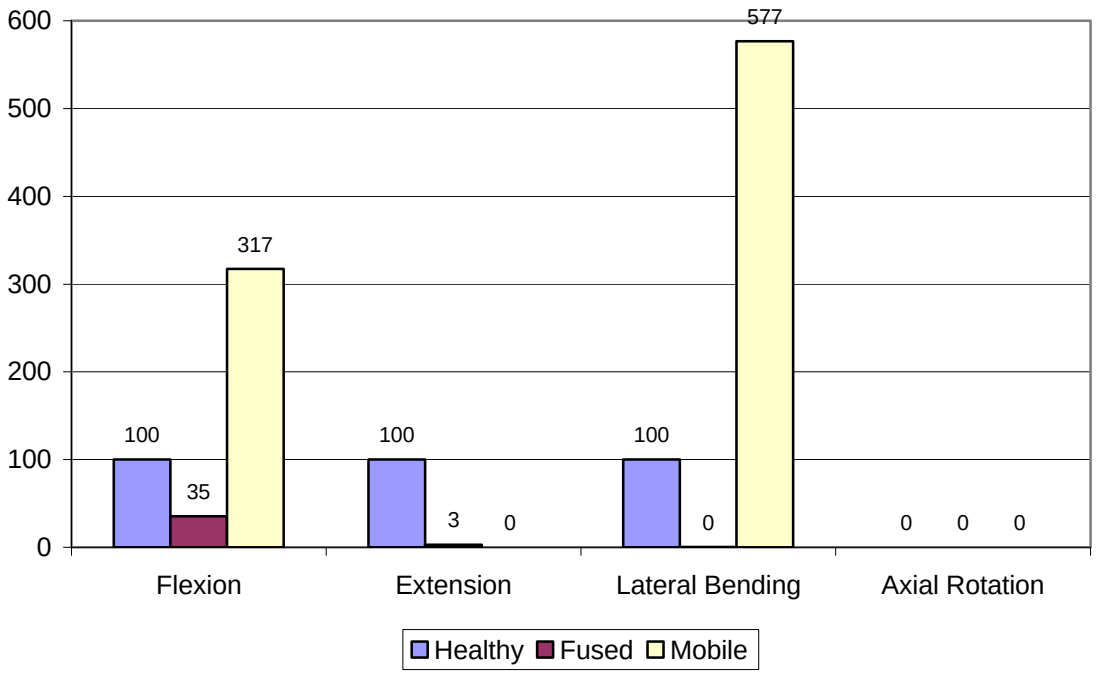

Figure 5-18: Comparison of the force transmitted through the upper left articular facets in the three modeled segments for the different rotational degrees of freedom; normalized to the results of the healthy model

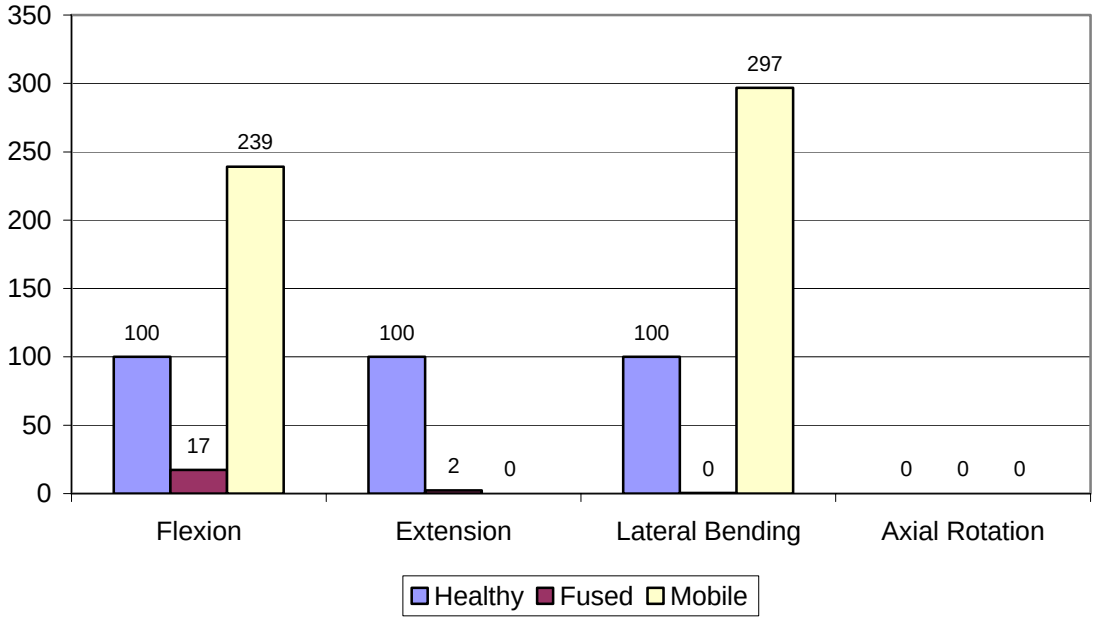

Figure 5-19: Comparison of the equivalent average pressure on the upper left articular facets in the three modeled segments for the different rotational degrees of freedom; normalized to the results of the healthy model

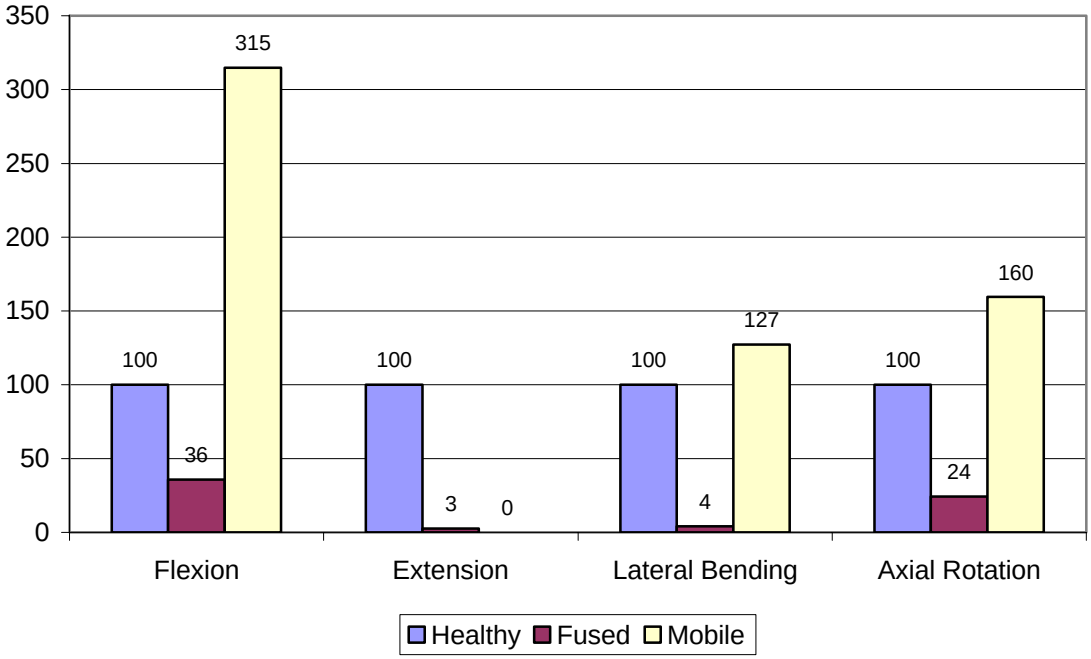

Figure 5-20: Comparison of the force transmitted through the upper right articular facets in the three modeled segments for the different rotational degrees of freedom; normalized to the results of the healthy model

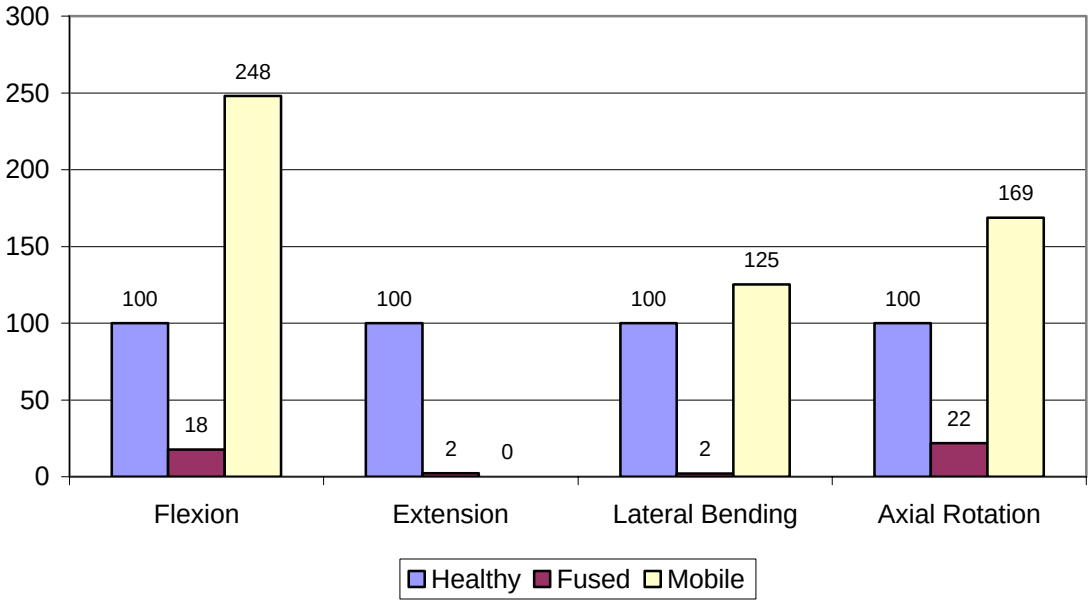

Figure 5-21: Comparison of the equivalent average pressure on the upper right articular facets in the three modeled segments for the different rotational degrees of freedom; normalized to the results of the healthy model

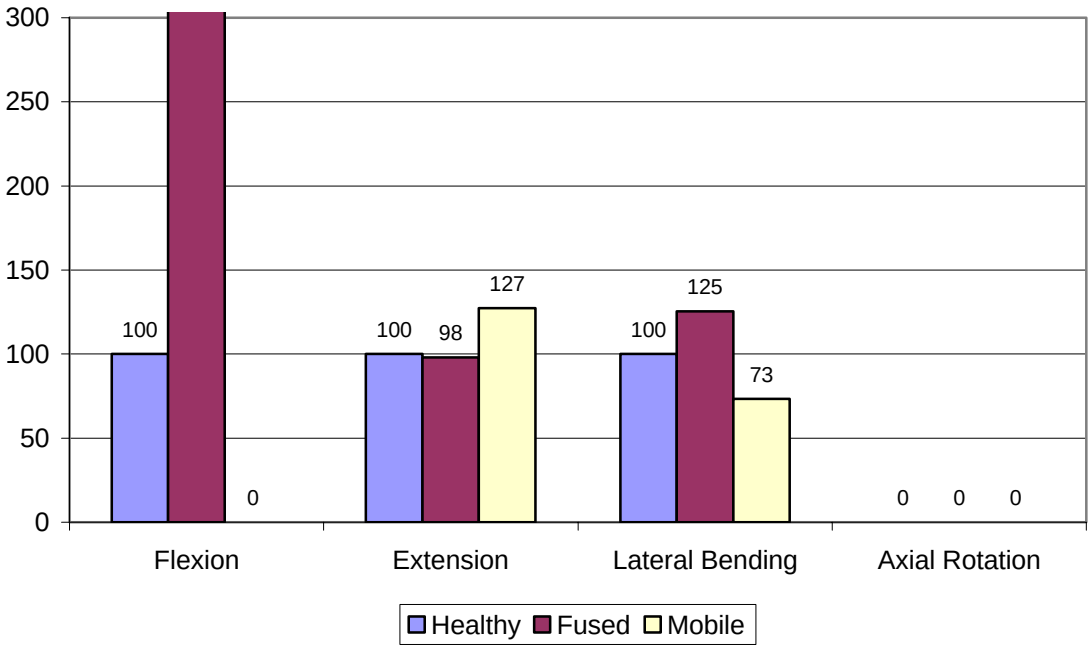

Figure 5-22: Comparison of the force transmitted through the lower left articular facets in the three modeled segments for the different rotational degrees of freedom; normalized to the results of the healthy model *(the relative value for the fused model in flexion is 4648)*

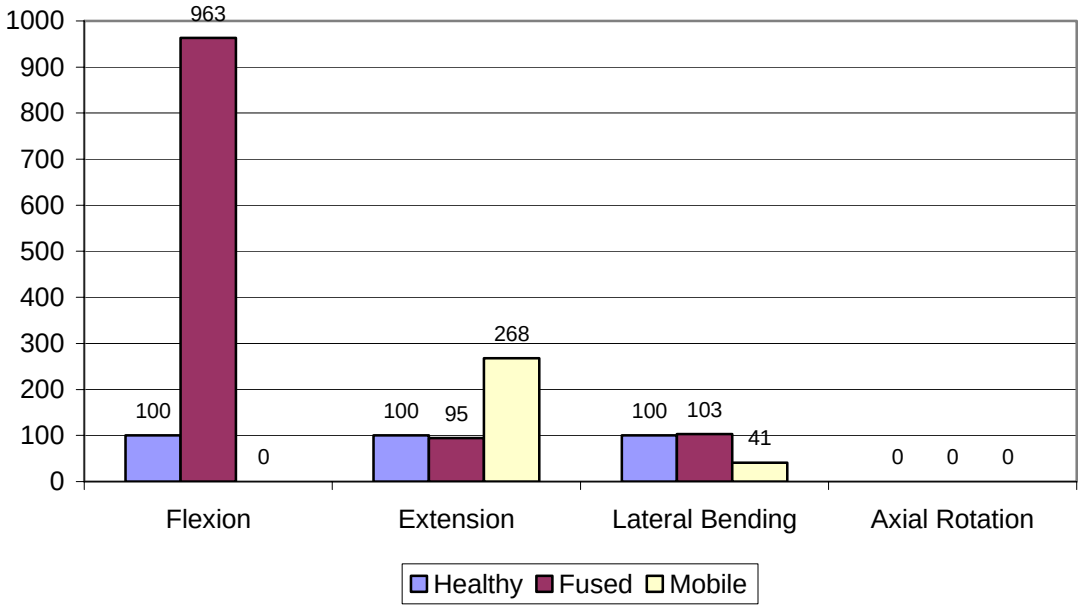

Figure 5-23: Comparison of the equivalent average pressure on the lower left articular facets in the three modeled segments for the different rotational degrees of freedom; normalized to the results of the healthy model

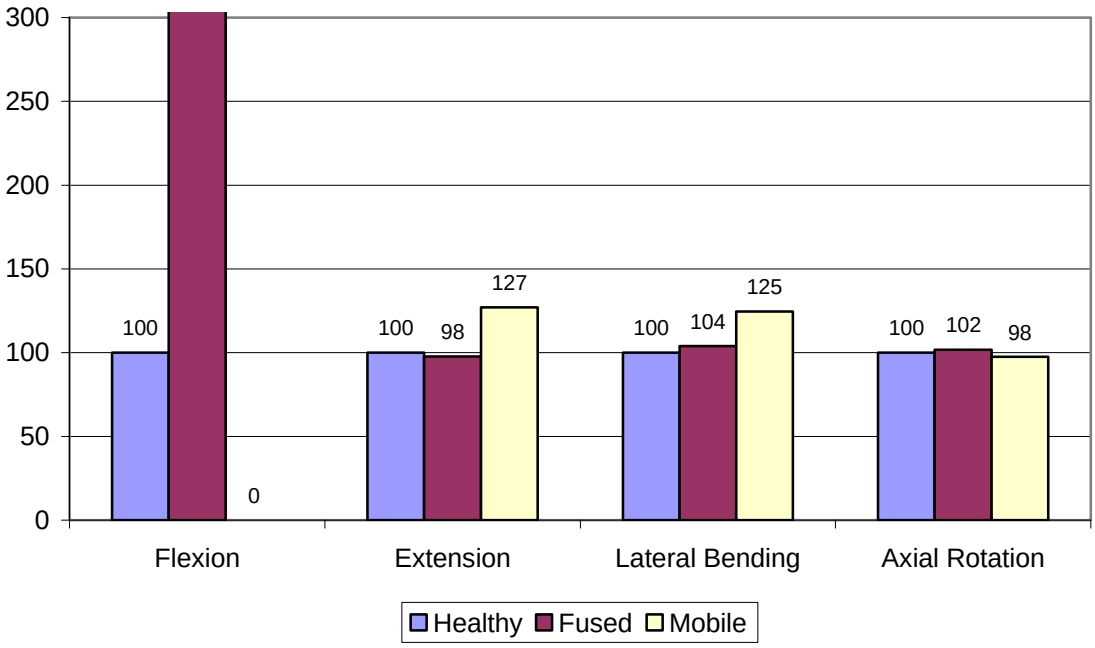

Figure 5-24: Comparison of the force transmitted through the lower right articular facets in the three modeled segments for the different rotational degrees of freedom; normalized to the results of the healthy model *(the relative value for the fused model in flexion is 4557)*

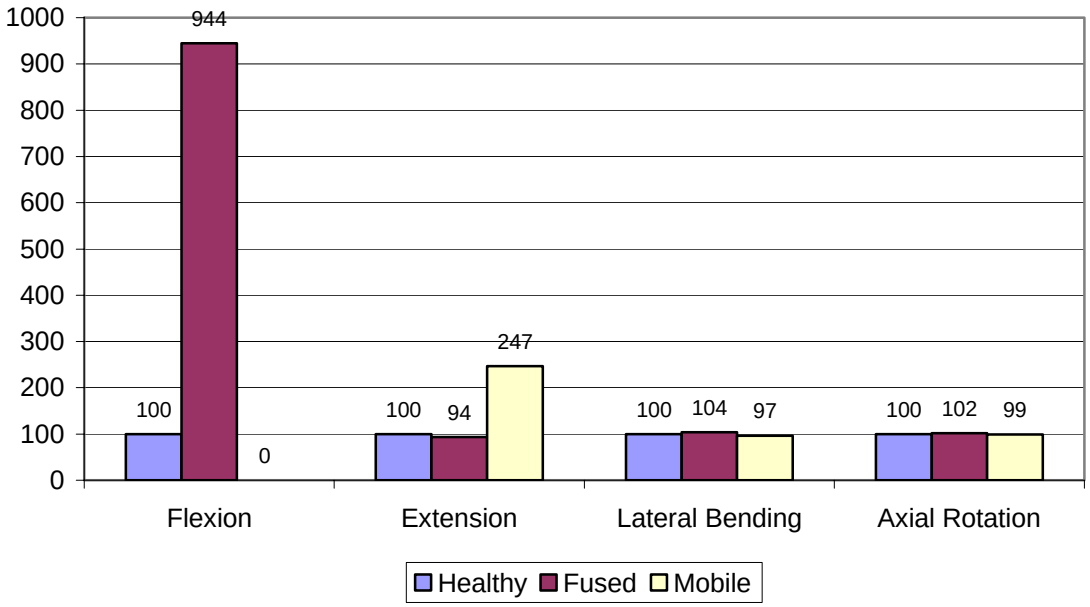

Figure 5-25: Comparison of the equivalent average pressure on the lower right articular facets in the three modeled segments for the different rotational degrees of freedom; normalized to the results of the healthy model

5.1.4 Bulge of the Adjacent Underlying Healthy Disc

Using the same technique described in section 4.7, the bulge of the lower healthy disc has been investigated and compared. Table B-9 to Table B-11 summarize the anterior, posterior, and right lateral bulge of the lower healthy disc in the three models in compression, flexion, extension, and right lateral bending. The relevant data, i.e. the anterior bulge in flexion, the posterior bulge in extension, and the right lateral bulge in right lateral bending, are illustrated in Figure 5-26.

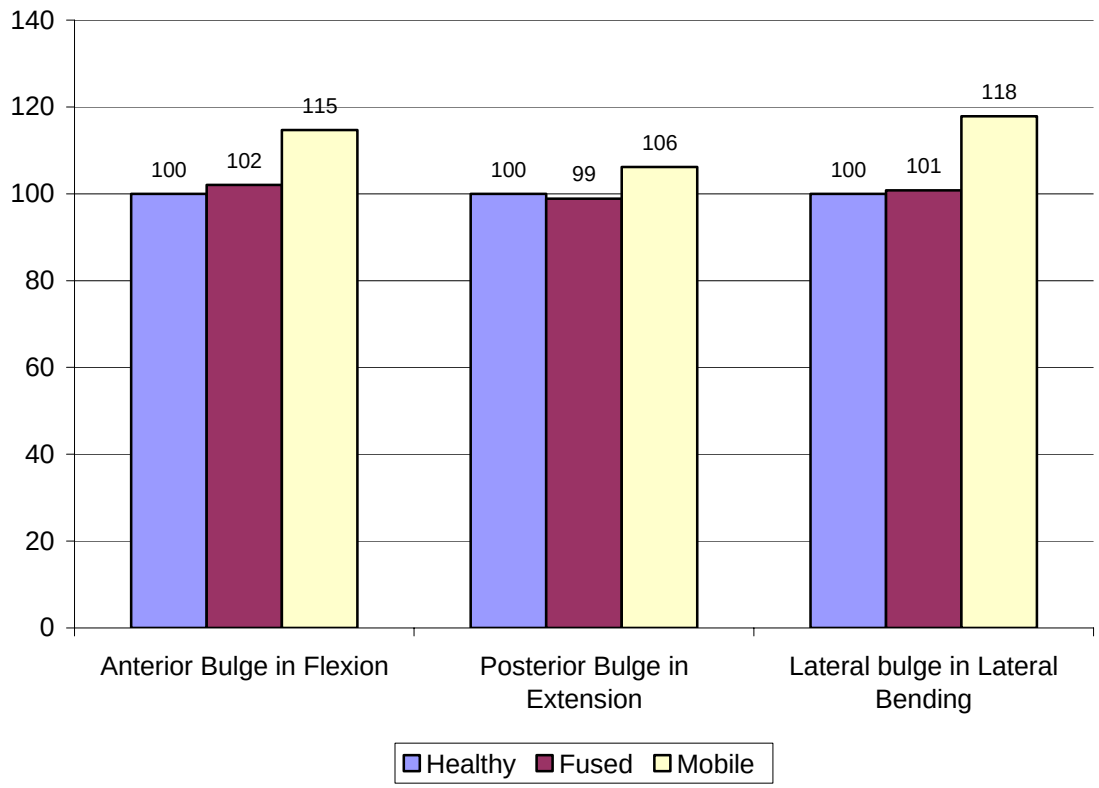

Figure 5-26: Comparison of the bulge of the lower healthy disc in the relevant directions for flexion, extension, and right lateral bending; normalized to the results of the healthy model

In general, the bulge of the lower healthy disc does not vary significantly from the healthy to the fused models, with a maximum increase of 2% for the anterior bulge in flexion. In the mobile model, it increases from 6% for the posterior bulge in extension, up to 18% for the right lateral bulge in right lateral bending.

With respect to the calculation method, the bulges reported are a function of the amount of the related rotational mobility (Figure 5-3) as well as the amount of the related translational mobility (Figure 5-4). Thus, the anterior bulge of the lower FSU of the fused model in flexion only increases by 2% (Figure 5-26). The 2% arises from a corresponding increase of 11% in the rotational mobility in flexion (Figure 5-3), and a reduction of 8% in the postero-anterior sagittal translation (Figure 5-4). This combination limits the augmentation of the reported anterior disc bulge in the lower FSU of the fused model.

5.1.5 Stresses in the Adjacent Underlying Disc

As discussed in Section 4.5, some truss elements in the intervertebral discs, which model the annulus fibers, reveal unrealistic high tensile stresses due to some of the approximations made in the geometrical modeling (Section 4.5). Those elements are fairly easy to identify. However, it is impossible to determine accurately the value of the maximum relevant Von Mises stress in the annulus fibers of the lower healthy disc. Therefore, in order to compare the stress of the annulus fibers of the lower disc in the three configurations, it was chosen to calculate the average stress in the fibers of each annulus. The comparative results and the related data are reported in Figure 5-27 and Table B-12, respectively.

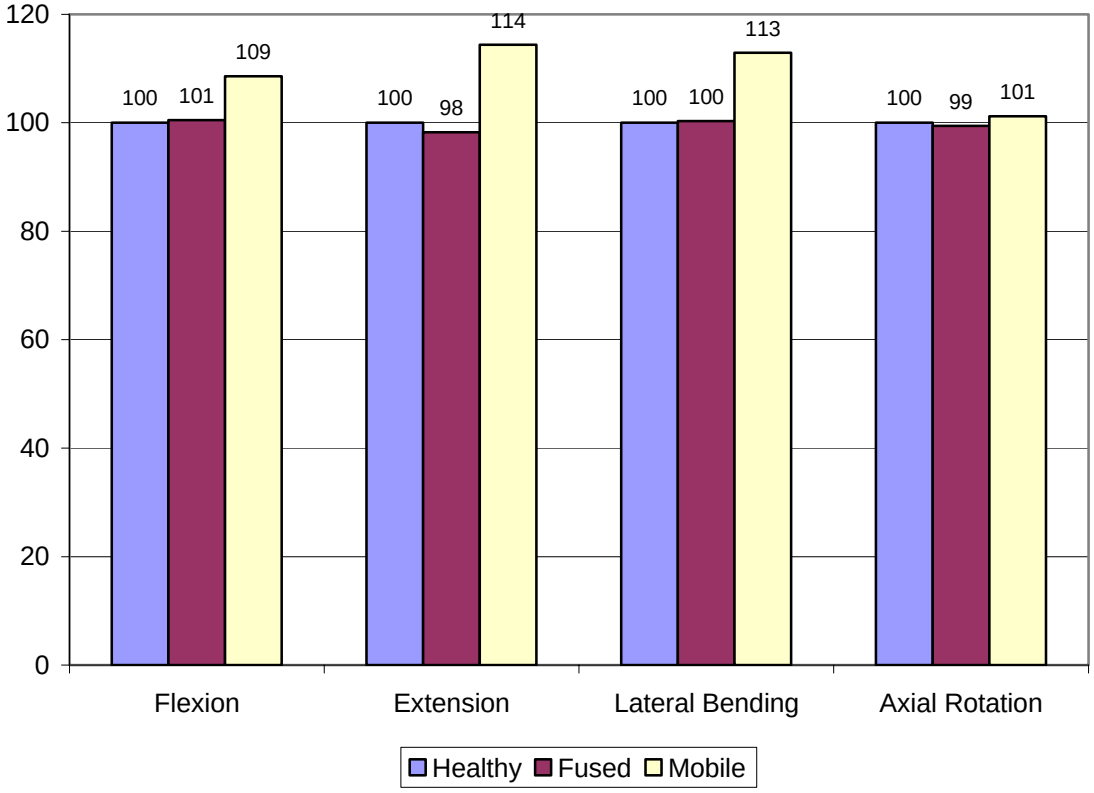

Figure 5-27: Comparison of the average Von Mises stress in the fibers if the lower healthy annulus in the three modeled segments for the different rotational degrees of freedom; normalized to the results of the healthy model

The changes in the average and maximum Von Mises stresses in the fibers of the lower annulus vary approximately in the same fashion. The differences between the healthy and the fused models are negligible. The increase of stress in the fibers of the lower annulus in the mobile model ranges from 9% to 14% in flexion, extension, and lateral bending. The maximum relevant Von Mises stress in the healthy model, reported in Section 4.5, is approximately 25 MPa. Compared to the estimated failure stress of 46 MPa, discussed in Section 4.5, the admissible increase of stress before failure of the

fibers in the lower annulus would be approximately 84%. As a consequence, the underlying adjacent annulus fibers do not seem to be endangered, from a static point of view, by the modeled surgical solutions of arthroplasty and arthrodesis.

It is interesting to note that the variation of the stress in the fibers of the lower annulus, for the different configurations and rotational degrees of freedom, is similar to the variation of the maximum disc bulge (Figure 5-26). This shows a significant correlation between the stress of the annulus fibers and the bulge of the disc.

A limitation of the model, discussed in Section 2.6, concerning the pressure in the disc was confirmed. Due to geometric and material models used in the study, the pressure in the discs is not homogeneous as would be expected in vivo. The pressure in the nucleus is significantly low, resulting from the weak mechanical properties used (Table 2-1), and do not exceed 0.05 MPa in all configurations and motions. In the annulus ground substance, where the pressure is not homogeneous, the maximum pressures, reported in Table B-13, are more important than the expected disc pressure (Figure 3-2) and reach up to 3.2 MPa in the anterior section of the lower disc of the mobile model in flexion. This is due to the fact that the hydrostatic pressure in the disc is not taken into consideration. As a consequence, the annulus, which is stiffer than the nucleus, bears most of the loads and displays greater pressures.

5.1.6 Stresses in the Vertebrae

Ignoring the unrelated peak stresses mentioned in Section 4.5, it is possible to estimate the variation of the maximum Von Mises stress in the main bony components of the vertebrae, namely the cortical and the cancellous bones.

Concerning the cancellous bone, the maximum Von Mises stress reported for the fused model is similar to the healthy model and does not exceed 3.5 MPa. The maximum stress is reached on the anterior section of the lower cancellous bone in flexion. In the mobile model, however, a new peak stress occurs, resulting from the presence of the artificial intervertebral disc. The Von Mises stress reaches a maximum of approximately 9 MPa on the anterior region of the interface between the lower plate of the artificial disc and the upper vertebral endplate of the intermediate vertebra in flexion. According to the failure stresses for the cancellous bone given in Table 4-3, specifically the value of 8.2±2.6 MPa, failure of the cancellous bone may occur in the mobile model. This may result in the subsidence of the artificial intervertebral disc into the adjacent vertebrae.

The relevant maximum Von Mises stress in the cortical bone of the fused model remains similar to the healthy model and reaches approximately 90 MPa on the anterior wall of the lowermost vertebral body in flexion. In the mobile model, the same area is also subject to the maximum stress, which reaches approximately 110 MPa in flexion. This increase of approximately 22% in the maximum Von Mises stress of the cortical bone is significant. However, the integrity of the cortical bone is not threatened since the value of 110 MPa is less than its expected failure stress, which ranges from 167 to 215 MPa (Table 4-3). A stress increase in the mobile model in flexion was observed on the anterior region of the interface between the prosthesis and the adjacent vertebral endplates. This increase results from the presence of the artificial intervertebral disc and is also responsible for the potential failure of the cancellous bone discussed above. The Von Mises stress ranges from 20 to 60 MPa in this particular region of the upper endplate of the intermediate vertebra, as illustrated in Figure 5-28. This value is not critical for the

cortical bone. Nevertheless, as the mechanical characteristics of the cortical bone are reduced in this area (Table 2-1), it was demonstrated above that the pressure transmits a significant stress to the cancellous bone and potentially generate the subsidence of the device into the adjacent vertebral bodies. The subsidence of the artificial disc into the intermediate vertebral body was evaluated to approximately 0.5 mm, even without considering the failure of the cancellous bone.

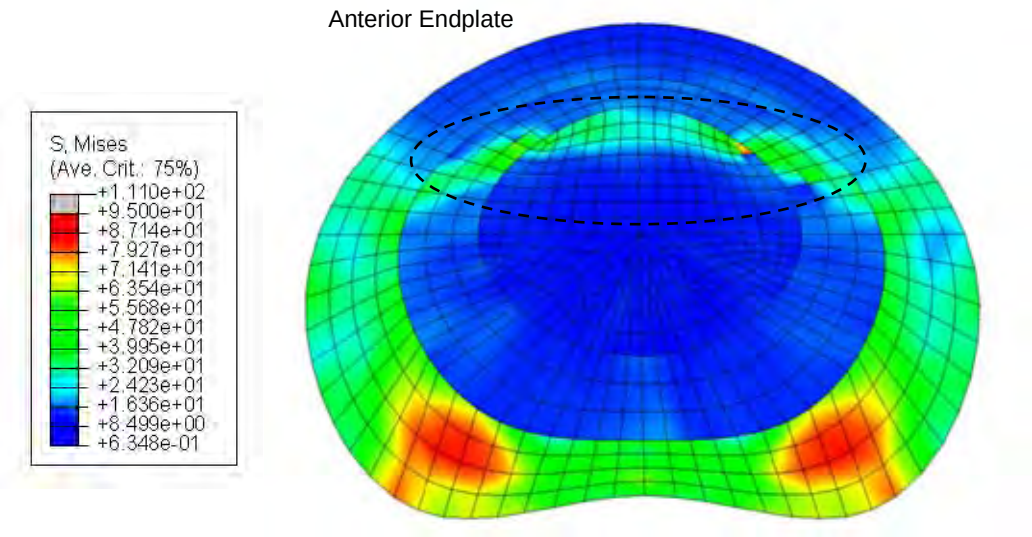

Figure 5-28: Illustration of the increase of compressive stress (circled by a dotted line) on the upper endplate of the intermediate vertebral body of the mobile model in flexion, resulting from the implantation of the artificial disc and potentially responsible for the subsidence of the device. The peak stresses on the posterior endplate are spurious tensile stresses and result from the rare coincidence of nodes from the residual annulus end the vertebral endplate

5.1.7Antero-posterior Position of the Artificial Disc

The antero-posterior position of the artificial disc was not deeply investigated in the current study. The artificial disc was located in order to maintain the balance of the lumbar segment in standing position, i.e. under simple compressive pressure. The

residual annulus, which provides additional stability, was not taken into consideration to determine the position of the artificial disc. Two additional simulations were run placing the artificial device in an anterior and a posterior position. It was shown that the static equilibrium of the FSU implanted with an artificial disc is extremely dependent on the antero-posterior position of the device. Figure 5-29 illustrates both posterior and anterior positions of the artificial disc when simulated in compression. Under simple compressive pressure, the segment becomes unstable with a slightly anterior device and the simulation fails to converge (Figure 5-29 (a)). With a posterior device, the segment remains stable because of the set of intervertebral ligaments and only a slight flexion is observed (Figure 5-29 (b)). The sagittal distance between the anterior and the posterior position of the artificial disc was only approximately equal to 3 mm.

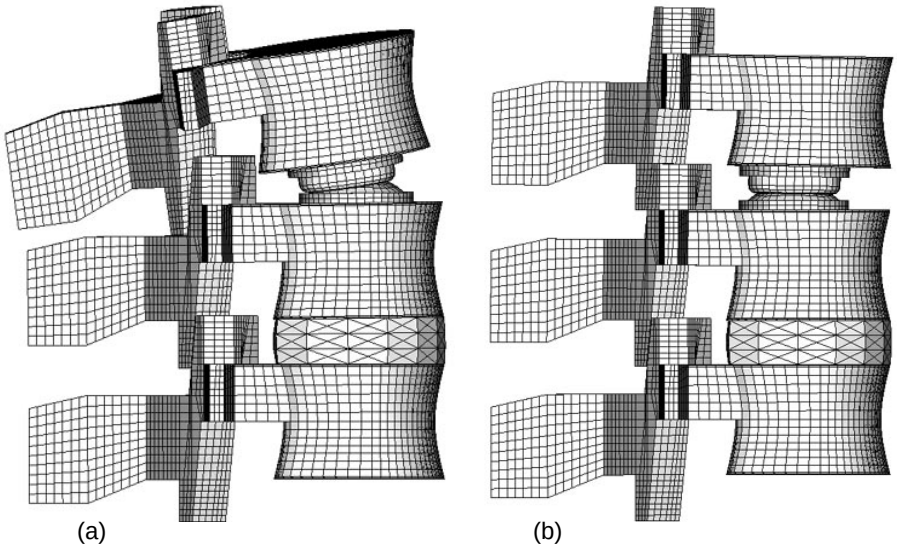

Figure 5-29: Influence of the antero-posterior position of the artificial disc in compression, without residual annulus. The ligaments are not represented. (a) The model becomes unstable and fails to converge with a slightly anterior device and in the absence of residual annulus. (b) The model remains stable in compression with a posterior device, and a slight flexion is observed

5.2 Discussion

5.2.1 Limitations

In view of the calculated results, this paragraph states the major limitations of the model.

- Density and distribution of mesh:

As expected during the construction of the model, the density and the distribution of the mesh of the different components limit the results provided by the model. In particular, spurious high peak stresses have been observed in several areas. However, those unrelated data are fairly easy to identify and have not been taken into consideration in the analyses of the results.

- Boundary and loading conditions:

In the healthy model, significant differences have been observed between the calculated forces on the components of the upper and lower FSUs, specifically on the ligaments and on the facet joints. This reveals that the combination of the boundary and the loading conditions affects the transmission of the load from one vertebra to another and the distribution between anterior and posterior intervertebral components. The influence of these edge effects concerns all numerical simulations but is particularly significant on short spinal segments.

- Clinical data:

Most of the properties of the model originate from clinical data. As a consequence limitations of the model arise from the relative accuracy of those clinical data. In

particular, the failure strengths of the different materials (ligaments, bone, annulus fibers) provide an order of magnitude to compare with the calculated results but should not be taken for granted as they are subject to large dispersions.

- Geometry of the artificial disc:

The geometry of the artificial disc used in the mobile model is similar to the SB Charité, the Prodisc, and the Maverick devices as it consists of a sliding ball-in-socket joint. The provided rotational ranges of motions are in the same order of magnitude than for these prostheses. The analysis of the results showed in particular that, in the mobile model, the facet joints were completely unloaded on the level implanted with the artificial disc in extension. Conversely, on the same FSU in flexion, the articular facets are overloaded. This reveals that the coupling of the rotational and translational displacements is not adapted as it is imposed. The above mentioned devices seem to have an alterative to this issue. The SB Charité propose an intermediate sliding core with two centers of rotation, which allows the prosthesis to disconnect, within a limited range, the rotational and translational displacements in the transverse plane. The Prodisc is alike the prosthesis used in the model; however, the surfaces of the ball-in-socket joint are not completely congruent, which allows a relative translational displacement in the transverse plane, independently from the rotational displacements. Finally, the Maverick offers a perfectly congruent ball-in-socket sliding joint that has a smaller radius of curvature. As a consequence, the translational displacements in the transverse plane are limited with respect to the rotational displacements and the facet joints are more likely to remain in contact and functional.

5.2.2 Loading Protocol

In view of the significant differences, specifically between the healthy and the mobile models reported in Section 5.1, and on the generally poor mechanics of the arthroplasty solution, it seems important to recall the general conditions of the loading protocol. The conditions simulated are appropriate to the upper limit of displacements and loads in physiological conditions. Those conditions are extreme, but may occur in daily life. Given that the aim of the surgical treatments of disc degeneration is to relieve the patients and to allow them to recover their normal range of daily activities, it is essential to understand the behavior of a treated spinal segment in all conditions, and in particular in the worst-case.

5.2.3 Antero-posterior Position of the Artificial Disc

Section 5.1.7 demonstrated that an anterior position of the artificial movable disc within the treated FSU can jeopardize the stability of the segment, whereas the segment remains stable with a posterior device, thanks to the set of intervertebral ligaments. This result confirms the observations of several other studies.

Dooris et al. have shown through a numerical model that an anterior placement of an artificial ball-in-socket joint greatly increases the facet loads in compression, which confirms a significant modification in the distribution of the load between anterior and posterior components of a FSU [14]. Moreover, Ooij et al. studied the complications with the SB Charité and have shown that the anterior placement of the prosthesis poses a risk of instability, as illustrated in Figure 5-30 [49].

Figure 5-30: Preoperative and 6 years postoperative lateral radiographs of a lumbar spine treated with the SB Charité device on the L4-L5 and L5-S1 levels. Note the anterior position of the prosthesis and the induced sharp angle in the spinal curvature at the L4-L5 level, similar to the model presented on Figure 5-29 (a) [49]

According to the findings of the current study, it is suggested, in order to reach an optimal stability of the treated segment, that the center of rotation of the artificial movable disc is located on the posterior area of the adjacent vertebral endplates. The posterior and anterior areas are delimited by the axis passing through the geometrical center of the vertebral endplate (O) and parallel to the lateral direction (x), as illustrated on Figure 5-31.

It is to note that the design of the Maverick prosthesis seems to have taken into consideration this issue. The center of rotation is located on the posterior part of the device (see Figure 2-12). This feature facilitates the implantation process as the prosthesis can still be located on the anterior area of the intervertebral space while guarantying a posterior position of the center of rotation.

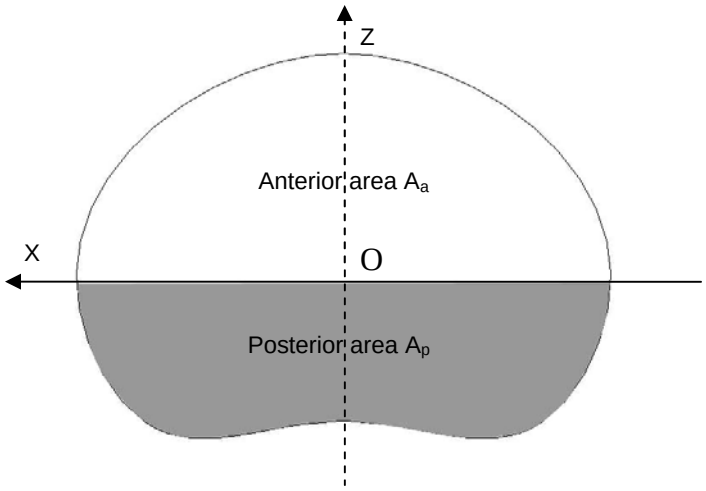

Figure 5-31: Delimitation of the anterior and posterior area of a vertebral endplate, X is oriented in the lateral direction; Z is oriented in the sagittal direction; O is the geometric center of the surface, defined such that the areas on each part of the Ox and Oz axes are equal (in particular Aa = Ap)

5.2.4 Significance of the Residual Annulus for the Arthroplasty Solution

Dooris et al. investigated, through a numerical model, the influence of the amount of residual annulus on the behavior of a FSU treated by implantation of a ball-in-socket artificial intervertebral joint. They demonstrated that slight variations in the amount of residual annulus do not significantly alter the ability of the implanted FSU to resist the intervertebral motions [14]. However, the presence of a residual annulus was shown to be absolutely necessary in the present study. Indeed, in absence of a residual annulus, the treated FSU of the mobile model has very little resistance, provided mainly by the ligaments. As a result, simulations of the rotational motions fail to converge, specifically in extension, lateral bending, and axial rotation for which the ligaments have a less significant role than in flexion. This reflects the importance of the residual annulus in

reducing the risks of instability after the implantation of an artificial intervertebral movable disc.

The mechanical behavior of the residual annulus, observed in the mobile model, is different without the presence of the nucleus. Stresses in the fibers and the annulus ground are less homogeneous and are not pertinent to the simulated motion. The maximum Von Mises stresses in the fibers, located in the lateral part of the residual annulus, are locally significantly higher, up to approximately 45 MPa in lateral bending, than the stresses reported in the lower annulus fibers (Section 5.1.5). This increased maximum stress, resulting from the excision of most of the disc and greater motion inflicted to the treated FSU, is dangerously close to the hypothesized failure stress of 46 MPa, discussed in Section 4.5. The maximum Von Mises stress calculated in the annulus ground remain similar to the one calculated in the lower disc (Table B-13), and do not exceed 3.3 MPa in the case of the residual annulus in lateral bending. With regard to the high peak stresses in the fibers, it seems clear that the residual annulus may be subject to further degeneration with the prosthesis that was used and under the considered loading conditions.

5.2.5 Complications Associated with the Treatment of Arthrodesis

The complications associated with the treatment of arthrodesis (fusion) reported in the literature, and discussed in Section 1.2.1, can be divided into two main groups: unsuccessful fusion of the treated FSU (failure of bony union, broken screw, instrument loosening, and migration of the implant), and degeneration of the levels adjacent to the treated FSU. Due to the simple geometric model of the fused FSU, the current model does not allow the investigation of complications in the prosthesis' area, such as broken

screw. Nevertheless, given a successful fusion of the treated FSU, the model allows an investigation into the behavior of the underlying adjacent level.

Concerning complications on the adjacent levels, the literature remains equivocal. The results reported by different authors are not definitive enough to conclude that arthrodesis significantly increases the degeneration of the adjacent FSUs [35], [55]. Conversely, other studies showed that fusion is more likely to accelerate the degeneration of adjacent levels [9], [36].

The key result of the present study concerning the arthrodesis treatment model is an average decrease of the whole segment's mobility in the rotational degrees of freedom of approximately 44%. Among the parameters investigated and specifically related to the FSU underlying the treated level (the mobility, the force in the ligaments, the force and pressure in the facets, the stress in the annulus fibers, and the tress in the vertebrae), the values were similar to the healthy configuration. With respect to the loading protocol appropriate to the upper limits of physiological conditions, the simulation of the fused model did not show any stress concentration that would suggest a subsequent or accelerated degeneration of the components of the adjacent underlying FSU.

5.2.6 Complications Associated with the Treatment of Arthroplasty

As discussed in Section 1.2.2, the main complications reported for the treatments of spinal arthroplasty are the degeneration of the facet joints on the treated level, the degeneration of the disc and facet joints on the adjacent levels, and the subsidence or migration of the artificial device [49]. The present mobile model considers a movable intervertebral prosthesis for total disc replacement consisting of sliding solid parts. The design of the prosthesis, described in Section 2.1.4, is similar to the Prodisc and Maverick

devices (Figure 2-12). As a consequence, the results provided by the mobile model are appropriate to this specific type of artificial device and should not be generalized to other arthroplasty solutions. The mobile model does allow the analysis of the behavior of both FSUs as well as their constitutive components.

With respect to the loading protocol, the mobile model showed significant differences relative to the healthy model on both treated and healthy underlying adjacent FSUs. The mobility of the whole segment was significantly increased in all rotational degrees of freedom by an average of approximately 52%.

For the mobile model, the underlying adjacent FSU exhibited increased values for all the parameters investigated. The mobility of the lower FSU was augmented in flexion, extension, and lateral bending by an average of 32%. The stretch forces on the ligaments were greater than in the healthy model and in particular reached 293 N for the lower right CL in right lateral bending, which exceeds the ligament's expected failure load of 284 N reported in Table 2-2. The pressure in the facet joints was significantly increased by approximately 150% (from 1 MPa in the healthy model to 2.5 MPa in the mobile model) in extension. This fairly high pressure pertains to a force of only 100 N, transmitted through a narrow area on each of the lower facets. The stress in the fibers of the annulus was also increased in flexion, extension, and lateral bending, by an average of approximately 12%. The only failure predicted for the components of the lower FSU is the right capsular ligament in right lateral bending. The general increased involvement of the components, relative to the healthy configuration, suggests that arthroplasty with a mobile artificial disc may lead to accelerated degeneration in the underlying adjacent FSU.

The investigated parameters are also significantly greater in the FSU implanted with the artificial movable disc than in the healthy model. The removal of most of the natural disc material decreases the ability of a FSU to resist intervertebral motions. As a consequence, the stability and the admissible mobility of the level rely as much on the geometry of the prosthesis as on the residual annulus, the facet joints, and the intervertebral ligaments. Given the geometry of the artificial disc employed, which allows a mobility of 12° in all combination of sagittal and frontal rotations (Section 2.1.4), an average increase of 65% was calculated for the mobility of the treated FSU in flexion, extension, and lateral bending. As a direct consequence, the force on the ligaments, the pressure in the facets and the stress in the residual annulus are greatly increased. Three ligaments are predicted to reach levels that exceed their reported failure loads. The force in the ISL reaches 145 N in flexion and the ligament may fail at 130 N (Table 2-2). In extension, a force of 503 N is attained in the CLs, which may fail at 284 N. It is possible to correlate this augmentation of the force on the CLs to the geometry of the prosthesis. In extension, the facet joints are no longer in contact due to the geometry of the artificial device. Indeed, a pressure of zero on the upper facets is then observed (Table B-8). As a result, the resistance provided by the upper facets of the healthy model in extension is transferred, in the mobile model, to the other intervertebral components, specifically the CLs. In addition, the pressure in the upper facets is greater in flexion and lateral bending, resulting from the geometry of the prosthesis and from the reduction of the treated FSU's stiffness. A pressure of 5.5 MPa, equivalent to a force of approximately 265 N transmitted through the facet joint, is reported in both facets in flexion. A pressure of 3.3 MPa, equivalent to a force of 205 N, is reported in the right

facet in right lateral bending. These values exceed the characteristic ultimate strength of articular cartilage, approximately equal to 3 MPa [5]. Other components of the FSU implanted with the artificial disc showed critical stresses. The fibers in the residual annulus attain a stress close to the hypothesized failure strength of 46 MPa (Section 5.2.4). The maximum Von Mises stress in the cancellous bone of the underlying vertebra adjacent to the artificial disc is increased by approximately 180% (from 3.5 MPa to 9 MPa) in flexion, which may result in the failure of the material and in the potential subsidence of the prosthesis into the vertebral body (Section 5.1.6).

In conclusion, the mobile model gave signs of the most common complications encountered in spinal arthroplasty when simulated with loading conditions appropriate to the upper limit of physiological conditions. The degrees of freedom and the range of motions allowed by the geometry of a movable artificial disc play a significant role in the outcomes of arthroplasty treatments considering such devices. Given the prosthesis used in the mobile model, the simulation of the segment treated by arthroplasty revealed major risks of instability and further degeneration in the treated FSU as well as risks of accelerated degeneration of the intervertebral components in the underlying adjacent FSU.

CHAPTER 6

CONCLUSIONS AND RECOMMENDATIONS

This chapter summarizes the accomplishments and conclusions of this study and proposes recommendations for future work.

6.1 Validation of the Model

A three-dimensional finite element model of a two-level ligamentous lumbar motion segment was developed. Three configurations of the model were considered in order to analyze and compare the behavior of a lumbar motion segment altered by the surgical treatments of arthrodesis and arthroplasty relative to a healthy configuration. The model was evaluated comparing the results calculated through the simulation of the healthy configuration to clinical data.

It was shown that the general behavior of the healthy model follows the same trends as a lumbar segment in vivo. The calculated results concerning the mobility of the segment, coupling of the different degrees of freedom, and the force provided by the intervertebral ligaments were reasonably close to physiological conditions. The evaluated maximum stresses in the different components (cancellous bone, cortical bone, annulus fibers and articular facets) were always less than the reported strength of the materials. Some limitations were, however, identified through the evaluation of the healthy model. The analysis of the strain in the ligaments revealed a defect in their initial conditions, which may limit the contribution of some ligaments in the static equilibrium of the segment. Some geometric approximations used in the model are responsible for unrelated

high peak stresses in several components as well as for an overestimation of the calculated disc bulge.

Nevertheless, these limitations did not prevent the model from comparing the three configurations. Indeed, the overall conditions being identical for the different configurations, the developed model is valid for the analysis and comparison of the influence of the considered surgical treatments on the biomechanics of a lumbar segment.

6.2 Evaluation of the Surgically Altered Models

6.2.1 Arthrodesis Solution

The modeled solution of arthrodesis showed a significant decrease in the mobility of the lumbar segment, by an average of 44%, in all rotational degrees of freedom (flexion, extension, lateral bending, and axial rotation). The changes of the biomechanics of the fused FSU were not specifically investigated. With regard to the uncertainties raised by clinical studies, the analysis focused on the potential alterations of the biomechanics of the adjacent healthy level underlying the treated FSU. Among the parameters investigated (mobility, force in the ligaments, pressure on the articular facets, tensile stress in the annulus fibers, and stress in the vertebrae) the results calculated in the lower healthy FSU were quite similar to the healthy configuration. In conclusion, the simulation of the fused model under severe physiological loading conditions did not raise any critical differences, relative to the healthy configuration, that would suggest a subsequent or accelerated degeneration of the intervertebral components of the adjacent healthy level underlying the treated FSU.

6.2.2 Arthroplasty Solution

In the model considering a treatment by arthroplasty, the alteration of the biomechanics was investigated in both FSUs while simulated in the different rotational degrees of freedom (flexion, extension, lateral bending, and axial rotation).

In the level implanted with a sliding ball-in-socket type of artificial disc, all the parameters investigated (mobility, force in the ligaments, pressure on the articular facets, tensile stress in the annulus fibers, and stress in the vertebrae) showed an increase in magnitude relative to the healthy configuration. The variation was, in some cases, significant enough to suggest that the failure of several intervertebral components may occur. As a result, the outcomes of arthroplasty may be particularly poor in the treated level under severe physiological conditions. This conclusion is mainly the result of the geometry and the type of prosthesis that was used in the mobile model. Indeed, the device allows a mobility that is not adapted for all of the rotational degrees of freedom. Moreover, the zero-stiffness of the device in the rotational degrees of freedom increases drastically the contributions of the other intervertebral components in resisting the motions of the treated FSU.

The alteration of the biomechanics of the treated FSU was transferred to the underlying healthy level. The intervertebral components of the underlying FSU conserved their integrity; however, a significant increase of the magnitude of the different parameters investigated was indicated.

In conclusion, under severe physiological loading conditions, the FSU of the mobile model implanted with the artificial movable disc gave signs of the most common complications encountered in spinal arthroplasty and showed risks of instability and

further degeneration. Alteration of the biomechanics of the spine is, among traumatic, nutritional, and genetic backgrounds, a cause of intensified degeneration of the intervertebral components. As a consequence, the increased stresses calculated in the underlying adjacent healthy FSU suggest risks of an accelerated degeneration of its intervertebral components.

6.3 Future Work

In spite of the approximations made in order to develop the model, it was shown (Chapter 4) that the model is a good tool for comparison of the global behavior of a lumbar segment in different configurations. Moreover, significant repercussions of the artificial disc's design on the alteration of the biomechanics of the segment were demonstrated. As a consequence, the model should be a particularly useful tool for comparing the biomechanics of lumbar segments implanted by different types of intervertebral prostheses. The category of prostheses considered in the mobile model (movable discs for total disc replacement) can be extended to flexible discs for total disc replacement, such as the Acroflex (J&J Depuy Acromed), and nucleus prostheses for partial disc replacement, such as the PDN (Raymedica). The postoperative behavior of a lumbar FSU implanted with an actual intervertebral cage is another possible field of investigation. The model may also be used to contribute to the optimization of a specific artificial device or to the development of a new design.

Instability of the mobile model was related to the presence of the residual annulus and to the anterior or posterior position of the artificial disc. Instability was predicted when the simulation failed to converge. Alternatively, instability could be obtained from

the amount of mobility predicted by convergent simulations and then incrementally changing the amount of residual annulus and the antero-posterior position of the device.

A succession of additional improvements would provide the model with more comprehensive validity and accordingly, the ability to run more specific analyses. The reduction of the limitations listed in Section 2.6 and the correction of the defects pointed out through the validation of the model (Chapter 4; in particular the initial conditions in the ligaments) should be the first steps in upgrading the model. The potential impact on further research could then be very broad, particularly related to the functional and structural analyses of the lumbar spine.

APPENDIX A

ABAQUS INPUT FILE

Following is an extract of the input file of the simulation of the healthy model, which summarizes the material properties, the interaction properties, the boundary conditions, the interactions, and the different steps simulated, i.e. flexion, extension, lateral bending and axial rotation.

```
** MATERIALS
**
*Material, name="ANNULUS FIBERS LAYER 1"
*Elastic
550.,0.
*Material, name="ANNULUS FIBERS LAYER 2"
*Elastic
485.,0.
*Material, name="ANNULUS FIBERS LAYER 3"
*Elastic
420.,0.
*Material, name="ANNULUS FIBERS LAYER 4"
*Elastic
360.,0.
*Material, name="ANNULUS GROUND SUBSTANCE"
*Elastic
4.2, 0.45
*Material, name="CANCELLOUS BONE"
*Elastic
100., 0.2
*Material, name="CORTICAL BONE"
*Elastic
12000., 0.3
*Material, name="END-PLATE CENTER"
*Elastic
2000., 0.3
*Material, name="END-PLATE MEDIAN"
*Elastic
6000., 0.3
*Material, name=NUCLEUS
*Elastic
 0.1, 0.499
*Material, name="POSTERIOR VERTEBRA"
*Elastic
3000., 0.3
*Connector Behavior, name=CL
*Connector Elasticity, nonlinear, component=1
  0.,  0.
 14., 1.2
200., 4.8
*Connector Behavior, name=TL
*Connector Elasticity, nonlinear, component=1
  0.,  0.
 3.2, 3.9
 90., 22.
*Connector Behavior, name=LF
*Connector Elasticity, nonlinear, component=1
   0.,   0.
 12.5,   1.
 375., 16.5
```

```
*Connector Behavior, name=ISL
*Connector Elasticity, nonlinear, component=1
  0.,  0.
 28., 1.8
234., 13.
*Connector Behavior, name=PLL
*Connector Elasticity, nonlinear, component=1
  0.,  0.
 7.3, 1.1
126., 10.
*Connector Behavior, name=ALL
*Connector Elasticity, nonlinear, component=1
  0.,  0.
 20., 1.2
400., 10.
*Connector Behavior, name=SSL
*Connector Elasticity, nonlinear, component=1
  0.,    0.
 48.,   2.8
408., 14.25
**
** INTERACTION PROPERTIES
**
*Surface Interaction, name="FACET JOINT"
1.,
*Friction, slip tolerance=0.005
0.,
*Surface Behavior, pressure-overclosure=exponential
0.1, 0.3
**
** BOUNDARY CONDITIONS
**
** Name: Disp-BC-1 Type: Displacement/Rotation
*Boundary
"INFERIOR ENDPLATE LOWERMOST VERTEBRA", 1, 1
** Name: Disp-BC-2 Type: Displacement/Rotation
*Boundary
"INFERIOR ENDPLATE LOWERMOST VERTEBRA", 2, 2
** Name: Disp-BC-3 Type: Displacement/Rotation
*Boundary
"INFERIOR ENDPLATE LOWERMOST VERTEBRA", 3, 3
**
** INTERACTIONS
**
** Interaction: FACET JOINT-1
*Contact Pair, interaction="FACET JOINT"
"LOWER FACET UPPERMOST VERT L", "UPPER FACET INTERMEDIATE VERT L"
** Interaction: FACET JOINT-2
*Contact Pair, interaction="FACET JOINT"
"LOWER FACET UPPERMOST VERT R", "UPPER FACET INTERMEDIATE VERT R"
** Interaction: FACET JOINT-3
*Contact Pair, interaction="FACET JOINT"
"LOWER FACET INTERMEDIATE VERT L", "UPPER FACET LOWERMOST VERT L"
** Interaction: FACET JOINT-4
*Contact Pair, interaction="FACET JOINT"
"LOWER FACET INTERMEDIATE VERT R", "UPPER FACET LOWERMOST VERT R"
** ----------------------------------------------------------------
**
** STEP: Comp preload
**
*Step, name="Comp preload"
*Static
.5, 1., 1e-05, 1.
```

```
**
** LOADS
**
** Name: SURFFORCE-1   Type: Pressure
*Dsload
_PickedSurf1829, P, 0.5
**
** OUTPUT REQUESTS
**
*Restart, write, frequency=1
**
** FIELD OUTPUT: F-Output-1
**
*Output, field, variable=PRESELECT, frequency=1
**
** Field OUTPUT: Ligaments
**
*Node Output, nset=ligaments
U
**
** HISTORY OUTPUT: H-Output-1
**
*Output, history, variable=PRESELECT, frequency=1
**
** HISTORY OUTPUT: Facet interactions
**
*Contact Output, master="LOWER FACET UPPERMOST VERT L",
slave="UPPER FACET INTERMEDIATE VERT L"
CFN, CAREA, XN
*Contact Output, master="LOWER FACET UPPERMOST VERT R",
slave="UPPER FACET INTERMEDIATE VERT R"
CFN, CAREA, XN
*Contact Output, master="LOWER FACET INTERMEDIATE VERT L",
slave="UPPER FACET LOWERMOST VERT L"
CFN, CAREA, XN
*Contact Output, master="LOWER FACET INTERMEDIATE VERT R",
slave="UPPER FACET LOWERMOST VERT R"
CFN, CAREA, XN
*Contact Output, master=Core, slave=Plate
CFT, CAREA, XN
**
*El Print, freq=999999
*Node Print, freq=999999
*End Step
** ----------------------------------------------------------------
**
** STEP: Flexion
**
*Step, name=Flexion
*Static
0.25, 1., 1e-05, 1.
**
** LOADS
**
** Name: FLEX-FORCE   Type: Body force
*Dload, op=NEW
Flexset, BZ, -7.7
**
*End Step
** ----------------------------------------------------------------
**** STEP: Extension
**
*Step, name=Extension
```

```
*Static
0.25, 1., 1e-05, 1.
**
** LOADS
**
** Name: EXT-FORCE   Type: Body force
*Dload, op=NEW
Extset, BZ, -2.2
**
*End Step
** ----------------------------------------------------------------
**
** STEP: Lateral Bending
**
*Step, name="Lateral Bending"
*Static
.25, 1., 1e-05, 1.
**
** LOADS
**
** Name: BEND-FORCE   Type: Body force
*Dload, op=NEW
Bendset, BZ, -3.6
**
*End Step
** ----------------------------------------------------------------
**
** STEP: Axial rot
**
*Step, name="Axial rot"
*Static
.25, 1., 1e-05, 1.
**
** LOADS
**
** Name: Axial rot 1   Type: Concentrated force
*Cload, follower
Rotset1, 2, -50.
** Name: Axial rot 2   Type: Concentrated force
*Cload, follower
Rotset2, 2, 50.
** Name: BEND-FORCE   Type: Body force
*Dload, op=NEW
**
*End Step
```

APPENDIX B

SUMMARY OF THE DATA CALCULATED

Table B-1: Rotational mobility (degree) of the whole model for the three configurations in the different rotational degrees of freedom, see calculation methods in Section 4.2

Motion	Healthy Model	Fused Model	Mobile Model
Flexion	16.4	9.9	21.6
Extension	8.5	4.1	13.6
Lateral Bending	11.6	6.3	18.0
Axial Rotation	2.9	1.8	4.7

Table B-2: Rotational mobility (degree) of the upper FSU for the three modeled configurations in the different rotational degrees of freedom, see calculation methods in Section 4.2

Motion	Healthy Model	Fused Model	Mobile Model
Flexion	8.2	0.7	11.4
Extension	4.3	0.1	7.7
Lateral Bending	5.8	0.3	10.2
Axial Rotation	1.5	0.5	3.3

Table B-3: Rotational mobility (degree) of the lower FSU for the three modeled configurations in the different rotational degrees of freedom, see calculation methods in Section 4.2

Motion	Healthy Model	Fused Model	Mobile Model
Flexion	8.6	9.5	10.5
Extension	4.3	4.0	6.0
Lateral Bending	5.9	6.1	7.9
Axial Rotation	1.5	1.5	1.5

Table B-4: Translational mobility (mm) in the sagittal direction for the upper and lower FSUs of the three modeled configurations in flexion, see calculation methods in Section 4.2

FSU	Healthy Model	Fused Model	Mobile Model
Upper FSU	1.3	0.0	4.3
Lower FSU	1.0	0.9	1.3

Table B-5: Translational mobility (mm) in the sagittal direction for the upper and lower FSUs of the three modeled configurations in extension, see calculation methods in Section 4.2

FSU	Healthy Model	Fused Model	Mobile Model
Upper FSU	0.7	0.0	2.6
Lower FSU	0.6	0.6	0.8

Table B-6: Translational mobility (mm) in the lateral direction for the upper and lower FSUs of the three modeled configurations in right lateral bending, see calculation methods in Section 4.2

FSU	Healthy Model	Fused Model	Mobile Model
Upper FSU	0.9	0.0	4.5
Lower FSU	0.5	0.5	0.7

Table B-7: Force in the ligaments in the three modeled segments for the different rotational degrees of freedom; *inf=inferior, sup= superior, l= left, r=right*; bold figures are exceeding the pre-defined failure load (Table 2-2), italic figures cannot be compared to the healthy model for which the force is zero

	Ligament Force - Healthy Model (N)				Ligament Force - Fused Model (N)				Ligament Force - Mobile Model (N)			
Ligament	**Flexion**	**Extension**	**Bending**	**Rotation**	**Flexion**	**Extension**	**Bending**	**Rotation**	**Flexion**	**Extension**	**Bending**	**Rotation**
ALL-inf	0	0	0	0	0	0	0	0	0	*4.5*	*2*	0
ALL sup	0	0	0	0	*1.4*	*0.11*	*0.66*	0	**N/A**	**N/A**	**N/A**	**N/A**
CL-inf-l	13.4	130.2	8.62	33.97	8.58	114.4	7.32	32.43	53.98	251.67	11.1	38.35
CL-inf-r	13.4	129.1	180.01	0.19	8.69	113.36	158.82	0	54.38	250.83	**292.57**	0
CL-sup-l	9.1	217.41	8.07	36.27	0.15	3.65	4.33	9.71	134.93	**502.59**	29.38	58.9
CL-sup-r	9.2	216.87	150.83	0	0.16	3.7	2.1	0	139.99	**502.63**	216.26	*1.16*
ISL-inf	78	0	0	5.92	73.08	0	0	5.14	107.97	0	0	9.1
ISL-sup	85.4	0	0	3.13	33.43	0	0	0	**145.3**	0	*17.78*	18.32
LF-inf	34.2	0	0	0	43.86	0	0	0	79.23	0	0	0
LF-sup	61.4	0	0	0	19.64	0	0	0	285.54	0	*26.95*	*5.38*
PLL-inf	0	0	0	0	0	0	0	0	0	0	0	0
PLL-sup	0	0	0	0	*2.78*	0	*0.46*	0	*83.12*	0	*11.68*	*1.78*
SSL-inf	69.1	0	0	1.43	62.18	0	0	1.19	113.37	0	0	3.1
SSL-sup	88.8	0	0	0	25.71	0	0	0	195.42	0	5.35	*7.1*
TL-inf-l	0.6	0	1.72	0	0.94	0	1.93	0	1.11	0	2.76	0
TL-inf-r	0.6	0	0	0	0.94	0	0	0	1.11	0	0	0
TL-sup-l	1.3	0	2.06	0	0.48	0	0.13	0	11.01	0	19.27	0
TL-sup-r	1.3	0	0	0	0.48	0	0	0	11.02	0	0	*1.66*

Table B-8: Forces and equivalent average compressive pressure on the facet joints in the three modeled segments for the different rotational degrees of freedom; *sup=superior*, *inf=inferior*; figures exceeding 200 N or 2 MPa are bolded

	Force Magnitude (N) - Healthy Model				Force Magnitude (N) - Fused Model				Force Magnitude (N) - Mobile Model			
Facet	**Flexion**	**Extension**	**Bending**	**Rotation**	**Flexion**	**Extension**	**Bending**	**Rotation**	**Flexion**	**Extension**	**Bending**	**Rotation**
Sup Left	115	54	16	0	41	1	0	0	**366**	0	94	0
Sup Right	116	54	161	109	42	1	7	27	**365**	0	**205**	174
Inf Left	1	79	24	0	40	77	30	0	0	100	17	0
Inf Right	1	79	140	114	40	77	145	116	0	100	174	111

	Equivalent Average Pressure (MPa) - Healthy Model				Equivalent Average Pressure (MPa) - Fused Model				Equivalent Average Pressure (MPa) - Mobile Model			
Facet	**Flexion**	**Extension**	**Bending**	**Rotation**	**Flexion**	**Extension**	**Bending**	**Rotation**	**Flexion**	**Extension**	**Bending**	**Rotation**
Sup Left	**2.2**	1	0.5	0	0.4	0	0	0	**5.3**	0	1.5	0
Sup Right	**2.2**	1	**2.6**	1	0.4	0	0.1	0.2	**5.5**	0	**3.3**	1.7
Inf Left	0.1	0.9	0.7	0	1.1	0.9	0.7	0	0	**2.5**	0.3	0
Inf Right	0.1	1	**2.3**	1	1.1	0.9	**2.4**	1.1	0	**2.4**	**2.2**	1

Table B-9: Anterior bulge (mm) of the lower healthy disc for the three modeled segments, calculated as described on Figure 4-7; bold figures are more likely to be compared considering the location of the reported bulge

Motion	Healthy Model	Fused Model	Mobile Model
Pre-compression	0.54	0.54	0.55
Flexion	**3.95**	**4.03**	**4.53**
Extension	0.44	0.48	0.10
Lateral Bending	1.34	1.41	1.24

Table B-10: Posterior bulge (mm) of the lower healthy disc for the three modeled segments, calculated as described on Figure 4-7; bold figures are more likely to be compared considering the location of the reported bulge

Motion	Healthy Model	Fused Model	Mobile Model
Pre-compression	0.66	0.66	0.65
Flexion	2.52	2.53	2.61
Extension	**1.79**	**1.77**	**1.90**
Lateral Bending	1.93	1.92	1.96

Table B-11: Right lateral bulge (mm) of the lower healthy disc for the three modeled segments, calculated as described on Figure 4-7; bold figures are more likely to be compared considering the location of the reported bulge

Motion	Healthy Model	Fused Model	Mobile Model
Pre-compression	0.44	0.44	0.44
Flexion	1.67	1.66	1.74
Extension	1.06	1.06	1.07
Lateral Bending	**2.63**	**2.65**	**3.10**

Table B-12: Average Von Mises stress (MPa) in the fibers of the lower healthy disc for the three modeled segments and in the different rotational motions

Motion	Healthy Model	Fused Model	Restored Model
Flexion	10.3	10.4	11.2
Extension	6.7	6.6	7.6
Lateral Bending	8.7	8.7	9.8
Axial Rotation	6.0	6.0	6.1

Table B-13: Maximum Von Mises stress (MPa) in the annulus ground substance of the lower healthy disc for the three modeled segments and in the different rotational motions

Motion	Healthy Model	Fused Model	Restored Model
Flexion	2.8	2.9	3.2
Extension	1.7	1.7	1.9
Lateral Bending	2.3	2.3	2.7
Axial Rotation	0.6	0.6	0.6

REFERENCES

[1] Adams, M.A., Hutton, W.C., **Mechanics of the intervertebral disc**, in: Ghosh, P., **The biology of the intervertebral disc**, Vol. 2, CRC Press LLC, Boca Raton, Florida, pp. 39-71, 1988

[2] Adams, M.A., Hutton, W.C., **The effect of posture on the role of the apophysial joints in resisting intervertebral compressive forces**, *The Journal of Bone and Joint Surgery*, Vol. 62-B, No. 3, pp. 368-362, 1980

[3] Alini, M., Roughley, P.J., Antoniou, J., Stoll, T., Aebi, M., **A biological approach to treating disc degeneration: not for today, but maybe for tomorrow**, *European Spine Journal*, Vol. 11, Suppl. 2, pp. S215-S220, 2002

[4] An, H., Boden, S.D., Kang, J., Sandhu, H.S., Abdu, W., Weinstein, J., **Summary statement, emerging techniques for treatment of degenerative lumbar disc disease**, *Spine*, Vol. 28, No. 15S, pp. S24-S25, 2003

[5] An, Y.H., **Mechanical properties of bone**, in: An, Y.H., Draughn, R.A., **Mechanical testing of bone and the bone-implant interface**, CRC Press LLC, Boca Raton, Florida, pp. 41-59, 2000

[6] Baldwin, N.G., **Lumbar disc disease: the natural history**, *Neurosurgical Focus*, Vol. 13, No. 2, Article 2, 2002

[7] Bao, Q.-B., McCullen, G.M., Higham, P.A., Dumbleton, J.H., Yuan, H.A., **The artificial disc: theory, design and materials**, *Biomaterials*, Vol. 17, pp. 1157-1167, 1996

[8] Baroud, G., Nemes, J., Heini, P., Steffen, T., **Load shift of the intervertebral disc after a vertebroplasty: a finite element study**, *European Spine Journal*, Vol. 12, No. 4, pp. 421-426, 2003

[9] Bastian, L., Lange, U., Knop, C., Tusch, G., Blauth, M., **Evaluation of the mobility of adjacent segments after posterior thoracolumbar fixation: a biomechanical study**, *European Spine Journal*, Vol. 10, No. 4, pp. 295-300, 2001

[10] Benoist, M., **Natural history of the aging spine**, *European Spine Journal*, Vol. 12, Suppl. 2, pp. S86-S89, 2003

[11] Bertagnoli, R., Kumar, S., **Indication for full prosthetic disc arthroplasty: a correlation of clinical outcome against a variety of indications**, *European Spine Journal*, Vol. 11, Suppl. 2, pp. S131-S136, 2002

[12] Bibby, S.R.S., Jones, D.A., Lee, R.B., Yu, J., Urban, J.P.G., **The pathophysiology of the intervertebral disc**, *Joint Bone Spine*, Vol. 68, pp. 536-542, 2001

[13] Calisse, J., Rohlmann, A., Bergmann, G., **Estimation of trunk muscle forces using the finite element method and in vivo loads measured by telemeterized internal spinal fixation devices**, *Journal of Biomechanics*, Vol. 32, pp. 727-731, 1999

[14] Dooris, A.P., Goel, V.K., Grosland, N.M., Gilbertson, L.G., Wilder, D.G., **Load sharing between anterior and posterior elements in a lumbar motion segment implanted with an artificial disc**, *Spine*, Vol. 26, No. 6, pp. E122-E129, 2001

[15] Dunlop, R.B., Adams, M.A., Hutton, W.C., **Disc space narrowing and the lumbar facet joints**, *The Journal of Bone and Joint Surgery*, Vol. 66-B, No. 5, 1984

[16] Dvorak, J., Panjabi., M.M., Chang, D.G., Theiler, R., Grob, D., Functional Radiographic Diagnosis of the Lumbar Spine, Spine, Vol. 16, No. 5, pp. 562-571, 1991

[17] Eijkelkamp, M.F., Van Donkelaar, C.C., Veldhuizen, A.G., Van Horn, J.R., Huyghe, J.M., Verkerke, G.J., **Requirements for an artificial intervertebral disc**, *Biomaterials*, Vol. 24, No. 5, pp. 311-332, 2001

[18] Ferguson, S.J., Steffen, T., **Biomechanics of the aging spine**, *European Spine Journal*, Vol. 12, Suppl. 2, pp. S97-S103, 2003

[19] Fritzell, P., Hägg, O., Nordwall, A., **Complications in lumbar fusion surgery for chronic low back pain: comparison of three surgical techniques used in a prospective randomized study. A report from the Swedish Lumbar Spine Study Group,** *European Spine Journal*, Vol. 12, pp. 178-189, 2003

[20] Frobin, W., Brinkmann, P., Biggemann, M., Tillotson, M., Burton, K., **Precision measurement of disc height, vertebral height and sagittal plane displacement from lateral radiographic views of the lumbar spine**, *Clinical Biomechanics*, Vol. 12, Suppl. 1, pp. S1-S63, 1997

[21] Fujiwara, A., Tamai, K., Yamato, M., An, H.S., Yoshida, H., Saotome, K., Kurihashi, A., **The relationship between facet joint osteoarthritis and disc degeneration of the lumbar spine: an MRI study**, *European Spine Journal*, Vol. 8, No. 5, pp. 396-401, 1999

[22] Goel, V.K., Kong, W., Han, J.S., Weinstein, J.N., Gilbertson L.G., **A combined finite element and optimization investigation of lumbar spine mechanics with and without muscles**, *Spine*, Vol. 18, No. 11, pp. 1531-1541, 1993

[23] Goel, V.K., Monroe, B.T., Gilbertson, L.G., Brinckmann, P., **Interlaminar shear stresses and laminae separation in a disc, finite element analysis if the L3-L4 motion segment subjected to axial compressive loads**, *Spine*, Vol. 20, No. 6, pp. 689-698, 1995

[24] Grant, J.P., Oxland, T.R., Dvorak, M.F., **Mapping the structural properties of the lumbosacral vertebral endplates**, *Spine*, Vol. 26, No. 8, pp. 889-896, 2001

[25] Gunzburg, R., Mayer, H.M., Szpalski, M., Aebi, M., **Arthroplasty of the spine: the long quest for mobility**, *European Spine Journal*, Vol. 11, Suppl. 2, pp. S63-S64, 2002

[26] Guyer, R.D., Ohnmeiss, D.D., **Intervertebral disc prosthesis**, *Spine*, Vol. 28, No. 15S, pp. S15-S23, 2003

[27] Hanley, E.N., David, S.M., **Lumbar arthrodesis for the treatment of back pain**, *Journal of Bone and Joint Surgery*, Vol. 81-A, No. 5, pp. 716-730, 1999

[28] Helmut, D.L., **History, design and biomechanics of the LINK SB Charité artificial disc**, *European Spine Journal*, Vol. 11, Suppl. 2, pp. S98-S105, 2002

[29] Homminga, J., McCreadie, B.R., Ciarelli, T.E., Weinans, H., Goldstein, S.A., Huiskes, R., **Cancellous bone mechanical properties from normals and patients with hip fractures differ on the structure level, not on the bone hard tissue level**, *Bone*, Vol. 30, No. 5, pp. 759-764, 2002

[30] Hukins, D.W.L., **Disc structure and function**, in: Ghosch, P., **The biology of the intervertebral disc**, Vol. 1, CRC Press LLC, Boca Raton, Florida, pp. 1-37, 1988

[31] Jin, D., Qu, D., Zhao, L., Chen, J., Jiang, J., **Prosthetic Disc Nucleus (PDN) replacement for lumbar disc herniation**, *Journal of Spinal Disorders & Techniques*, Vol. 16, No. 4, pp. 331-337, 2003

[32] Kabel, J., Odgaard, A., Van Rietbergen, B., Huiskes, R., **Connectivity and the elastic properties of cancellous bone**, *Bone*, Vol. 24, No. 2, pp. 115-120, 1999

[33] Kabel, J., Van Rietbergen, B., Odgaard, A., Huiskes, R., **Constitutive relationships of fabric, density, and elastic properties in cancellous bone architecture**, *Bone*, Vol. 25, No. 4, pp. 481-486, 1999

[34] Kleuver, M. de, Oner, F.C., Jacobs, W.C.H., **Total disc replacement for chronic back pain: background and a systematic review of the literature**, *European Spine Journal*, Vol. 12, pp. 108-116, 2003

[35] Kumar, M.N., Baklanov, A., Chopin, D., **Correlation between sagittal plane changes and adjacent segment degeneration following lumbar spine fusion**, *European Spine Journal*, Vol. 10, pp. 314-319, 2001

[36] Kumar, M.N., Jacquot, F., Hall, H., **Long-term follow-up of functional outcomes and radiographic changes at adjacent levels following lumbar spine fusion for degenerative disc disease**, *European Spine Journal*, Vol. 10, pp. 309-313, 2001

[37] Langrana, N.A., Lee, C.K., Yang, S.W., **Finite-element modeling of the synthetic intervertebral disc**, *Spine*, Vol. 16, No. 6, pp. S245-S252, 1991

[38] Lavaste, F., Skalli, W., Robin, S., Roy-Camille, R., Mazel, C., **Three-dimensional geometrical and mechanical modeling of the lumbar spine**, *Journal of Biomechanics*, Vol. 25, No. 10, pp. 1153-1164, 1992

[39] LeHuec, J.C., Kiaer, T., Friesem, T., Mathews, H., Liu, M., Eisermann, L., **Shock absorption in lumbar disc prosthesis, a preliminary mechanical study**, *Journal of Spinal Disorders & Techniques*, Vol. 16, No. 4, pp. 346-351, 2003

[40] Lemaire, J.-P., Skalli, W., Lavaste, F., Templier, A., Mendes, F., Diop, A., Sauty, V., Laloux, E., **Intervertebral disc prosthesis: result and prospects for the year 2000**, *Clinical Orthopaedics and Related Research*, Vol. 337, pp. 64-76, 1997

[41] Linde, F., **Elastic and viscoelastic properties of trabecular bone by a compression testing approach**, *Danish Medical Bulletin*, Vol. 41, No. 2, pp. 119-138, 1994

[42] Long, M., Rack, H.J., **Titanium alloys in total joint replacement – a materials science perspective**, *Biomaterials*, Vol. 19, pp. 1621-1639, 1998

[43] Madan, S.S., Harley, J.M., Boeree, N.R., **Anterior lumbar interbody fusion: does stable anterior fixation matter?**, *European Spine Journal*, Vol. 12, pp. 186-392, 2003

[44] Marchesi, D.G., **Spinal fusion: bone and bone substitutes**, *European Spine Journal*, Vol. 9, pp. 372-378, 2000

[45] Martin, M.D., Boxell, C.M., Malone, D.G., **Pathophysiology of lumbar disc degeneration: a review of the literature**, *Neurosurgical Focus*, Vol. 13, No. 2, Article 1, 2002

[46] McAfee, P.C., **Interbody fusion cages in reconstructive operations on the spine**, *Journal of Bone and Joint Surgery*, Vol. 81-A, No. 6, pp. 859-880, 1999

[47] Moore, R.J., Fraser, R.D., Vernon-Roberts, B., Finnie, J.W., Blumbergs, P.C., Haynes, D.R., Hutchens, M.J., Walters, R.M., Kamat, A.S., Koszyca, B., **The biologic response to particles from a lumbar disc prosthesis**, *Spine*, Vol. 27, No. 19, pp. 2088-2094, 2002

[48] Niv, D., Gofeld, M., Devor, M., **Causes of pain in degenerative bone and joint disease: a lesson from vertebroplasty**, *Pain*, Vol. 105, pp. 387-392, 2003

[49] Ooij, A. van, Oner, F.C., Verbout, A.J., **Complications of artificial disc replacement, a report of 27 patients with the SB Charité Disc**, *Journal of Spinal Disorders & Techniques*, Vol. 16, No. 4, pp. 368-383, 2003

[50] Oxland, T.R., Lund, T., **Biomechanics of stand-alone cages and cages in combination with a posterior fixation: a literature review**, *European Spine Journal*, Vol. 9, Suppl. 1, pp. S95-S101, 2000

[51] Panjabi, M.M., Goel, V.K., Takata, K., **Physiological strains in the lumbar spinal ligaments**, *Spine*, Vol. 7, pp. 192-203, 1977

[52] Panjabi, M.M., Oxland, T., Takata, K., Goel, V., Duranceau, J., Krag, M., **Articular facets of the human spine, quantitative three-dimensional anatomy**, *Spine*, Vol. 18, No. 10, pp. 1298-1310, 1993

[53] Panjabi, M.M., Yamamoto, I., Oxland, T., Crisco, J., **How does posture affect coupling in the lumbar spine?**, *Spine*, Vol. 14, pp. 1002-1011, 1989

[54] Patwardhan, A.G., Havey, R.M., Meade, K.P., Lee, B., Dunlap, B., **A follower load increases the load-carrying capacity of the lumbar spine in compression**, *Spine*, Vol. 24, No. 10, pp. 1003-1009, 1999

[55] Penta, M., Sandhu, A., Fraser, R.D., **Magnetic resonance imaging assessment of disc degeneration 10 years after anterior lumbar interbody fusion**, *Spine*, Vol. 20, pp. 743-747, 1995

[56] Pitzen, T., Geisler, F.H., Matthis, D., Müller-Storz, H., Pederson, K., Steudel, W.-I., **The influence of cancellous bone density on load sharing in human lumbar spine: a comparison between an intact and a surgically altered motion segment**, *European Spine Journal*, Vol. 10, No. 1, pp. 23-29, 2001

[57] Polikeit, A., Ferguson, S.J., Nolte, L.P., Orr, T.E., **Factors influencing stresses in the lumbar spine after the insertion of intervertebral cages: finite element analysis**, *European Spine Journal*, Vol. 12, No. 4, pp. 413-420, 2003

[58] Polikeit, A., Ferguson, S.J., Nolte, L.P., Orr, T.E., **The importance of the endplates in the lumbar spine**, *European Spine Journal*, Vol. 12, No. 6, pp. 556-561, 2003

[59] Ray, C.D., **The PDN prosthetic disc-nucleus device**, *European Spine Journal*, Vol. 11, Suppl. 2, pp. S137-142, 2002

[60] Rothoerl, R.D., Woertgen, C., Brawanski, A., **When should conservative treatment for lumbar disc herniation be ceased and surgery considered?**, *Neurosurgical Review*, Vol. 25, pp. 162-165, 2002

[61] Sharma, M., Langrana, N.A., Rodriguez, J., **Modeling of facet articulation as a nonlinear moving contact problem: sensitivity study on lumbar facet response**, *Journal of Biomechanical Engineering*, Vol. 120, pp. 118-125, 1998

[62] Sharma, M., Langrana, N.A., Rodriguez, J., **Role of ligaments and facets in lumbar spinal stability**, *Spine*, Vol. 20, No. 8, pp. 887-900, 1995

[63] Shirazi-Adl, A., **Finite element evaluation of contact loads on facets of an L2-L3 lumbar segment in complex loads**, *Spine*, Vol. 16, No. 5, pp. 533-541, 1991

[64] Shirazi-Adl, A., **Nonlinear stress analysis of the whole lumbar spine in torsion – mechanics of facet articulation**, *Journal of Biomechanics*, Vol. 27, No. 3, pp. 289-299, 1994

[65] Shirazi-Adl, A., Sadouk, S., Parnianpour, M., Pop, D., El-Rich, M., **Muscle force evaluation and the role of posture in human lumbar spine under compression**, *European Spine Journal*, Vol. 11, No. 6, pp. 519-526, 2002

[66] Shirazi-Adl, S.A., Shrivastava, S.C., Ahmed, A.M., **Stress analysis of the lumbar disc-body unit in compression, a three-dimensional nonlinear finite element study**, *Spine*, Vol. 9, No. 2, pp. 120-134, 1984

[67] Silva, M., Keaveny, Y.M., Hayes, W.C., **Load sharing between the shell and centrum in the lumbar vertebral body**, *Spine*, Vol. 22, No. 2, pp. 140-150, 1997

[68] Silva, M.J., Wang, C, Keaveny, T.M., Hayes, W.C., **Direct and computed tomography thickness measurements of he human, lumbar vertebral shell and endplate**, *Bone*, Vol. 15, No. 4, pp. 409-414, 1994

[69] Skaggs, D.L., Weidenbaum, M., Iatridis, J.C., Ratcliffe, A., Mow, V.C., **Regional variation in tensile properties and biochemical composition of the human lumbar annulus fibrosus**, *Spine*, Vol. 19, No. 12, pp. 1310-1319, 1994

[70] Smit, T.H., Odgaard, A., Schneider, E., **Structure and function of vertebral trabecular bone**, *Spine*, Vol. 22, No. 24, pp. 2823-2833, 1997

[71] Szpalski, M., Gunzburg, R., Mayer, M., **Spine arthroplasty: a historical review**, *European Spine Journal*, Vol. 11, Suppl. 2, pp. S65-S84, 2002

[72] Thompson, R.E., Pearcy, M.J., Downing, K.J.W., Manthey, B.A., Parkinson, I.H., Fazzarali, N.L., **Disc lesions and the mechanics of the intervertebral joint complex**, *Spine*, Vol. 25, No. 23, pp. 3026-3035, 2000

[73] Traynelis, V.C., **Spinal arthroplasty**, *Neurosurgical Focus*, Vol. 13, No. 2, Article 10, 2002

[74] Vernon-Roberts, B., **Disc pathology and disease state**, in: Ghosch, P., **The biology of the intervertebral disc**, Vol. 2, CRC Press LLC, Boca Raton, Florida, pp. 73-119, 1988

[75] Welch, W.C., Gerszten, P.C., **Alternative strategies for lumbar discectomy: intradiscal electrothermy and nucleoplasty**, *Neurosurgical Focus*, Vol. 13, No. 2, Article 7, 2002

[76] White III, A.A., Panjabi, M.M., **Clinical biomechanics of the spine, second edition**, J.B. Lippincott Company, Philadephia, 1990

[77] Wilke, H.-J., Neef, P., Caimi, C., Hoogland, T., Claes, L.E., **New *in vivo* measurements of pressure in the intervertebral disc in daily life**, *Spine*, Vol. 24, No. 8, pp. 755-762, 1999

[78] Zander, T., Rohlmann, A., Klöckner, C., Bergmann, G., **Influence of graded facetectomy and laminectomy on spinal biomechanics**, *European Spine Journal*, Vol. 12, No. 4, pp. 427-434, 2003

[79] Zhao, J., Hou, T., Wang, X., Ma, S., **Posterior lumbar interbody fusion using one diagonal fusion cage with transpedicular screw/rod fixation**, *European Spine Journal*, Vol. 12, No. 2, pp. 173-177, 2003